Micron- and submicron-scale high porosity polymer membranes and their use for cell isolation

J. Alejandro Hernández Castro

Doctor of Philosophy

McGill University
Montréal, Québec
June 2019

Submitted to McGill University in partial fulfillment of the requirements for the degree of Doctor of Philosophy

DEDICATION

This dissertation is dedicated to my family, especially to my wife, Maria, whose love and support helped me get through this journey successfully, thank you for believing in me and loving me like you always do.

To my mother, Norma, who was always my best teacher, friend, guide, and role model, thank you for dedicating your life to your family, I wouldn't be the person I am today without you, I will always miss you.

To my father, Jorge, who instilled in me a love for science and studying, always pushing me forward to aspire for greatness, and for reminding me that a work worth doing is that which is in the service of others.

TABLE OF CONTENTS

LIST OF TABLES

LIST OF FIGURES

ABSTRACT

Cell isolation is defined as the process of separating individual living cells from a solid block of tissue or cell suspension. Isolating cells is necessary for downstream analysis of the cells of interest, which can be rare (such as circulating tumor cells) or abundant cells (like white blood cells). Many different methods, including the use of hydrodynamic, sonic, dielectrophoretic, and magnetic forces have been proposed, however, these techniques usually suffer from low throughput, high cost, need of complex setups, and are not easily translatable to the clinical setting.

Microfilters have also been proposed for the isolation and enrichment of specific rare and abundant cells, especially due to their capacity to process samples with a higher throughput than with microfluidic devices (larger volumes and higher flow rates), relative simple operation, capacity for cell recovery, and integrated on-chip washing and staining. Even though many different microfiltration cell capture platforms can be found in the literature, many rely on the use of silicon microfilters, which are costly to produce and suffer from lack of optical transparency and brittleness.

Only two commercially available alternatives of polymer microfilters with controllable pore size exist, track-etched membranes and PET mesh filters. The first ones lack a regular pore distribution and have limited porosity values; the second have high autofluorescence, are not transparent, and their pores are not perfectly uniform due to the mesh construction characteristics. There is thus a need for low-cost, large-area, freestanding polymer microfilters with regular pore distribution and the related production process capable of precise control of pore size, shape, porosity, and thickness.

This thesis proposes a solution to meet the aforementioned needs through a novel fabrication method for submicron- and microporous polymer membranes. This powerful technique allows for the fabrication of very large-area filters (up to 9×9 cm^2), with high porosity (up to 60%), pores as small as 500 nm and of different shapes, that are easy to manipulate and can be readily integrated into microfluidic devices.

Successful use of these membranes for the capture of rare circulating tumor cells (CTCs) from buffer solutions and whole blood samples is also shown. Isolation efficiencies of up to $\approx 95\%$ were obtained by using a combination of molecular and physical capture of the target cells.

Finally, efficient capture ($\approx 97\%$), multi-step staining and release ($\approx 95\%$) of white blood cells (WBCs) obtained from healthy blood samples is also demonstrated. This platform can be useful for applications where minimizing cell loss is critical, or for enriching cells from samples with very low cell concentrations.

RÉSUMÉ

L'isolement de cellules est défini comme le processus consistant à séparer des cellules vivantes individuelles d'un bloc solide de tissu ou d'une suspension cellulaire. L'isolement de cellules est une étape nécessaire à l'analyse en aval de cellules d'intérêt, qui peuvent être rares (telles que les cellules tumorales circulantes) ou abondantes (comme les globules blancs). De nombreuses méthodes, utilisant des forces hydrodynamiques, soniques, diélectrophorétiques ou magnétiques, ont été proposées. Cependant, ces techniques sont généralement limitées par un faible rendement, un coût élevé, et par le besoin d'installations complexes, les rendant alors difficilement transférables en clinique.

Les microfiltres ont également été proposés pour l'isolement et l'enrichissement de cellules rares ou abondantes spécifiques, notamment en raison de leur capacité à traiter des échantillons avec un rendement supérieur à celui des dispositifs microfluidiques (volumes et débit plus élevés), leur fonctionnement relativement simple, leur taux de récupération de cellules, et la possibilité d'intégrer les étapes de rinçage et marquage directement sur puce. Bien que de nombreuses plateformes de capture de cellules par microfiltration ont été rapportées dans la littérature, beaucoup utilisent des microfiltres en silicium, qui sont coûteux, fragiles et manquent de transparence optique.

Il existe seulement deux alternatives commerciales de microfiltres en polymère à taille de pore contrôlable : les membranes en polycarbonate Track-etch et les filtres à mailles en PET. Les premières présentent une distribution de pores irrégulière limitant leur porosité; les deuxièmes possèdent une autofluorescence élevée, ne sont pas transparents et leurs pores ne sont pas parfaitement uniformes en raison des caractéristiques de construction de la maille. Il existe donc un besoin réel de microfiltres en polymère, indépendants, de grande surface et avec une distribution régulière des pores et donc de mettre au point un processus de production à faible coût permettant un contrôle précis de la taille et de la forme des pores, ainsi que de la porosité et de l'épaisseur des microfiltres.

Cette thèse propose une solution répondant aux exigences susmentionnées et décrit la mise au point d'un nouveau procédé de fabrication de membranes submicro- et microporeuses en polymère. Cette technique puissante permet la fabrication de filtres de très grande surface (jusqu'à 9×9 cm^2), de porosité élevée (jusqu'à 60%), transparents, faciles à manipuler et à intégrer en dispositifs microfluidiques, et possédant des pores de formes différentes et de taille variant de plusieurs dizaines de microns à 500 nm.

L'utilisation de ces membranes pour la capture efficace de cellules tumorales circulantes (CTCs) rares à partir de solutions tampons et d'échantillons de sang complet est également présentée. Une rendement d'isolation d'environ 95% a été obtenu en combinant la capture moléculaire et mécanique des cellules cibles.

Finalement, la capture (environ 97%), la libération (environ 95%) et le marquage des globules blancs présents au sein d'échantillons de sang complet de donneurs seins, sont également démontrés. Cette plateforme peut être utile pour les applications dans lesquelles il est essentiel de minimiser la perte de cellules ou pour l'enrichissement de cellules à partir d'échantillons contenant de très faibles concentrations cellulaires.

ACKNOWLEDGEMENTS

First and foremost, I thank my advisors, Prof. David Juncker and Dr. Teodor Veres for granting me the opportunity to embark on this journey with them over the last 5 years and guiding my scientific, professional, and personal growth along the way. It has been a challenging road, and I couldn't have made it through without their guidance.

I would also like to thank my committee members, Profs. Richard Leask, Srikar Vengallatore, and Maryam Tabrizian for always asking the tough questions and ensuring that high standards were maintained in my research, presentations, and writings.

I was extremely fortunate to be part of two world-class laboratories that have allowed me to work side-by-side with amazing colleagues and researchers. Special thanks go to my mentors: Dr. Kebin Li, who showed me the ropes in the clean room, helping me take my first steps in this journey, and with whose help we developed the fabrication process that is the foundation of this thesis; Dr. Anne Meunier, who did an amazing work to take our developed technology through to performing very interesting clinical tests; Dr. Jamal Daoud, for always being open to provide guidance and comments to improve my work, as well as for working with me on the development of the WBC isolation platform, and helping me revise this thesis; Dr. Lidija Malic, for her help brainstorming for projects, and also for her comments and suggestions to improve the writing of this thesis; Dr. Keith Morton, for his invaluable help in the revision of this manuscript.

On a personal note, I would like to thank the friends I made along the way, Ayo, Jamal, Lidija, Matthias, Liviu, Jeff, Véro. You have encouraged and counseled me, helped me clear my mind with those football games, jam sessions, and coffee chats. Some memories will fade with time, but the ones I made with you will remain with me forever.

To my friends back home, all those jokes, silly chats, and late gaming nights were part of the fuel that kept me going.

This work could not have been completed without the help, support, and guidance of my family too, who made sure I remained strong throughout the ride. Lastly, I owe my

greatest gratitude to my wife, Maria, for believing in me and following me in this long and challenging journey away from home, your constant support, patience, and understanding mean everything to me, I'm a better man because of you.

PREFACE

The original motivation of this research work was to develop a platform for cell isolation, both for the capture of rare (CTCs) and abundant cells (WBCs) from blood samples.

With the onset of MEMS technology, the ability to fabricate devices in the micro- and nanoscale has enhanced our capacity to interact with particles, microorganisms, and cells in ways we had never been able to before. Microfluidic devices where magnetic, acoustic, dielectrophoretic, and hydrodynamic forces are used for sorting of specific cell populations can be found in the literature, adaptation of MEMS fabrication techniques have also been explored for the production of microfilters or micro-gap microfluidic devices that can also be used for successful cell isolation.[1,2]

Among the different types of cells that can be isolated, CTCs have had a prominent role in the past decade due to their potential to be used as a cancer biomarker or a form of liquid minimally invasive biopsy, as well as their role in the metastatic process.[3,4] Even though the presence of these cancer cells in circulating blood was first reported by Dr. Thomas Ashworth in 1869,[5] it was not until more recent times when they were begun to be studied in more detail.

CTC isolation is challenging because of their very low numbers in blood (typically < 10/mL); they must be extracted from a background of millions of WBCs and billions of RBCs per milliliter of blood; their size overlap with that of WBCs; short life in circulation (less than 24 h); size and molecular heterogeneity; and the fact that they can be found as single or clustered cells. The first examples of CTC isolation experiments using track-etched polymer microfilters date back to the 1960s[6] (an approach still used in some modern commercial CTC isolation platforms like ScreenCell®), while these porous membranes are relatively easy to fabricate and use, and are commercially available, they suffer from low porosity ($< 20\%$), random pore distribution, and autofluorescence, which

limits the throughput, increases the chances of non-specific cell capture in the space between the pores, and makes on-filter fluorescence imaging challenging.

With the emergence of the MEMS and lab-on-a-chip fields (from the late 1980s), the use of acoustics, magnetism, dielectrophoresis, optical tweezers, and hydrodynamics in microfluidic devices have been effectively explored for cell isolation. While good capture rates ($> 70\%$) and very specific CTC isolation have been demonstrated with these techniques, they still have some important drawbacks that have not been overcome yet, namely: low throughput, need for complex instrumentation, operation constrictions from the device's geometry, or the inability to target single or clustered cells simultaneously. These microfabrication advances have also allowed us to produce complex structures, such as microfilters with high porosity and regularly distributed pores, which can be fabricated using silicon substrates or polymers, the former lack optical transparency and are brittle, making them harder to manipulate and prone to breaking during filtration procedures; microfabricated polymer filters are more mechanically robust, but most current fabrication methods are complex and/or yield autofluorescent membranes.

Cell isolation by filtration has the advantages of being simple to operate, achieving higher throughput rates than other techniques, targeting a wider range of cells (regardless of their size or molecular heterogeneity), and capturing clustered and single cells at the same time; however, efforts must be made to select optimal filtration parameters that increase CTC capture efficiency while reducing unwanted capture of background blood cells.

Although the importance of CTCs has been established by now, and many researchers have proposed different methods for the separation of these rare cells from blood samples, there's still no gold standard for CTC isolation, and there are still many unknowns related to the biology of these cancer cells.

Capture of WBCs is usually a problem when the interest are CTCs, however, in other cases, WBC separation and isolation from peripheral blood is the precursor to many

downstream analytical assays. While for CTCs the biggest challenge to capture them lies on their rarity, in the case of WBCs, their abundance can be a source of issues, especially when using a filtration method, filter clogging can occur rapidly if the filtration area is not considered in relation to the volume of the filtered sample. Another challenge for WBC isolation by filtration is the high deformability of these cells, they are able to course through small capillaries ($4 - 5$ µm in diameter) and even smaller gaps between endothelial cells during extravasation ($\approx 1.6 - 2.3$ µm in diameter),[7] meaning submicron pores may be necessary to ensure high efficiency capture of WBCs.

The isolation and counting of WBCs finds many applications in disease diagnosis, including infection, myeloma, lymphoma, leukaemia, as well as for HIV/AIDS diagnostics.[8–11] To isolate WBCs, standard clinical methods involve density gradient centrifugation or red blood cell (RBC) depletion,[12–17] however, the use of centrifugation risks cellular damage and results can be highly variable depending on user expertise.[17] These centrifugation methods are also used during sample preparation for fluorescence activated cell sorting (FACS), which is commonly used in clinical settings for the analysis of WBC populations; fluorescent multi-staining of cells is necessary for FACS analysis, which usually involves several centrifugation and resuspension steps, increasing the chance of cell loss and damage, and are also a source of result variability.

As with CTCs, various efforts have been made to conceive more efficient WBC sample preparation technologies in miniaturized and automated platforms. A popular approach involves the use of antibody-coated magnetic beads,[19] however, this technique relies on label-dependent capture, with efficiency correlated with antibody activity. A widely used label-free approach involves the use of microporous membranes for size-based cell capture, recovery, and perfusion of buffers, commercially available track-etched or polymer mesh filters are commonly used, but intrinsic limitations due to their construction restrict the throughput and capture efficiencies of these systems.

After analyzing and comparing current approaches for cell isolation, our hypothesis was that: *"Microfiltration is the most promising method since, by using precisely microfabricated filters, it can simultaneously offer high throughput (by using large diameter filters), it can be tailored for label-free high efficiency capture of rare or abundant cells (by carefully selecting the pore size), it can isolate both single and clustered cells, on-filter staining and imaging are possible (reducing sample manipulation during buffer exchange), it is easy to operate (not requiring complex chips or instruments), and it could be coupled with immunocapture to enhance isolation of specific target cells".*

To prove our hypothesis, we divided the work into four projects, whose results became the overall contributions of this work, by the end I can claim to have:

1. **Developed a robust fabrication method for polymer microfilters which allows for the fabrication of porous membranes across a wide range of sizes, thickness, porosity, and pore size.** No commercially available polymer filters had the desired characteristics for the platforms we built: We required freestanding membranes, that were optically transparent, non-autofluorescent, non-cytotoxic, had high porosity, regular pore distributions, and that were not cytotoxic. This combination of characteristics could not be found in commercially available polymer microfilters or in other experimental microfabricated ones found in the literature. Published as a *Research Article* in ***Lab on a Chip***. It was highlighted in the back cover of Issue 11 in 2017.
2. **Showed that the antibodies on a filter surface enhance the capture efficiency of target cells.** One of the advantages of using physical filtration for cell isolation is that all cells are forced to interact with the filters at some point during the filtration process, we hypothesized that by attaching antibodies onto the filters' surface, it would be possible to increase the capture efficiency of specific target cells, since cells that would otherwise squeeze through the pores would be captured by the secondary molecular isolation method, a concept that had not been explored before in the literature. We proved this hypothesis first using silicon microfilters, and then applied the same

principle for enhanced CTC isolation using microporous polymer membranes. Published as part of the Proceedings of the ***The 18th International Conference on Miniaturized Systems for Chemistry and Life Sciences (μTAS 2014)***.

3. Helped develop a powerful tool for CTC capture. The developed microfilters are robust enough to allow filtration of samples at high flow rates (as high as 6 mL/min was tested without filter breakage or deformation), they are easy to handle, can be cut to size according to the design of a given filtration cartridge, and can be functionalized with capture antibodies. Thanks to these characteristics, we could develop a platform that allows capture of CTCs of different sizes by using a stack of filters of different pore sizes, and can also be used for efficient CTC cluster capture by optimizing the filtration parameters accordingly. Published as a *Research Article* in ***Analytical Chemistry*** in 2016.

4. Built a platform for integrated capture, imaging, staining, buffer exchange, and recovery of WBCs from blood samples. By being able to fabricate submicron-porous polymer filters, we could have a membrane where a full population of WBCs could be captured with very high efficiency (97%), this capture rate could not be achieved with commercial PET mesh filters with a nominal pore size of 1 μm, thus, achieving this capture rate wouldn't have been possible without the use of the newly developed submicron-porous membranes. Furthermore, the smaller pores avoid cells getting stuck inside the pores, facilitating their subsequent release, which we also achieved with a similar efficiency as the capture rate (95%). Published as a *Research Article* in ***Lab on a Chip***. It was highlighted in the back cover of Issue 4 in 2019.

References

1. G.-H. Lee, S.-H. Kim, K. Ahn, S.-H. Lee and J. Y. Park, *J. Micromechanics Microengineering*, 2016, **26**, 013003.
2. Z. Shen, A. Wu and X. Chen, *Chem. Soc. Rev.*, 2017, **46**, 2038–2056.
3. Attard and J. S. de Bono, *Curr. Opin. Genet. Dev.*, 2011, **21**, 50–58.

4. K.-A. Hyun, J. Kim, H. Gwak and H.-I. Jung, *Analyst*, 2016, **141**, 382–392.

5. S. K. Arya, B. Lim and A. R. A. Rahman, *Lab. Chip*, 2013, **13**, 1995–2027.

6. S. H. Seal, *Cancer*, 1964, **17**, 637–642.

7. J. Escribano, M. Chen, E. Moeendarbary, X. Cao, V. Shenoy, J. M. Garcia-Aznar, R. Kamm, and F. Spill, *PLOS Computational Biology*, 2019, **15(5)**, e1006395.

8. J. J. M. van Dongen, V. H. J. van der Velden, M. Brüggemann and A. Orfao, *Blood*, 2015, blood–2015–03–580027.

9. U. Hassan, N. N. Watkins, B. Reddy Jr, G. Damhorst and R. Bashir, *Nat. Protoc.*, 2016, **11**, 714–726.

10. N. N. Watkins, U. Hassan, G. Damhorst, H. Ni, A. Vaid, W. Rodriguez and R. Bashir, *Sci. Transl. Med.*, 2013, **5**, 214ra170–214ra170.

11. U. Hassan, T. Ghonge, B. R. Jr, M. Patel, M. Rappleye, I. Taneja, A. Tanna, R. Healey, N. Manusry, Z. Price, T. Jensen, J. Berger, A. Hasnain, E. Flaugher, S. Liu, B. Davis, J. Kumar, K. White and R. Bashir, *Nat. Commun.*, 2017, **8**, 15949.

12. P. K. Dagur and J. P. McCoy, Curr. Protoc. Cytom. Editor. Board J Paul Robinson Manag. Ed. Al, 2015, **73**, 5.1.1–5.1.16.

13. C. Iliescu, G. Xu, E. Barbarini, M. Avram and A. Avram, *Microsyst. Technol.*, 2009, **15**, 1157–1162.

14. H. M. Ji, V. Samper, Y. Chen, C. K. Heng, T. M. Lim and L. Yobas, *Biomed. Microdevices*, 2008, **10**, 251–257.

15. X. Chen, D. F. Cui, C. C. Liu and H. Li, *Sens. Actuators B Chem.*, 2008, **130**, 216–221.

16. Y. Cheng, X. Ye, Z. Ma, S. Xie and W. Wang, *Biomicrofluidics*, 2017, **11**.

17. V. VanDelinder and A. Groisman, *Anal. Chem.*, 2007, **79**, 2023–2030.

18. M. Delahaye, K. Lawrence, S. J. Ward and M. Hoare, *Biotechnol. Bioeng.*, **112**, 997–1011.

19. S. Miltenyi, W. Müller, W. Weichel and A. Radbruch, *Cytometry*, 1990, **11**, 231–238.

CONTRIBUTION OF AUTHORS

In accordance with McGill University's "Guideline for Thesis Preparation" policy, this thesis is presented as a collection of manuscripts written by the PhD candidate with the collaboration of co-authors, as detailed below. The manuscripts and thesis presented here are based on experiments designed and conducted by the candidate. Additionally, the candidate analyzed and interpreted the experimental datasets, organized the results, and composed the manuscripts. Reflecting my role in the research, I am first author on all manuscripts included in this thesis as main chapters, and second author in the manuscript of Appendix I.

The PhD supervisors (Dr. Teodor Veres and Prof. David Juncker) appear as co-authors on all manuscripts to reflect their supervisory role in the projects and their contribution to data interpretation and manuscript preparation. Likewise, Dr. Kebin Li, a research officer in Dr. Veres' group appears as a co-author on all manuscripts to reflect his contribution to research design, the interpretation of datasets, and to the editing of the manuscripts presented here.

The thesis has been organized in five main chapters and one appendix, short prefaces have been added to serve as transitions between each chapter, where appropriate.

Chapter 1 contains a brief introduction to cell isolation techniques, and a review of polymer microfilter fabrication technologies.

Chapter 2 shows that the combined use of microfilters and capture antibodies on the membranes' surface can enhance the capture of a specific population of cells. We show that, when using filters that were only functionalized on one half, a larger number of cells are captured on the antibody-coated side when the cells express the antibody's target marker on their surface. This work was performed using silicon microfilters, but it's important in the context of this research project as it served as a basis to show that we could indeed enhance the capture of specific cells by adding capture antibodies on the filters' surface, which was a principle used later for the work presented in Appendix I.

Chapter 3 presents the developed fabrication method to produce polymer microfilters. We show that the proposed protocol is highly flexible, allowing the fabrication of polymer membranes with several different physical characteristics (pore size and shape, membrane thickness and area), and that they can be successfully used for the enrichment of populations of microbeads or cells from solution. The fabrication method is presented in detail and is the basis for the following chapters. This chapter has been published in *Lab on a Chip* as an article and highlighted in the back cover of Issue 11 in 2017. The protocol was developed alongside Dr. Kebin Li, a research officer at the NRC, which is why he appears as a first-coauthor in the article.

Chapter 4 describes a modification to the fabrication process discussed in Chapter 3 that allows the production of polymer membranes with pores in the submicron range (500 nm). These submicron-porous membranes were then successfully used to develop a technique for high efficiency isolation, on-filter immunostaining, and recovery of cells from solution, showing that a system like this could be used to replace standard sample preparation protocols where several steps of centrifugation and resuspension steps are required for cell separation and staining, which are tied to cell loss and damage. The contents of this chapter have been published as a research article in *Lab on a Chip* and highlighted in the back cover of Issue 4 in 2019.

Chapter 5 serves as a conclusion to the thesis, and includes a summary of the work carried out, as well as a discussion of the findings and formal conclusions drawn from the research. The dissertation ends with a discussion of the main drawbacks of our current research, as well as an overview of future research directions motivated by the present work.

Appendix I is a work where we show the first use of our polymer microfilters for the isolation of CTCs from blood samples based on both, physical and biochemical properties of the cells. The results obtained from the experiments in Chapter 2 had shown that by attaching antibodies on the surface of a filter, the capture efficiency of specific target cells

could be enhanced. The work in Appendix I was led by Dr. Anne Meunier, I contributed on the design of the polymer microfilters, the development of a technique to encapsulate the membranes onto PMMA frames, and the design of an antibody functionalization protocol on our polymer filters. The filtration parameters optimized by Dr. Meunier helped to achieve a high efficiency and purity capture of CTCs from blood samples. The contents of this chapter were published as a research article in *Analytical Chemistry*.

CHAPTER 1 | INTRODUCTION AND LITERATURE REVIEW

1.1 Cell isolation

Defined as the process of separating individual living cells from a solid block of tissue or a cell suspension, cell isolation has been a focus of modern medicine and biomedical science for its potential applications in the study of rare or abundant cells of interest. In the past two decades, interest in the use of microfabrication and microfluidic platforms for the isolation of cells has arisen, with many different cell sorting and separation techniques being proposed, the use of acoustics, magnetism, dielectrophoresis, microfiltration, optical tweezers, and hydrodynamics have been explored for this purpose.[1,2]

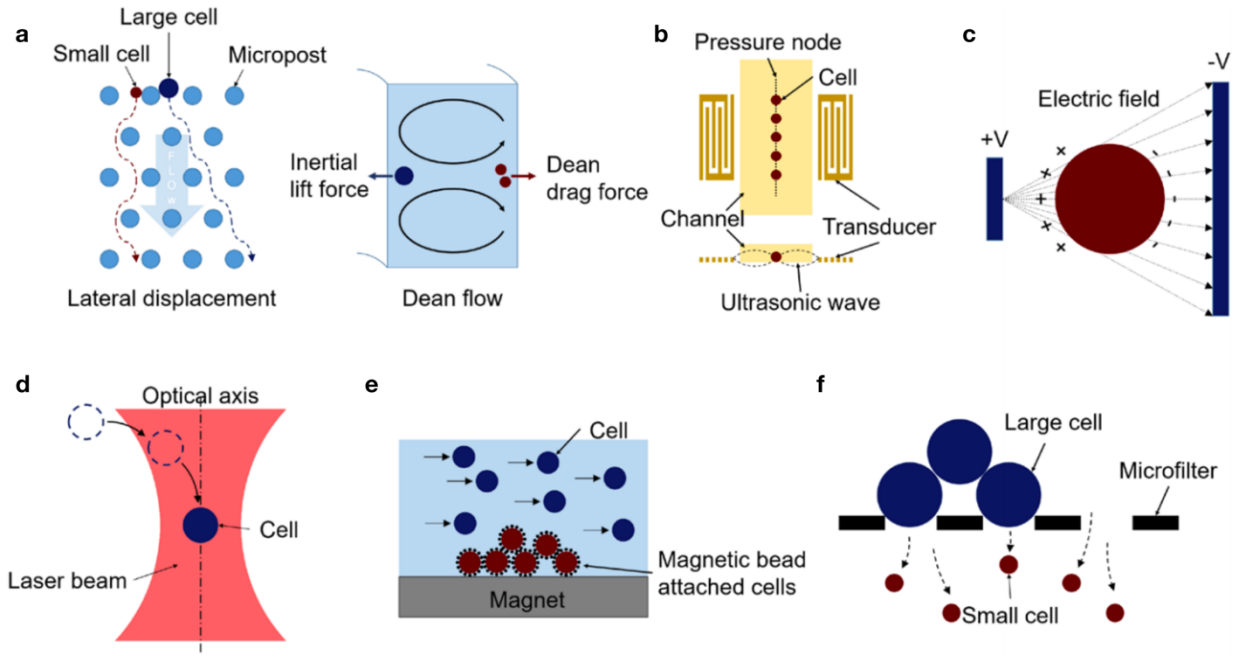

*Figure 1-1 | **Schematic of cell separation principles**.[1] (a) Hydrodynamic forces (drag, lift, and shear forces) can be used to separate cells based on their physical properties. (b) The acoustic cell separation utilizes acoustic primary radiation force from the ultrasonic waves. (c) Dielectrophoretic force utilizes the electrokinetic motion of polarizable cells in non-uniform electric fields. (d) Optical tweezers can be used to precisely manipulate single cells. (e) Cells tagged with magnetic particles can be separated by the use of an external magnetic field. (f) Microfiltration is based on the use of physical barriers for cell separation*

based on their size and deformability. (Figure adopted and reprinted with permission from Institute of Physics Publishing).

Separation of rare or abundant cells have their specific sets of needs and challenges, even though the previously mentioned isolation techniques can be adapted for both cases, some are better suited for one or the other. For example, optical tweezers allow for very precise manipulation of cells - single-cell manipulation is possible, which is very good when very precise cell isolation is sought. However, this is a slow, serial process and as the number of target cells grows larger, the advantages of very precise cell manipulation are lost.

In the context of rare cell isolation and analysis, the capture of circulating tumor cells (CTCs) has gained a lot of attention in the past decades due to their potential use as cancer biomarkers, or a form of non-invasive liquid biopsy. Cancer is a very complex disease that remains a challenge for modern medicine, even in developed countries like Canada, where mortality rates are as high as 25%.[3] It has been shown that early detection and effective treatment have a high impact on positive outcomes for the disease.[4] Poor outcomes are usually related to metastatic disease. More specifically, the presence of CTCs has been found to be a characteristic of this dissemination process, i.e. the presence of CTCs is directly correlated with recurrence, higher mortality rates and resistance to therapy in cancer.[5–7] Accurate detection of CTCs can be valuable for both predictive and prognostic cancer screenings or as a tool for assessing the effectiveness of cancer therapies.

Thus, the capability to isolate these rare, circulating cells from patient blood samples is of utmost importance. However, due to that rarity and heterogeneity, this is an extremely challenging task. The number of CTCs present in one ml of blood is typically less than 200, which, when compared to red ($\approx 5\times10^9$/mL) and white blood cells ($\approx 7\times10^6$/mL),[8] the challenge is analogous to finding a needle in the haystack. The issue is further compounded by the fact that CTCs possess quite heterogeneous characteristics,[9] rendering CTC capture a highly complex and difficult endeavor. Research interest in recent years has led to the development of several different methods for isolating CTCs;[8,10]

so far only the CellSearch system has been approved for clinical use by the FDA. This device is based on the use of anti-EpCAM coated magnetic micro-beads for the detection of CTCs. While successful rare cell isolation has been demonstrated with this system, it is quite complex and rather expensive. Additional limitations include its low sensitivity and ability to detect only EpCAM positive CTCs, and the requirement for cell fixation which prevents any further downstream analysis of the cells.[11–13]

Enrichment of more abundant cells, like WBCs, from blood is also of interest. Many analytical assays are based on the analysis of the populations of WBCs obtained from patient samples. To isolate WBCs, most clinical methods involve density gradient centrifugation or red blood cell (RBC) depletion.[14–19] Subsequent WBC manipulation is then required to prepare samples for specific analyses, often resulting in cell loss or damage. There's still a need for integrated platforms for WBC isolation, buffer exchange, and sample preparation for downstream assays whose performance is independent of the operator's expertise and that minimize cell loss or damage during the serial sample preparation steps.

Among the diseases related to WBC physiology, HIV/AIDS remains a global concern: It is estimated that in 2015 alone there were 1.1 million AIDS-related deaths worldwide.[20] Even though significant advances have been made in the fight to eradicate AIDS, according to the World Health Organization (WHO) there were approximately 2.1 million new HIV infections worldwide in 2015, for a total of 36.7 million people living with HIV. [20] More than 90% of whom live in developing countries.[21] Since most of these patients live in resource limited areas, there is still a need for the development of inexpensive but robust and accurate tools for diagnosis and monitoring of HIV infection.[22,23] Even in a country like Canada, an estimated 21% (approximately 16000 persons) of all HIV-infected people in the country are believed to be unaware of being HIV-positive.[24] Developing a simple device for lymphocyte enumeration might prove useful for a rapid assessment of AIDS status in a patient, considering that the current gold standard for these tests is flow

cytometry (an expensive instrument requiring specialized training to operate). Thus, simpler devices could help lower costs for these kind of tests, as well as provide the opportunity to employ them in low resource settings. In the following sections, some rare and abundant cell isolation techniques will be discussed in more detail.

1.2 Rare cell isolation technologies

CTCs are thought to play an important role in the process of metastasis (Figure 1-2); this cancer dissemination process is strongly related to high mortality rates and relapse in cancer. Identifying the presence of CTCs in the blood of cancer patients could potentially be used for risk-stratification of different cancer types, molecular sub-classification of disseminated cancer cells, as well as for therapeutic efficacy studies.[25,26] Further optimization of the capture mechanisms could even lead to early detection of metastatic disease or relapse. Also, by being able to isolate and study CTCs, a deeper understanding on how the process of metastasis works could be obtained, and new therapies could then be developed aimed at stopping cancer dissemination in patients.

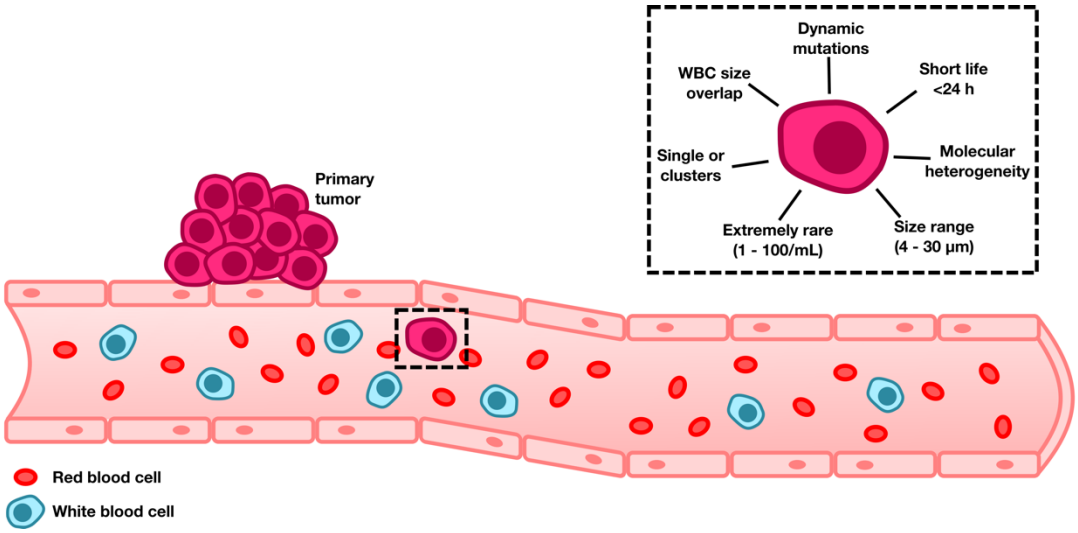

*Figure 1-2 | **Circulating tumor cells.** CTCs are known to detach from a primary tumor site and travel in the blood stream, some of these cells will exit the blood vessels and colonize distant organs. (Insert) Several characteristics of these cells make them challenging to isolate from the large background of normal blood cells.*

The first reports on the presence of CTCs in the blood of cancer patients dates back to 1869, when physician Thomas Ashworth casually identified cancer-like cells while

observing the blood of cancer patients on the microscope.[27] Almost 150 years later from that discovery, the relevance of CTCs has been noted, but there are still large gaps in the knowledge base related to the biology of these CTCs or the process of metastasis itself; this is largely because the technology needed to consistently isolate these cells from blood samples had not yet been developed.

Isolation of CTCs from blood samples is not a trivial problem because 1) CTCs are a rare occurrence when compared to the background of normal cells in blood. Even for very aggressive cancers or for patients in advanced stages of the disease, a mere few hundreds of CTCs can be found per mL of blood, in comparison to a background of billions of RBCs and millions of platelets and WBCs that are present – this is generally referred to as the "needle in the haystack" problem of CTC isolation. Another challenge is that 2) CTCs are themselves cancer cells, which means that they are highly heterogeneous due to the many different mutations they might have. As such, CTCs may have different biophysical (e.g. size, stiffness) and biochemical properties (e.g. protein and genetic content, cell surface protein expression or metabolic rate) which is why developing a single strategy to target all CTCs simultaneously is very difficult. Furthermore, when we consider that, in actual patient blood samples, the characteristics and numbers of CTCs that are being introduced into the isolation device are initially completely unknown, the problem becomes even more complex as such systems must be designed to target the widest possible range of CTCs, otherwise, the risk of false negative results is increased.

Within the past decades, advances in the field of microfabrication have provided researchers with the necessary tools to develop new technologies for the effective isolation of CTCs. A variety of creative solutions have been proposed for this purpose. These are designed around isolation based on either biophysical or biochemical properties of CTCs and, more recently, a combination of microfabrication and bio-sensitive approaches. While the proposed solutions show promise for the development of the field, there are still unresolved issues related to capture efficiency, specificity and purity of the captured

samples, as well as ease of use of the system, flexibility, and the range of targeted CTCs. These are discussed in more details below.

1.2.1 Isolation by physical barriers

Among the first category are those devices that rely on the use of physical obstacles for the trapping of the CTCs;[28] porous membranes or micro-posts arrays have both been proposed as alternatives for this method. Some of the first approaches using micro-porous membranes as a filtering structure date back to the 1960s, through the use of the then newly developed track-etched membranes[29] and some attempts were done towards the isolation of CTCs from blood.[30] These membranes have been commercially available ever since and are still used in more recent experiments on CTC isolation.[31–38] The holes in these membranes are created by bombardment of a thin polymer film with heavy, high-energy particles, which leave trails of radiation-damaged material that can be etched away with solvents,[29] but since particle bombardment is a random process, a regular distribution of the pores cannot be achieved,[30,39] and membrane porosity is limited to 2% to guarantee there will be no hole overlaps.[29] Some of the issues encountered when using these track-etched membranes are low throughput of the system given the high flow resistance, higher risk of filter clogging due to the low porosity, and higher trans-membrane pressures (which might damage the cells).

Advances and techniques developed in the field of CMOS fabrication made possible the production of microfilters with controlled pore size and distribution geometry. Silicon and polymer porous membranes have been successfully fabricated through standard photolithography techniques,[35,40–45] electroforming,[46–48] nanoimprint lithography (NIL),[49–51] and phase separation on micromolds.[52,53] Fabricating filters this way helps to increase the porosity of the membranes to ranges between 39%[40] and 50%,[54] and include precise control of the pores distribution and size as well. There are reported results of capture efficiencies higher than 80%[35,39–41,43] using these kind of filter-based devices, however, purity of the captured samples is usually low (this is not usually mentioned in the

publications). It is important to note that it is hard to compare the performance of these devices since there is still no consensus on a standard protocol to characterize CTC capture systems. Even though all these methods can be used for successful fabrication of microfilters, the processes involved are complex and costly which limits their adoption for clinical applications that require disposable filter devices.

The use of micro-gaps has also been proposed as alternatives to capture CTCs based on their size and stiffness.[55–58] Some of these device use arrays of pillars closely packed together to provide gaps that are small enough to trap the target cells.[57,59,60] Other approaches use more complex structures that try to improve flow patterns within the microfluidic chips to achieve better capture rates.[61,62] In addition, the use of shallow microchannels as the physical barriers that stop the CTCs has also been reported in the literature.[63–65] These approaches usually exhibit good capture efficiency, but suffer from very low purity of the captured samples, similar to the filter membranes. While they have the advantage of being less prone to clogging than microfilters, their throughput remains low. These shallow microchannel devices operate in the few µL/min range of the flow rates, which translates to several hours of operation to process a conventional blood sample volume of 7.5 mL. This can be a serious limitation, considering that a long sample processing time is not desired since the viability of CTCs in circulation is still unknown. Longer sample processing and analysis could lead to false negative results or prevent further processing, like culture, of the captured cells.

1.2.2 Isolation by hydrodynamic forces

Particles suspended in a fluid flowing through a microfluidic device experience a variety of hydrodynamic forces that are dependent on the physical properties (size, density) of the particles in the fluid, and on the properties of the fluid as well. This proves to be helpful in discriminating particles of very similar sizes, something that cannot be achieved by the devices based solely on the use of physical barriers.

A wide variety of microfluidic devices that take advantage of centripetal, drag, and inertial forces that arise in microfluidic laminar fluid flows have been proposed as an alternative to separate cells according to their size and density. Pinched-flow focusing devices, for example, use hydrodynamic forces that arise from sudden widening and narrowing of microchannels to force suspended cells in the sample solution to migrate into specific portions of the channel: Larger cells tend to migrate to the channel center where the flow rates are higher, while smaller cells disperse towards the walls after a final channel widening,[66–69] with reported capture efficiencies of approximately 80%.

Particles flowing in spiral channels are subject to additional forces that pull them towards or away from the inner wall of the microfluidic channel. The use of spiral channels has also been explored for the separation of cells, whereas particles or cells in the solution will migrate towards the inner or outer walls of the spiral channel depending on their size.[70] Different designs with slanted,[71,72] or double-spiral[73] microchannels have been shown in the literature. These devices have good capture efficiencies (over 85%), but they must be very carefully designed to target cells in specific size ranges. The operational flexibility is thus limited since the working parameters of these devices are heavily dependent on the channel geometry and flow rate, which remains fixed once the devices are designed and fabricated.

Another less explored way of isolating CTCs due to hydrodynamic phenomena comes from the use of vortices within microchannels to separate the rare cells from the mix. Herein, very abrupt widening of the channels lead to the creation of recirculating vortices in the wider channel regions, were the bigger cells are trapped since they experience larger forces that push them towards these cavities.[74]

It's possible to obtain very high capture rates using this sort of microfluidic devices, however they have some drawbacks, especially in terms of throughput. This is because 1) the volume of sample that can be contained inside microfluidic channels is very small (in the ranges of nL), and 2) typical flow speeds in these devices usually ranges in a few

hundred µL/min; so, processing of large volumes of samples, like the ones from normal blood samples is not practical. Also, in this kind of devices, separation of particles is typically done in two populations, those that are larger or smaller that a given value. The performance of the device depends heavily, as mentioned before, on the geometry of the channels, which cannot be modified once the device is fabricated which limits operation flexibility.

1.2.3 Isolation by dielectrophoretic (DEP) forces

Dielectrophoretic forces arise when a dielectric particle suspended on a dielectric medium is subjected to a non-uniform electric field.[75] These forces are dependent on the size and dielectric properties of the particles and the suspension medium, as well as on the characteristics of the applied electric field, i.e. waveform, frequency, amplitude, etc.; depending on the combination of these factors, DEP forces can be either attractive or repulsive. This is a highly versatile technique: Some approaches have been presented where the cells are deflected to a given equilibrium position or path within a microfluidic channel and separated according to their different characteristics,[75–79] or the systems can be designed in such a way that a sum of DEP forces traps the cells in certain locations on the chip.[80]

Since the resulting forces can be tailored by modifications of the applied electric signals to the system, the devices can be easily modified to target different types of cells. However, this method requires pre-processing steps to re-suspend the cells in a dielectric medium of known properties to have a better control on the output of the system. Additionally, the sample volumes that can be processed by DEP-based devices is usually very small (a couple hundred µL), which makes these very low throughput devices. Another important drawback is the unavoidable need of using electrical signal generators or power sources, which are usually expensive and bulky equipment, and they also require special training for their appropriate use, which makes the translation of the technology to the clinical setting a complicated task.

1.2.4 Immunocapture

The profile of a cell's surface proteins depends on its gene expression characteristics. By knowing the type of surface protein that a certain cell type expresses, it is possible to use antibodies that target those specific proteins to be able to capture them due to molecular interactions between antigen and antibody. For isolating CTCs from blood, the ideal scenario would be to find a specific marker that is expressed in all cancer cells but in none of the normal hematopoietic cells. However, cancer cells are in constant mutation which makes them highly heterogeneous, and so, finding a common marker expressed in all cancer cells is virtually impossible.

Some common markers have been found through different cancer cell types, and several approaches have been developed to use the surface protein expression properties of cancer cells for their capture. Epithelial cancer is the most common type of cancer, with a reported incidence between 80% to 90%,[81] this is why epithelial cell surface markers have been commonly used as targets for CTC isolation. Also, normal hematopoietic cells don't express epithelial markers; this helps to discriminate between blood and cancer cells. The epithelial cell adhesion molecule (EpCAM) is the most widely used target for CTC isolation. The most basic devices that utilize EpCAM for cell isolation have the anti-EpCAM coated on the surface (either flat or nano/micro-structured), which is then exposed to the sample that is flowed or allowed to sediment on the surface where the antigen-antibody interaction takes place. When the cells are highly expressing the antibody's target protein, the capture efficiency of these devices can be higher than 90%,[82] but efficiency drops considerably if the cells' surface protein expression differs, as the absence of the target protein eliminates any possibility of specific interaction between the cells and the capture antibodies.

Some other more complex approaches rely on the coating of one of the walls in a rectangular microchannel with a capture antibody. A solution containing the target cells is then flowed through the channel, and the cells that interact with the antibodies will be

trapped. Interaction between the target cells and the activated surface can be promoted by the generation of turbulent flow patterns in the microchannels,[83,84] or by the introduction of antibody- or aptamer-coated obstacles, which effectively increases the surface-area-to-volume ratio of the microchannels.[59,85–87] As with previous biochemical capture devices, capture efficiency is very high (close to 90%) and it rapidly decreases with lower expression of the target protein. However, by increasing the interaction of the cells with the activated surface, the throughput of the system can be increased.

Approaches using antibody-coated microbeads have also been explored. The principle also relies on surface-based interactions, but here the antibodies are attached to the bead surface and dynamic mixing of the cells with the beads helps promote interaction between them.[88] However, microbead labeling of CTCs by itself is not enough to capture and isolate these rare cells. Bead-coating of CTCs is useful to amplify their size compared to the background of blood cells, which can then be used to increase the sensitivity, purity, and capture efficiency of size-based isolation techniques.[43,61,62] However, further analysis or culture of the isolated cells can be complicated by the presence of these beads. Other methods use paramagnetic particles to label the cells and then manipulate them through the use of external magnetic fields,[44,63,89,90] this is the approach used by the CellSearch system.

In general, molecular-based approaches for the isolation and capture of CTCs are very specific and can capture cells of any size (given they express the target marker), yielding a high purity capture sample, however this same characteristic makes them perform poorly when trying to capture a heterogeneous population of cancer cells, or populations of cells with unknown surface protein expression profiles. This is because most of these devices use a single capture antibody, which means that cells that don't express the target antigen will not be detected. Furthermore, recent studies have shown that many CTCs go through a phenomenon known as the epithelial-mesenchymal transition (EMT) during their detachment from the primary tumor sites.[91,92] During this transformation,

the CTCs lose the expression of epithelial markers, which means their presence will not be detected with devices using anti-EpCAM as the capture antibody. Some recent works have begun to take the EMT phenomenon into account by functionalizing magnetic beads with a panel of different antibodies,[93] trying to target a wider range of cells.

1.2.5 Hybrid methods

The previously presented methods have been shown to successfully capture CTCs with varying degrees of efficiency, however, some issues remain unsolved, heterogeneity of CTCs is not being tackled by most these methods, purity of captured samples remains low (which makes it difficult to use the captured cells for genetic or proteomic analysis) and most methods are expensive and complex to use, which makes them not suitable for translation into extended clinical applications. While trying to address these problems, some approaches have been made by combining different capture methods, like the combination of magnetic arrest followed by physical filtration.[11,94] Hydrodynamic and DEP or magnetophoretic forces have also been tested in conjunction, with enhancing effects on the flow patterns' separation of cells according to their size.[95,96] A capture efficiency of close to 99% is reported for this device in experimental conditions, the purity of the captured samples was also increased compared to the results obtained solely from the hydrodynamic-based separation of the cells. This shows that combination of different techniques to tackle the heterogeneous CTC population can have positive results both in terms of increased capture efficiency and purity.

1.3 White blood cell isolation techniques

In general, white blood cells (WBCs) can be separated by similar means as the ones presented before for rare cell capture. The use of mechanical traps,[16–19,97–100] microfluidic devices,[18,66,101–103] DEP forces,[104] and magnetic labeling,[15,101] among others, have been explored.

Depending on whether a full WBC population or only a subset of all WBCs are being targeted for capture, some different considerations must be made compared to CTC

isolation. For example, given the large abundance of WBCs ($\approx 7\times10^3$ cells/μL), techniques relying on mechanical barriers for their capture must be prepared to handle this large cell numbers without clogging, so considerations on the volume of the samples used, filtration area available, and membrane porosity are important for correct operation of these platforms.

Microfluidic devices can rely on the use of DEP or magnetic forces for selection of cells from a mixture. Depending on the desired composition of the final solution, different tags might be necessary for each different cell subpopulation. Some of the disadvantages of microfluidic devices for cell separation is the relative slow flow rate usually used in these devices (tens of μL/min). Also, when specific cells are targeted, it is commonly necessary to rely on the use of antibody-functionalized microbeads for the positive selection of these specific populations. These antigen-antibody interactions are sometimes not as strong and specific as we would hope, which can cause inadvertent loss of some of the target cells, or the capture of undesired cells as well.

The following table summarizes the advantages and limitations of the different cell isolation methods presented above:

Table 1-1 | Advantages and limitations of different cell isolation techniques.

Method	Advantages	Limitations
Microfilters	• High throughput • Customizability • Buffer exchange capability • For rare or abundant cells • Simple operation • On-filter imaging • For single or clustered cells • Stackable filtration stages	• Filter clogging • Must optimize for best results • Capture some non-target cells
Micro-gaps	• Simple operation • On-chip imaging • Buffer exchange capability	• Low throughput • Geometry constraints
Hydrodynamic	• For rare or abundant cells • High specificity • High sample purity	• Low throughput • Geometry constraints • Not good for clusters

	• Simple operation	• Complex design • Only targets cells with very specific characteristics • Can't target single and clusters at the same time
DEP	• For rare or abundant cells • High specificity • High sample purity	• Low throughput • Can't target single and clusters at the same time • Complex operation • Complex instrumentation • Only targets cells with very specific characteristics
Immunocapture	• For rare or abundant cells • For single or clustered cells • High throughput • High specificity • Customizability	• Depends on antibody specificity • Expensive reagents
Gradient centrifugation	• High throughput • Simple operation • Clinic standard	• Possible cell damage • Possible cell loss • High results variability
FACS	• High specificity • Sorts different cell populations • For rare or abundant cells	• Complex instrumentation • Complex operation • Cluster detection can be challenging

1.4 Microfilters for cell isolation

Use of microfilters for cell isolation falls into the category of the use of physical barriers for separation. Their use is particularly interesting since, by selecting the appropriate parameters like pore size, membrane area, and flow rates, they can be just as easily used for rare or abundant cell capture.

Several different microfilter fabrication methods have been developed in the past decades (Figure 1-3). Photolithography techniques from CMOS manufacturing have been adapted to produce microfilters using materials like silicon or silicon oxide.[40,44,45] Precise control on pore dimensions can be achieved with this technology, however, shortcomings like high manufacturing cost, brittleness, or optical opacity can limit their use in clinical applications. Considering these limitations, there has been a growing interest in developing

fabrication protocols for microfilters using polymers, which could provide better mechanical and optical properties at a lower cost. However, achieving production of free-standing, through-hole membranes in polymers comes with its own set of challenges.

Fabrication of polymer microfilters with controllable pore size and distribution has been explored for many purposes including selection, capture, and identification of low abundance targets in clinical applications.[105,106] In this work, a new and low-cost method for the fabrication of free-standing polymer submicro- and microfilters is presented, showing successful and reliable fabrication of very large area polymer membranes with regular distribution, high aspect ratio, and narrow size variation of the pores. The description of a novel polymer microfilter fabrication method and the subsequent characterization of these porous membranes for the capture of different populations of cells is the main purpose of this work.

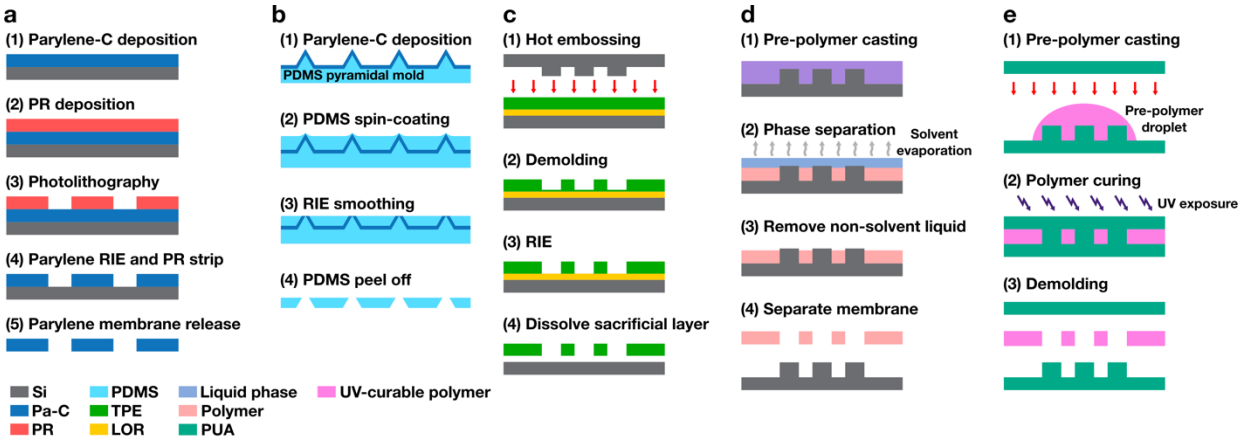

*Figure 1-3 | **Polymer membrane fabrication methods**. (a) Photolithography methods can be used to pattern polymer films to make microfilters either by using photoresists (PR) as masks for reactive ion etching (RIE) patterning of an underlying polymer, or for direct patterning of UV-curable materials, like SU-8. (b) In polymer casting methods, liquid pre-polymers are deposited on top of microstructured molds via spin-coating, by a subsequent RIE smoothing step, through hole structures can be achieved in a polymer membrane. (c) Microstructured metal or silicon molds can be used as stamps to replicate patterns onto thermoplastic elastomers (TPE) by hot embossing, RIE must be used to remove thin residual layers to achieve through hole structures on the polymer film before their release from the substrate. (d) Similar to polymer casting, phase separation methods begin with casting of a pre-polymer solution onto a microstructured mold, a phase separation is induced by polymerization of one or more, but not all of the components of a mixture and evaporation of solvents, usually leaving a solidified polymer separated from a liquid phase. (e) Mold-based dewetting relies on the use of highly hydrophilic (or hydrophobic) molds and covers, and hydrophobic (or hydrophilic) UV-curable pre-polymer solutions that*

are sandwiched between the cover and the mold before crosslinking, the wettability difference between the mold and the pre-polymer avoid the appearance of residual layers within the micropores.

Production of freestanding, isoporous (with high density through-holes), residual-layer-free polymer membranes with good replication fidelity and membrane integrity is challenging. Many different methods for the fabrication of such polymer membranes have been explored in the literature, including techniques such as polymer casting,[107–109] hot embossing or nanoimprint lithography (NIL),[49–51,110,111] photolithography,[41,112] phase separation microfabrication,[52,53,113] and more recently, mold-based dewetting,[114] have been explored for this purpose. Successful proof-of concept demonstrations have been achieved using these techniques, however, the involved processes present some limitations, especially in terms of the complexity involved, auto-fluorescence of the materials used, low maximum porosity values achievable, and cost. The advantages and limitations of these methods will be discussed in the following sections.

1.4.1 Photolithography

The development of the semiconductor integrated circuits (ICs) brought about the standardization of photolithography protocols, which allowed the precise patterning of microfeatures onto photoresistive materials and the transfer of these patterns onto metal and semiconductor layers. For IC fabrication, polymers usually only play a transient role in the form of photoresists that can be patterned to mask underlying layers during etching steps, however, with the onset of the micro-electro-mechanical-systems (MEMS) field, standard photolithography protocols have been adapted to include polymers as functional layers in microfabricated devices.

Chemical vapor deposited (CVD) polymers like Parylene are usually used as moisture and dielectric barriers, they can also be etched by reactive ion etching (RIE), which makes them compatible with standard photolithography processes. Some examples of the use of Parylene-C, combined with sacrificial and etch mask layers, have shown that the fabrication of membranes with through-hole structures is possible using standard photolithography equipment and materials.[35,41,115,116] Furthermore, Parylene-C has several

properties that make it interesting for use in the processing of biological samples: it's highly biocompatible, has low bio-fouling, excellent mechanical properties (strong but flexible), it's a good isolating material for electronic-compatible applications, and it's transparent in the UV and visible ranges.[35] Photolithographic processes allow for the fabrication of Parylene-C microfilters with precise control of the filter pore size and height, however, some important limitations can be observed: first, there are no reusable layers in these processes, which means that every time a new batch of membranes has to be fabricated, the whole process must be performed; second, Parylene-C cannot be patterned directly with UV light, which makes the use of extra patterned layers necessary for transferring the desired patterns onto the Parylene, making the process more complex as several steps of CVD, patterning, and etching are required to achieve the end-result; third, CVD deposition of Parylene allows for precise control of the height of the deposited layer, however, CVD processes were developed to deposit relatively thin layers (< 10 µm), which limits the maximum thickness achievable for the microfilters; finally, even though the material is transparent, its autofluorescence can be an obstacle for its use in applications requiring fluorescence imaging.[117]

Another alternative in photolithography-based polymer microfilter fabrication presented in the literature is the use of photoresist materials like SU-8 as the building material for the polymer membranes. Since SU-8 is a photoresist, patterns in a photomask can be transferred directly without the need of the deposition, patterning, and etching of extra layers. An intriguing application uses a special optical setup to create interference patterns that create regular arrays of features onto an SU-8 substrate,[112] this removes the need of photomasks, but it's limited by the need of special optical components, which in turn limits the variety of features that can be created by interference holography. Also, the thickness range for the final membranes is constrained by light dispersion effects, and SU-8 has autofluorescence problems like Parylene-C.

Photolithography technologies are well established, and very precise features can be replicated onto polymers by using these techniques, however, there are some important limitations like the variety of materials that can be used, the necessity of having access to a mask aligner and other clean room equipment, complex processes with several steps of material deposition and etching, or costly modifications to the optical path of a standard aligner.

1.4.2 Polymer casting

Pre-polymer liquid solutions can be thermally or UV-crosslinked, which allows the replication of structures from a solid mold structure, the principle behind the soft lithography process of replicating features using polydimethylsiloxane (PDMS), a thermally-cured silicone material very commonly used for the fabrication of microfluidic chips.

During PDMS replication, fabrication of through hole structures is possible through a combination of spin-coating of thin PDMS onto protruding structures in the underlying mold, and the use of a gas stream.[118] The process is simple and can be performed in most laboratories without the need of very specialized equipment. However, it is a slow and labor-intensive protocol that yields very limited range of the hole size. In addition, ensuring open structures in the micrometer range in PDMS is very difficult, it would require very precise control on the thickness of the spin-coated layer as well as of the speed of the gas stream used to uncover the protruding features.

Another alternative in terms of polymer casting is to use a combination of casting onto pointy microstructures, like pyramids, and then using a plasma etching process to etch away a thin section of the top surface of the casted polymer as well as part of the pyramids' apices, creating through-hole structures in the casted polymer.[107] Contrary to the previously mentioned method, arrays of micropores can be created using this process, however, precise control on the thickness of the casted polymer layer is necessary and the pore size can vary in relation to the plasma etching process, which may affect

reproducibility of the process. Additionally, single-use sacrificial PDMS molds are used which take several hours to prepare, and the need of a high-power plasma etching machine means a process like this can be hardly transferred outside of a clean room facility or specialized lab.

Another creative approach relies on the use of droplet arrays, printed with an inkjet printer, as the mold from which a polymer porous membrane can be casted.[109] By not requiring a solid mold, detaching the final membrane can be done by a simple peel-off process, however, precise control on the size of the pores is difficult, since it is related to the height of the casted polymer layer, the size of the printed droplets, and evaporation effects. The shape of the fabricated pores will always be a truncated hemisphere, which can be advantageous for certain applications, but might not be optimal for others, limiting the applicability of these type of polymer microfilters.

1.4.3 Nanoimprint lithography (NIL)

Also known as hot embossing, NIL is a process by which, a pattern from a master mold is transferred onto a substrate by means of pressurized contact between the two, often involving heat, when the substrate is a thermoplastic material. NIL is a low cost, high throughput, and high resolution method, but it does require a significant initial investment, especially when precise control of all variables involved is needed.

Patterning features even in the nanometer range is possible by NIL, however, obtaining through hole structures is not straightforward with this technique, an issue usually encountered when trying to replicate micro-holes is the presence of a residual layer covering the pores,[50,110] which must be then removed through an extra etching step, usually by reactive ion etching, with the etch time depending on the thickness of the residual layer.

By using more complex molds, with extra sacrificial layers, it's possible to obtain through hole structures directly from a hot embossing process, but the range of pore sizes achievable is limited, and there's an added complexity in the assembly of the molds

used,[49,111] the added intricacies require the use of more precise machines, and also makes the translation of the method into a mass production system more troublesome.

In a similar fashion, it has been proposed to use microneedle arrays to punch holes through thin polymer films, thus creating microporous membranes with regularly distributed pores.[51] However, microneedle fabrication is itself a complex problem, the size and density of the needles that can be made is limited, the size of the array is also constrained by the complexity of the fabrication method. In addition, there is also a high probability of breaking the needles when punching through a film, and the edge of the needles will become blunt with use. All these make the process unviable for mass production of polymer microporous membranes.

In general, the use of NIL for microfilter fabrication is a possibility, however, it is limited in terms of the size, density, and aspect ratio of the pores that can be produced due to the nature of the method. Furthermore, the need of extra sacrificial layers or etching steps to ensure that pores are open-through adds to the complexity and cost of the process, which makes it hard to be translated to most facilities or adapted for mass production.

1.4.4 Phase separation micromolding

Phase separation micromolding (PSμM)[53] is based on the principle of polymerization induced phase separation (PIPS) to obtain microstructured polymer replicas by casting a thin polymer film on a master mold. PIPS occurs when a phase separation is induced by polymerization of one or more, but not all of the components of a mixture, usually leaving a solidified part separated from a liquid phase not forming part of the polymer.

PSμM is usually done in two phase separation steps, a vapor-induced (VIPS), and a liquid-induced phase separation (LIPS). The first one is related to a vertical or thickness shrinkage, which results in perforation of the polymer film by the mold microstructures to ensure open holes to be obtained. Lateral shrinking during the LIPS allows loosening of the polymer from the mold. To ensure that the final microstructures are indeed open-

though pores when using PSµM, it is necessary to have precise control on the thickness of the casted pre-polymer solution, the composition of the solution, moisture levels, and temperature during the VIPS. Replication of polymer microsieves from a silicon mold can be done in approximately four to five hours, however, the necessary preparation and post processing steps are performed overnight, making the whole process a $>$ 24 h endeavor. Thorough cleaning of the master silicon molds is necessary between each fabrication replicate, and using the master mold for every replication increases the chances of damaging it, probably requiring fabrication of silicon molds on a regular basis.

While consistent open micropore structures can be obtained by PSµM, due to the shrinking stages, the thickness or the shape and size of the final through-hole structures is harder to replicate consistently. Another characteristic of this process is that the polymerized material has an intrinsic porous structure, due to the nature of the phase separation method.[52,53,113] Depending on the intended application, the porous structure of the polymer might be an advantage or a disadvantage. For biological applications, such as size-based cell separation, cells might adhere more strongly to porous materials, causing non-specific attachment of cells on the filter surface for example.

Finally, the polymers usually used for PSµM are not thermally stable, with glass transition temperatures of approximately 150° C. The fabricated membranes can be heated to densify their structure, reducing the intrinsic porosity. Thermal treatment can also be used to reduce the size of the replicated micropores, however this also results in deformation of the original shape of the holes. This makes the use of these membranes in high temperature applications not recommended, which is usually not a problem for biological purposes, however integration of membranes onto monolithic chips sometimes requires their embedding through hot embossing, which would not be possible with these PSµM microsieves.

1.4.5 Mold-based dewetting

This process[114] is the one that more closely resembles the fabrication method we propose in this work, both in approach and materials used, as it also relies on the use of UV-curable polymers, typically perfluoropolyether (PFPE), for the fabrication of nano- and microporous polymer membranes. Mold-based dewetting relies on the spontaneous dewetting of a hydrophobic resin against a hydrophilic mold, or vice versa to ensure the fabricated membranes are residual layer free.

The method works by placing a droplet of a UV-curable pre-polymer on a microstructured mold, and sandwiching it with a flat or nanostructured cover to spread the pre-polymer along the whole area of the mold. The large difference in wettability between the resin and the mold material is needed to ensure that the nano- and microstructures are open-through. Mold filling and membrane curing can be done in a matter of minutes, and this process has the advantage of being compatible with high viscosity resins, as long as the wettability difference requirement is achieved.

Membranes with an area as large as 2×2 cm^2 and with features as small as 50 nm are possible by mold-based dewetting. However, this technique still has some limitations, for instance, the trapping of air bubbles between the mold features during the droplet spreading often results in defects on the membrane area; other defects can be caused by damage caused to the mold structures due to the pressing needed to bring the cover and underlying mold in contact during the filling and curing steps of the process; demolding is done manually, which can produce tears; finally, local wettability variations can result in pore shape deformations, especially noticeable for the smallest structures.

Our proposed fabrication method also uses a PFPE material for the membrane production, while addressing some of the shortcomings of mold-based dewetting. First, we employ vacuum assisted mold filling, which eliminates the possibility of trapping air bubbles between the mold structures, the defects caused by local wettability differences, and removes the need of applying a pressing force during filling and curing. We also

propose a solvent bath self-demolding protocol to avoid membrane tearing. This approach has allowed us to successfully fabricate microporous membranes having an area as large as 9×9 cm^2, and pore diameter as small as 500 nm.

The following table summarizes the advantages and limitations of the different polymer microfilter fabrication methods presented above, as well as for the method presented in this work (explained in detail in Chapter 3):

Table 1-2 | Advantages and limitations of different polymer microfilter fabrication techniques.

Method	Advantages	Limitations
VAUM (this work)	• Precise pore size control • Self-demolding • Large-area membranes • High porosity membranes • Pore size range (≥ 0.5 µm) • Low autofluorescence • Not cytotoxic • Optically transparent • No bubble trapping during mold filling • Can have complex pore shapes	• Manual process • Need of a disposable PDMS mold • Sensitive to UV lamp power changes
Photolithography	• Precise pore size control • High porosity membranes • Optically transparent	• Requires complex equipment • Complex process • Autofluorescent membranes
Polymer casting	• Simple process	• Mechanical peel-off • High fabrication variability • Requires very precise control of fabrication parameters
NIL	• Fast process • Mass-production compatible	• Residual layers must be etched away • High chance of master mold breaking
Phase separation	• Direct replication from a Si master mold	• Long process (> 24h) • Requires very precise control of fabrication parameters in every step • Membrane materials have intrinsic porosity

		• Not thermally stable (harder to integrate in a chip)
Mold-based dewetting	• Precise pore size control • High porosity membranes • Pore size range (≥ 0.05 µm) • Low autofluorescence • Not cytotoxic • Optically transparent	• Manual process • Sensitive to UV lamp power changes • Mechanical peel-off • Possible bubble trapping during mold filling

1.5 Conclusions

Polymer microfilters with precise pore size control and regular pore distribution have many different applications in biology, however, commercially available polymer membranes do not have the optimal porosity values or pore distribution necessary for taking full advantage of their use, especially for applications related to cell isolation. Different alternatives have been proposed in the literature for the fabrication of polymer microfilters, however these solutions often come with limitations which prevents their adoption in real-world applications. Our proposed solution has considerable advantages over previously developed methods, in terms of cost, reproducibility, and reliability of the process. Namely, we don't require the use of photolithography equipment every time a new membrane is to be fabricated; our method is more flexible in terms of pore size, shape, maximum porosity, membrane thickness and size, the fabricated membranes are optically transparent, and have low autofluorescence. In addition, we have successfully, reliably, and repeatedly fabricated polymer microfilters with the highest pore aspect ratio reported to date and the largest overall membrane extents.

In a similar way, cell isolation has been explored using a variety of techniques, each with its own set of advantages and limitations. We believe that the use of microfilters with high porosity allows for a faster throughput and analysis of biological samples, which is a critical factor when looking for CTCs, as it is known that these cells remain viable for less than 24 hours in circulation. As such, if downstream analysis of the CTCs is desired, it's important to process the samples as fast as possible, since it is impossible to

determine how long they've been in circulation by the time a blood sample is acquired. Microfilters also have the advantage of allowing buffer exchange on-chip while retaining the captured cells on the membrane, which permits sequential staining and washing of the cells in a gentle manner and without the need of sample centrifugation, commonly associated with cell loss and damage.

As will be presented in the following chapters, we successfully used these new polymer membranes for the separation of a mixture of microbead populations, isolation of CTCs from blood samples, capture and release of full WBC populations, and multi-step cell staining. We have also demonstrated the versatility of these membranes through their use as masks for specific patterning of a plastic substrate surfaces.[119] This shows that although our original motivation was to use the fabricated polymer membranes for cell isolation, they can be used in a variety of other applications, thus enlarging our contributions to the field.

References

1. G.-H. Lee, S.-H. Kim, K. Ahn, S.-H. Lee and J. Y. Park, *J. Micromechanics Microengineering*, 2016, **26**, 013003.

2. Z. Shen, A. Wu and X. Chen, *Chem. Soc. Rev.*, 2017, **46**, 2038–2056.

3. Canadian Cancer Society's Advisory Committee on Cancer Statistics, 2013.

4. O. M. Ginsburg, T. P. Hanna, T. Vandenberg, A. A. Joy, M. Clemons, M. Game, R. MacCormick, L. M. Elit, B. Rosen, Y. Rahim, W. Geddie, S. B. Sutcliffe and M. Gospodarowicz, *Can. Med. Assoc. J.*, 2012, **184**, 1699–1704.

5. C. Criscitiello, C. Sotiriou and M. Ignatiadis, *Curr. Opin. Oncol. Novemb. 2010*, 2010, **22**, 552–558.

6. B. P. Negin and S. J. Cohen, *Curr. Treat. Options Oncol.*, 2010, **11**, 1–13.

7. M. J. S. Fernández, J. C. Á. Merino, I. M. Zubiaurre, A. F. García, P. S. Rovira and J. A. L. Acosta, *Clin. Transl. Oncol.*, 2009, **11**, 659–668.

8. Y. Dong, A. M. Skelley, K. D. Merdek, K. M. Sprott, C. Jiang, W. E. Pierceall, J. Lin, M. Stocum, W. P. Carney and D. A. Smirnov, *J. Mol. Diagn.*, 2013, **15**, 149–157.

9. M. Yu, S. Stott, M. Toner, S. Maheswaran and D. A. Haber, *J. Cell Biol.*, 2011, **192**, 373–382.

10. N. Gerges, J. Rak and N. Jabado, *Br. Med. Bull.*, 2010, **94**, 49–64.

11. Y.-K. Chung, J. Reboud, K. C. Lee, H. M. Lim, P. Y. Lim, K. Y. Wang, K. C. Tang, H. Ji and Y. Chen, *Biosens. Bioelectron.*, 2011, **26**, 2520–2526.

12. K. F. Ho, N. E. Gouw and Z. Gao, *TrAC Trends Anal. Chem.*, 2015, **64**, 173–182.

13. N. Yu, J. Zhou, F. Cui and X. Tang, *Lung*, 2015, **193**, 157–171.

14. P. K. Dagur and J. P. McCoy, *Curr. Protoc. Cytom. Editor. Board J Paul Robinson Manag. Ed. Al*, 2015, **73**, 5.1.1-5.1.16.

15. C. Iliescu, G. Xu, E. Barbarini, M. Avram and A. Avram, *Microsyst. Technol.*, 2009, **15**, 1157–1162.

16. H. M. Ji, V. Samper, Y. Chen, C. K. Heng, T. M. Lim and L. Yobas, *Biomed. Microdevices*, 2008, **10**, 251–257.

17. X. Chen, D. F. Cui, C. C. Liu and H. Li, *Sens. Actuators B Chem.*, 2008, **130**, 216–221.

18. Y. Cheng, X. Ye, Z. Ma, S. Xie and W. Wang, *Biomicrofluidics*, 2017, **11**.

19. V. VanDelinder and A. Groisman, *Anal. Chem.*, 2007, **79**, 2023–2030.

20. UNIAIDS, 2016.

21. X. Cheng, A. Gupta, C. Chen, R. G. Tompkins, W. Rodriguez and M. Toner, *Lab. Chip*, 2009, **9**, 1357–1364.

22. M. T. Glynn, D. J. Kinahan and J. Ducrée, *Lab. Chip*, 2013, **13**, 2731–2748.

23. W. G. Lee, Y.-G. Kim, B. G. Chung, U. Demirci and A. Khademhosseini, *Adv. Drug Deliv. Rev.*, 2010, **62**, 449–457.

24. Government of Canada, *Global AIDS Response*, 2016.

25. Attard and J. S. de Bono, *Curr. Opin. Genet. Dev.*, 2011, **21**, 50–58.

26. K.-A. Hyun, J. Kim, H. Gwak and H.-I. Jung, *Analyst*, 2016, **141**, 382–392.

27. S. K. Arya, B. Lim and A. R. A. Rahman, *Lab. Chip*, 2013, **13**, 1995–2027.

28. P. Patil, Madhuprasad, T. Kumeria, D. Losic and M. Kurkuri, *RSC Adv.*, 2015, **5**, 89745–89762.

29. R. L. Fleischer, P. B. Price and E. M. Symes, *Science*, 1964, **143**, 249–250.

30. S. H. Seal, *Cancer*, 1964, **17**, 637–642.

31. T. G. Ntouroupi, S. Q. Ashraf, S. B. McGregor, B. W. Turney, A. Seppo, Y. Kim, X. Wang, M. W. Kilpatrick, P. Tsipouras, T. Tafas and W. F. Bodmer, *Br. J. Cancer*, 2008, **99**, 789–795.

32. G. Vona, A. Sabile, M. Louha, V. Sitruk, S. Romana, K. Schütze, F. Capron, D. Franco, M. Pazzagli, M. Vekemans, B. Lacour, C. Bréchot and P. Paterlini-Bréchot, *Am. J. Pathol.*, 2000, **156**, 57–63.

33. L. Zabaglo, M. G. Ormerod, M. Parton, A. Ring, I. E. Smith and M. Dowsett, *Cytometry A*, 2003, **55A**, 102–108.

34. V. De Giorgi, P. Pinzani, F. Salvianti, J. Panelos, M. Paglierani, A. Janowska, M. Grazzini, J. Wechsler, C. Orlando, M. Santucci, T. Lotti, M. Pazzagli and D. Massi, *J. Invest. Dermatol.*, 2010, **130**, 2440–2447.

35. S. Zheng, H. Lin, J.-Q. Liu, M. Balic, R. Datar, R. J. Cote and Y.-C. Tai, *J. Chromatogr. A*, 2007, **1162**, 154–161.

36. T.-H. Kim, M. Lim, J. Park, J. M. Oh, H. Kim, H. Jeong, S. J. Lee, H. C. Park, S. Jung, B. C. Kim, K. Lee, M.-H. Kim, D. Y. Park, G. H. Kim and Y.-K. Cho, *Anal. Chem.*, 2017, **89**, 1155–1162.

37. D. Chudasama, J. Barr, J. Beeson, E. Beddow, N. Mcgonigle, A. Rice, A. Nicholson and V. Anikin, *Anticancer Res.*, 2017, **37**, 169–173.

38. J. Kuvendjiska, P. Bronsert, V. Martini, S. Lang, M. B. Pitman, J. Hoeppner and B. Kulemann, *Cancers*, 2019, **11(3)**, 397.

39. I. Desitter, B. S. Guerrouahen, N. Benali-Furet, J. Wechsler, P. A. Jänne, Y. Kuang, M. Yanagita, L. Wang, J. A. Berkowitz, R. J. Distel and Y. E. Cayre, *Anticancer Res.*, 2011, **31**, 427–441.

40. L. S. Lim, M. Hu, M. C. Huang, W. C. Cheong, A. T. L. Gan, X. L. Looi, S. M. Leong, E. S.-C. Koay and M.-H. Li, *Lab. Chip*, 2012, **12**, 4388–4396.

41. T. Xu, B. Lu, Y.-C. Tai and A. Goldkorn, *Cancer Res.*, 2010, **70**, 6420–6426.

42. J.-M. Park, J.-Y. Lee, J.-G. Lee, H. Jeong, J.-M. Oh, Y. J. Kim, D. Park, M. S. Kim, H. J. Lee, J. H. Oh, S. S. Lee, W.-Y. Lee and N. Huh, *Anal. Chem.*, 2012, **84**, 7400–7407.

43. H. J. Lee, J. H. Oh, J. M. Oh, J.-M. Park, J.-G. Lee, M. S. Kim, Y. J. Kim, H. J. Kang, J. Jeong, S. I. Kim, S. S. Lee, J.-W. Choi and N. Huh, *Angew. Chem. Int. Ed.*, 2013, **52**, 8337–8340.

44. C. M. Earhart, C. E. Hughes, R. S. Gaster, C. C. Ooi, R. J. Wilson, L. Y. Zhou, E. W. Humke, L. Xu, D. J. Wong, S. B. Willingham, E. J. Schwartz, I. L. Weissman, S. S. Jeffrey, J. W. Neal, R. Rohatgi, H. A. Wakelee and S. X. Wang, *Lab. Chip*, 2013, **14**, 78–88.

45. Y. Koh, H. Kang, S. H. Lee, J.-K. Yang, J.-H. Kim, Y.-S. Lee and Y.-K. Kim, *Lab. Chip*, 2013, **14**, 237–243.

46. M. Hosokawa, T. Yoshikawa, R. Negishi, T. Yoshino, Y. Koh, H. Kenmotsu, T. Naito, T. Takahashi, N. Yamamoto, Y. Kikuhara, H. Kanbara, T. Tanaka, K. Yamaguchi and T. Matsunaga, *Anal. Chem.*, 2013, **85**, 5692–5698.

47. M. Hosokawa, T. Hayata, Y. Fukuda, A. Arakaki, T. Yoshino, T. Tanaka and T. Matsunaga, *Anal. Chem.*, 2010, **82**, 6629–6635.

48. E. H. Kim, J. K. Lee, B. C. Kim, S. H. Rhim, J. W. Kim, K. H. Kim, S. M. Jung, P. S. Park, H. C. Park, J. Lee and B. H. Jeon, *Anal. Biochem.*, 2013, **440**, 114–116.

49. J. Chou, N. Du, T. Ou, P. N. Floriano, N. Christodoulides and J. T. McDevitt, *Biosens. Bioelectron.*, 2013, **42**, 653–660.

50. H. Schift, S. Bellini and J. Gobrecht, *Microelectron. Eng.*, 2006, **83**, 873–875.

51. T. Shibata, S. Yukizono, T. Kawashima, M. Nagai, T. Kubota and M. Mita, *Microelectron. Eng.*, 2011, **88**, 2121–2125.

52. M. Bikel, P. Z. Çulfaz, L. A. M. Bolhuis-Versteeg, J. G. Pérez, R. G. H. Lammertink and M. Wessling, *J. Membr. Sci.*, 2010, **347**, 93–100.

53. M. Gironès, I. J. Akbarsyah, W. Nijdam, C. J. M. van Rijn, H. V. Jansen, R. G. H. Lammertink and M. Wessling, *J. Membr. Sci.*, 2006, **283**, 411–424.

54. R. A. Harouaka, M. Nisic and S.-Y. Zheng, *J. Lab. Autom.*, 2013, **18(6)**, 455–468.

55. S. J. Tan, L. Yobas, G. Y. H. Lee, C. N. Ong and C. T. Lim, *Biomed. Microdevices*, 2009, **11**, 883–892.

56. W. Sun, C. Jia, T. Huang, W. Sheng, G. Li, H. Zhang, F. Jing, Q. Jin, J. Zhao, G. Li and Z. Zhang, *PLoS ONE*, 2013, **8(9)**.

57. H. Mohamed, M. Murray, J. N. Turner and M. Caggana, *J. Chromatogr. A*, 2009, **1216**, 8289–8295.

58. J. S. Kuo, Y. Zhao, P. G. Schiro, L. Ng, D. S. W. Lim, J. P. Shelby and D. T. Chiu, *Lab. Chip*, 2010, **10**, 837–842.

59. S. Nagrath, L. V. Sequist, S. Maheswaran, D. W. Bell, D. Irimia, L. Ulkus, M. R. Smith, E. L. Kwak, S. Digumarthy, A. Muzikansky, P. Ryan, U. J. Balis, R. G. Tompkins, D. A. Haber and M. Toner, *Nature*, 2007, **450**, 1235–1239.

60. A. F. Sarioglu, N. Aceto, N. Kojic, M. C. Donaldson, M. Zeinali, B. Hamza, A. Engstrom, H. Zhu, T. K. Sundaresan, D. T. Miyamoto, X. Luo, A. Bardia, B. S. Wittner, S. Ramaswamy, T. Shioda, D. T. Ting, S. L. Stott, R. Kapur, S. Maheswaran, D. A. Haber and M. Toner, *Nat. Methods*, 2015, **12**, 685–691.

61. M. S. Kim, T. S. Sim, Y. J. Kim, S. S. Kim, H. Jeong, J.-M. Park, H.-S. Moon, S. I. Kim, O. Gurel, S. S. Lee, J.-G. Lee and J. C. Park, *Lab. Chip*, 2012, **12**, 2874–2880.

62. M. S. Kim, J. Kim, W. Lee, S.-J. Cho, J.-M. Oh, J.-Y. Lee, S. Baek, Y. J. Kim, T. S. Sim, H. J. Lee, G.-E. Jung, S.-I. Kim, J.-M. Park, J. H. Oh, O. Gurel, S. S. Lee and J.-G. Lee, *Small*, 2013, **9**, 3005–3005.

63. B. P. Casavant, R. Mosher, J. W. Warrick, L. J. Maccoux, S. M. F. Berry, J. T. Becker, V. Chen, J. M. Lang, D. G. McNeel and D. J. Beebe, *Methods*, 2013, **64**, 137–143.

64. T. Huang, C.-P. Jia, Jun-Yang, W.-J. Sun, W.-T. Wang, H.-L. Zhang, H. Cong, F.-X. Jing, H.-J. Mao, Q.-H. Jin, Z. Zhang, Y.-J. Chen, G. Li, G.-X. Mao and J.-L. Zhao, *Biosens. Bioelectron.*, 2014, **51**, 213–218.

65. X. Qin, S. Park, S. P. Duffy, K. Matthews, R. R. Ang, T. Todenhöfer, H. Abdi, A. Azad, J. Bazov, K. N. Chi, P. C. Black and H. Ma, *Lab. Chip*, 2015, **15**, 2278–2286.

66. A. A. S. Bhagat, H. W. Hou, L. D. Li, C. T. Lim and J. Han, *Lab. Chip*, 2011, **11**, 1870–1878.

67. K.-A. Hyun, K. Kwon, H. Han, S.-I. Kim and H.-I. Jung, *Biosens. Bioelectron.*, 2013, **40**, 206–212.

68. J. M. Martel, K. C. Smith, M. Dlamini, K. Pletcher, J. Yang, M. Karabacak, D. A. Haber, R. Kapur and M. Toner, *Sci. Rep.*, 2015, **5**, 11300.

69. J. Che, V. Yu, E. B. Garon, J. W. Goldman and D. D. Carlo, *Lab. Chip*, 2017, **17**, 1452–1461.

70. H. W. Hou, M. E. Warkiani, B. L. Khoo, Z. R. Li, R. A. Soo, D. S.-W. Tan, W.-T. Lim, J. Han, A. A. S. Bhagat and C. T. Lim, *Sci. Rep.*, 2013, **3**, 1259.

71. M. E. Warkiani, G. Guan, K. B. Luan, W. C. Lee, A. A. S. Bhagat, P. K. Chaudhuri, D. S.-W. Tan, W. T. Lim, S. C. Lee, P. C. Y. Chen, C. T. Lim and J. Han, *Lab. Chip*, 2013, **14**, 128–137.

72. M. E. Warkiani, A. K. P. Tay, G. Guan and J. Han, *Sci. Rep.*, 2015, **5**, 11018.

73. J. Sun, M. Li, C. Liu, Y. Zhang, D. Liu, W. Liu, G. Hu and X. Jiang, *Lab. Chip*, 2012, **12**, 3952–3960.

74. E. Sollier, D. E. Go, J. Che, D. R. Gossett, S. O'Byrne, W. M. Weaver, N. Kummer, M. Rettig, J. Goldman, N. Nickols, S. McCloskey, R. P. Kulkarni and D. D. Carlo, *Lab. Chip*, 2013, **14**, 63–77.

75. J. Yang, Y. Huang, X.-B. Wang, F. F. Becker and P. R. C. Gascoyne, *Anal. Chem.*, 1999, **71**, 911–918.

76. P. R. C. Gascoyne, J. Noshari, T. J. Anderson and F. F. Becker, *ELECTROPHORESIS*, 2009, **30**, 1388–1398.

77. A. Alazzam, I. Stiharu, R. Bhat and A.-N. Meguerditchian, *ELECTROPHORESIS*, 2011, **32**, 1327–1336.

78. M. Aghaamoo, A. Aghilinejad, X. Chen and J. Xu, *ELECTROPHORESIS*, 2019, **40**, 1486–1493.

79. N.-V. Nguyen and C.-P. Jen, *Biosens. Bioelectron.*, 2018, **121**, 10–18.

80. F. Fabbri, S. Carloni, W. Zoli, P. Ulivi, G. Gallerani, P. Fici, E. Chiadini, A. Passardi, G. L. Frassineti, A. Ragazzini and D. Amadori, *Cancer Lett.*, 2013, **335**, 225–231.

81. National Cancer Institute, *Cancer Classification*, 2019.

82. Y.-S. Hsiao, S.-C. Luo, S. Hou, B. Zhu, J. Sekine, C.-W. Kuo, D.-Y. Chueh, H. Yu, H.-R. Tseng and P. Chen, *Small*, 2014, **10**, 3012.

83. S. L. Stott, C.-H. Hsu, D. I. Tsukrov, M. Yu, D. T. Miyamoto, B. A. Waltman, S. M. Rothenberg, A. M. Shah, M. E. Smas, G. K. Korir, F. P. Floyd, A. J. Gilman, J. B. Lord, D. Winokur, S. Springer, D. Irimia, S. Nagrath, L. V. Sequist, R. J. Lee, K. J. Isselbacher, S. Maheswaran, D. A. Haber and M. Toner, *Proc. Natl. Acad. Sci.*, 2010, **107**, 18392–18397.

84. W. Sheng, O. O. Ogunwobi, T. Chen, J. Zhang, T. J. George, C. Liu and Z. H. Fan, *Lab. Chip*, 2013, **14**, 89–98.

85. G. Galletti, M. S. Sung, L. T. Vahdat, M. A. Shah, S. M. Santana, G. Altavilla, B. J. Kirby and P. Giannakakou, *Lab. Chip*, 2013, **14**, 147–156.

86. Z. Wang, D. Xu, X. Wang, Y. Jin, B. Huo, Y. Wang, C. He, X. Fu and N. Lu, *Nanoscale*, 2019, **11**, 6677–6684.

87. Y. Zhao, D. Xu and W. Tan, *Integr. Biol.*, 2017, **9**, 188–205.

88. M. X. Lin, K.-A. Hyun, H.-S. Moon, T. S. Sim, J.-G. Lee, J. C. Park, S. S. Lee and H.-I. Jung, *Biosens. Bioelectron.*, 2013, **40**, 63–67.

89. J. Ko, N. Bhagwat, S. S. Yee, T. Black, C. Redlinger, J. Romeo, M. O'Hara, A. Raj, E. L. Carpenter, B. Z. Stanger and D. Issadore, *Lab. Chip*, 2017, **17**, 3086–3096.

90. W. Zhao, Y. Liu, B. D. Jenkins, R. Cheng, B. N. Harris, W. Zhang, J. Xie, J. R. Murrow, J. Hodgson, M. Egan, A. Bankey, P. G. Nikolinakos, H. Y. Ali, K. Meichner, L. A. Newman, M. B. Davis and L. Mao, *Lab. Chip*, 2019, **19**, 1860–1876.

91. H. Liu, X. Zhang, J. Li, B. Sun, H. Qian and Z. Yin, *J. Cancer Res. Clin. Oncol.*, 2014, **141**, 189–201.

92. M. Yu, A. Bardia, B. S. Wittner, S. L. Stott, M. E. Smas, D. T. Ting, S. J. Isakoff, J. C. Ciciliano, M. N. Wells, A. M. Shah, K. F. Concannon, M. C. Donaldson, L. V.

Sequist, E. Brachtel, D. Sgroi, J. Baselga, S. Ramaswamy, M. Toner, D. A. Haber and S. Maheswaran, *Science*, 2013, **339**, 580–584.

93. N.-N. Lu, M. Xie, J. Wang, S.-W. Lv, J.-S. Yi, W.-G. Dong and W.-H. Huang, *ACS Appl. Mater. Interfaces*, 2015, **7**, 8817–8826.

94. B. P. Casavant, L. N. Strotman, J. J. Tokar, S. M. Thiede, A. M. Traynor, J. S. Ferguson, J. M. Lang and D. J. Beebe, *Lab. Chip*, 2013, **14**, 99–105.

95. H.-S. Moon, K. Kwon, S.-I. Kim, H. Han, J. Sohn, S. Lee and H.-I. Jung, *Lab. Chip*, 2011, **11**, 1118–1125.

96. N. M. Karabacak, P. S. Spuhler, F. Fachin, E. J. Lim, V. Pai, E. Ozkumur, J. M. Martel, N. Kojic, K. Smith, P. Chen, J. Yang, H. Hwang, B. Morgan, J. Trautwein, T. A. Barber, S. L. Stott, S. Maheswaran, R. Kapur, D. A. Haber and M. Toner, *Nat. Protoc.*, 2014, **9**, 694–710.

97. D.-H. Lee, X. Li, N. Ma, M. A. Digman and A. P. Lee, *Lab. Chip*, 2018, **18**, 1349–1358.

98. D. Okuzaki, S. Kimura, N. Yabuta, T. Ohmine and H. Nojima, *BMC Clin. Pathol.*, 2011, **11**, 9.

99. N. J. Panaro, X. J. Lou, P. Fortina, L. J. Kricka and P. Wilding, *Biomol. Eng.*, 2005, **21**, 157–162.

100. H. Wei, in *Studying Cell Metabolism and Cell Interactions Using Microfluidic Devices Coupled with Mass Spectrometry*, ed. H. Wei, Springer Berlin Heidelberg, Berlin, Heidelberg, 2013, pp. 61–82.

101. E. Ozkumur, A. M. Shah, J. C. Ciciliano, B. L. Emmink, D. T. Miyamoto, E. Brachtel, M. Yu, P. Chen, B. Morgan, J. Trautwein, A. Kimura, S. Sengupta, S. L. Stott, N. M. Karabacak, T. A. Barber, J. R. Walsh, K. Smith, P. S. Spuhler, J. P. Sullivan, R. J. Lee, D. T. Ting, X. Luo, A. T. Shaw, A. Bardia, L. V. Sequist, D. N. Louis, S. Maheswaran, R. Kapur, D. A. Haber and M. Toner, *Sci. Transl. Med.*, 2013, **5**.

102. J. K. S. Tan, S. Park, H. L. Leo and S. Kim, *IEEE Trans. Biomed. Circuits Syst.*, 2017, **11**, 1431–1437.

103. U. Hassan, T. Ghonge, B. R. Jr, M. Patel, M. Rappleye, I. Taneja, A. Tanna, R. Healey, N. Manusry, Z. Price, T. Jensen, J. Berger, A. Hasnain, E. Flaugher, S. Liu, B. Davis, J. Kumar, K. White and R. Bashir, *Nat. Commun.*, 2017, **8**, 15949.

104. M. Borgatti, L. Altomare, M. Baruffa, E. Fabbri, G. Breveglieri, G. Feriotto, N. Manaresi, G. Medoro, A. Romani, M. Tartagni, R. Gambari and R. Guerrieri, *Int. J. Mol. Med.*, 2005, **15**, 913–920.

105. J. de Jong, R. G. H. Lammertink and M. Wessling, *Lab Chip*, 2006, **6**, 1125–1139.

106. X. Chen and J. Shen, *J. Chem. Technol. Biotechnol.*, 2016, **92(2)**, 271–282.

107. K. Atsuta, H. Noji and S. Takeuchi, *Lab. Chip*, 2004, **4**, 333–336.

108. T. Masters, W. Engl, Z. L. Weng, B. Arasi, N. Gauthier and V. Viasnoff, *PLoS ONE*, 2012, **7(8)**, e44261.

109. S. F. Jahn, L. Engisch, R. R. Baumann, S. Ebert and W. A. Goedel, *Langmuir*, 2009, **25**, 606–610.

110. J. Choi, A. Roychowdhury, N. Kim, D. E. Nikitopoulos, W. Lee, H. Han and S. Park, *J. Micromechanics Microengineering*, 2010, **20**, 085011.

111. T. Yanagishita, K. Nishio and H. Masuda, *J. Vac. Sci. Technol. B Microelectron. Nanometer Struct.*, 2007, **25**, L35–L38.

112. A. M. Prenen, J. C. A. "Hans" van der Werf, C. W. M. Bastiaansen and D. J. Broer, *Adv. Mater.*, 2009, **21**, 1751–1755.

113. E. J. Vriezekolk, A. J. B. Kemperman, M. Gironès, W. M. de Vos and K. Nijmeijer, *J. Membr. Sci.*, 2013, **446**, 10–18.

114. H. Cho, J. Kim, H. Park, J. Won Bang, M. Seop Hyun, Y. Bae, L. Ha, D. Yoon Kim, S. Min Kang, T. Jung Park, S. Seo, M. Choi and K.-Y. Suh, *Nat. Commun.*, 2014, **5**, 3137.

115. S. Zheng, H. K. Lin, B. Lu, A. Williams, R. Datar, R. J. Cote and Y.-C. Tai, *Biomed. Microdevices*, 2011, **13**, 203–213.

116. Y. Liu, W. Wang, W. Wu, F. Yang, W. Wang and H. Li, in *2015 Transducers - 2015 18th International Conference on Solid-State Sensors, Actuators and Microsystems (TRANSDUCERS)*, 2015, pp. 1767–1769.

117. B. Lu, S. Zheng, B. Q. Quach and Y.-C. Tai, *Lab. Chip*, 2010, **10**, 1826–1834.

118. J. H. Kang, E. Um and J.-K. Park, *J. Micromechanics Microengineering*, 2009, **19**, 045027.

119. D. Polcari, J. A. Hernández-Castro, K. Li, M. Geissler and J. Mauzeroll, *Anal. Chem.*, 2017, **89**, 8988–8994.

PREFACE TO CHAPTER 2

In the previous chapter, we introduced several different capture methods for rare cells in cell suspensions. We also pointed out the advantages and limitations of the currently available methods, the fact that no gold standard yet exists for the isolation of CTCs, and why we consider microfiltration as the best approach to tackle this challenge.

One of the hypotheses of this work was that the combination of mechanical and molecular capture methods would enhance the efficient arrest of CTCs, *i.e.* the use of antibody-coated microfilters would yield a higher capture rate than by using bare filters. The idea of coupling immunocapture with microfilters for CTC isolation had not been explored before in the literature.

In this chapter, we developed a technique to prove this hypothesis, by using a hemi-functionalized microfilter and comparing the capture rate of a given cell type on each half of the filter we showed that the use of a molecular and mechanical capture platform does increase the capture efficiency of cells that express the target antigen to the antibody on the filter surface. The findings in this chapter served as part of the foundation for the work presented in Appendix I.

The work of this thesis began with the use of silicon microfilters, which gave promising results, however, they had two major drawbacks: first, they were expensive and complicated to fabricate, and second, they were brittle, with a tendency to break during handling or filtration.

The following manuscript was published as part of the Proceedings of the ***The 18th International Conference on Miniaturized Systems for Chemistry and Life Sciences (μTAS 2014)***.

CHAPTER 2 | HEMI-FUNCTIONALIZED SILICON FILTERS FOR SIMULTANEOUS CAPTURING AND TYPING OF CIRCULATING TUMOR CELLS

J. Alejandro Hernández Castro,[1,2] K. Turner,[1,2] A. Sanati Nezhad,[1,2] and D. Juncker[1,2,3]

[1]McGill University and Génome Québec Innovation Centre, 740 Dr. Penfield Avenue, Montréal, Québec, H3A 0G1, Canada

[2]Department of Biological and Biomedical Engineering, McGill University, 3775 rue University, Montréal, Québec, H3A 2B4, Canada

[3]Department of Neurology and Neurosurgery, McGill University, 3801 rue University, Montréal, Québec, H3A 2B4, Canada

2.1 Abstract

We report a novel method for circulating tumor cell (CTC) capturing and typing using silicon filters that have been selectively functionalized with an anti-EpCAM IgG only on one half of the filter. We found that a significantly higher number of EpCAM-expressing cancer cells are captured on the antibody-coated section of the filters compared to the non-coated portion. Based on the distribution of the captured cells on the filter surface, it may be possible to simultaneously assess the overall CTC number along with relative EpCAM expression without the need for specific staining.

2.2 Introduction

CTC capture using molecular or size-based enrichment has been widely explored, but CTC isolation is challenging owing to the very low concentration of CTCs in blood and their similarity to white blood cells. The efficiency of CTC isolation is further confounded by the heterogeneity of CTCs, both in size and in the expression of various molecular receptors.[1] Despite increasing appreciation of the heterogeneity of CTCs, many purification methods only target a single parameter, be it a receptor such as the epithelial cell adhesion molecule (EpCAM) using an antibody,[2] or the size by using size-based filtering.[3,4] Finally, following isolation, the identification and enumeration of CTCs require

cell staining with multiple markers, which is slow and cumbersome. Here, we introduce hemi-coated microfilters that on one half isolate cells based on size only, and on the other half isolate cells based on size and EpCAM expression. Hence, by comparing the cells trapped on each half of the filter, the relative contribution of EpCAM expression can be directly derived, without the need of receptor staining, from the difference in CTC counts.

2.3 Experimental

Microfilters with a 15 µm thick circular active surface of 10 mm diameter were fabricated by photolithography techniques. The pores on the filters were etched onto the Si, with diameters ranging from 6 to 20 µm. The antibodies were coupled to the surface using an EDC/NHS chemistry protocol, only one half was functionalized using a custom built hemi-coating chamber requiring only 84 µL of the 5 µg/ml of EpCAM antibody in PBS (Figure 2-1). Next, the filters were incubated with 1% BSA in PBS for 10 minutes for surface blocking.

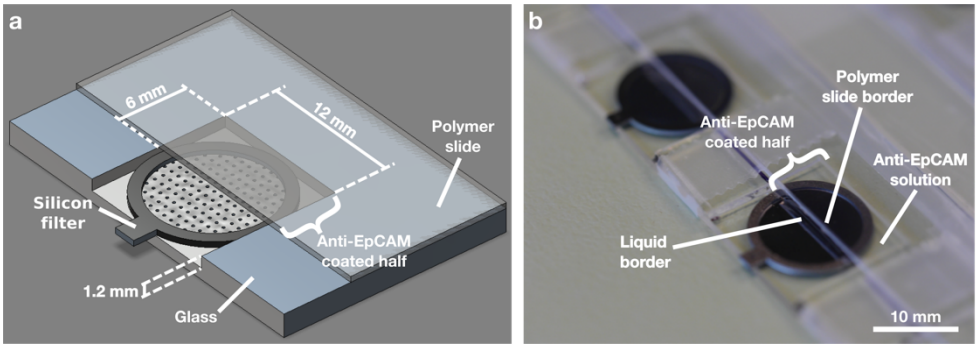

*Figure 2-1 | **Hemi-functionalization of the filter**. (a) Schematic showing the filter installed in the hemi-functionalization device. (b) Incubation with EpCAM antibody solution on one half of the filter.*

The anti-EpCAM hemi-functionalized filter was mounted in a custom cartridge that directs the sample fluid flow and allows for visualization of the filter in cell capture experiments without additional manipulation of the filter (Figure 2-2). The filters were aligned to ensure equal volumetric flow of the solution through both halves of the filter (Figure 2-2b). MCF-7 (strongly expressing EpCAM) breast cancer cells spiked in PBS (used instead of whole blood to avoid confounding effects) were used as CTC model. The cells were stained with Vybrant green dye before flowing them at a rate of 0.5 mL/min

through the cartridge. The captured cells were visualized using an inverted fluorescence microscope with a 10× objective. The cells are round (usually presenting a fluorescent halo), and they are found on or within the filter pores, which helps to discriminate them from other fluorescent particles that are randomly present on the filters.

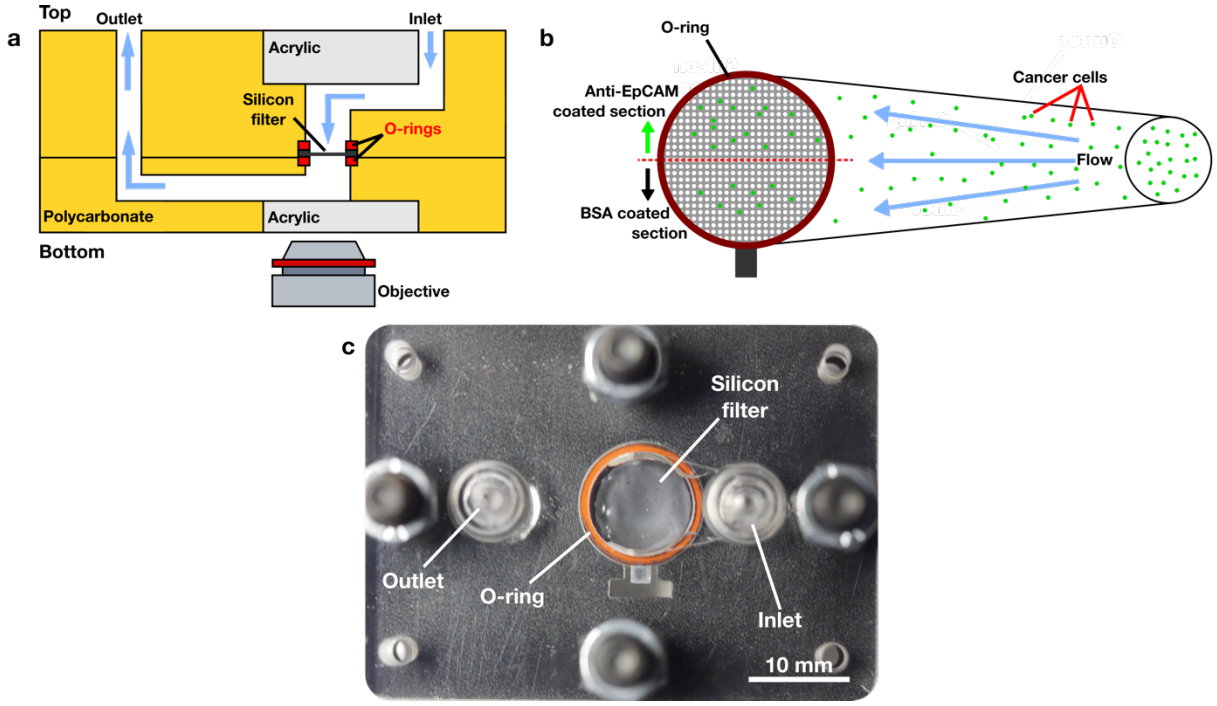

*Figure 2-2 | **Filter cartridge for cell capture**. (a) Cross-section schematic view of the cartridge with filter. The flow path is shown using arrows. (b) Top view schematic showing how the filter was positioned inside the cartridge to achieve equal flow patterns on the antibody-functionalized and non-functionalized halves of the filter. (c) Top view of the assembled cartridge.*

2.4 Results and discussion

For the CTC capture experiments, silicon filters with pores from 11 µm to 17 µm were used, and it was found, regardless of the pore size, that the number of captured cells was approximately two times higher on the anti-EpCAM functionalized half of the filter. Figure 2-3 shows representative sections of each half of one filter, and it is apparent that more cells are captured, for the same area, on the antibody-coated half. Figure 2-4 summarizes the results obtained from the cell capture experiments with non-coated (control) and the hemi-functionalized filters. The results from control experiments show that similar numbers of cells were captured on both halves of the filters for positive

controls using hemi-functionalized filters and cells with low expression of EpCAM, and for negative controls using completely uncoated filters and EpCAM$^+$ cells.

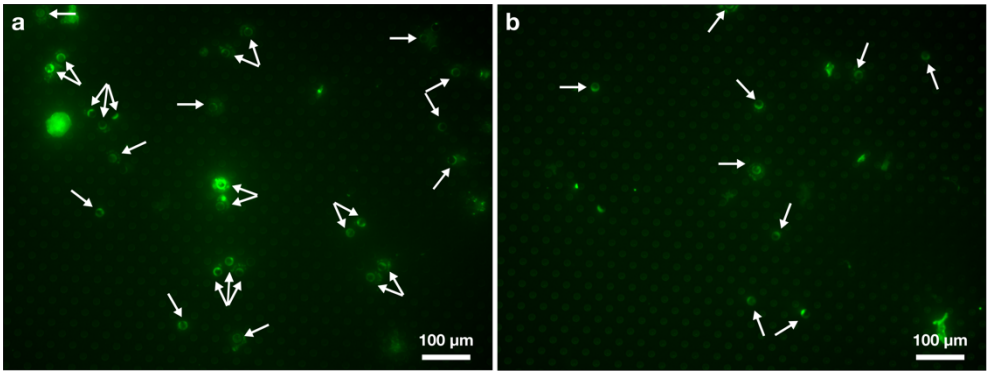

*Figure 2-3 | **MCF-7 cancer cells (average diameter ≈ 18 µm) captured on a hemi-functionalized filter with 15 µm pores**. Arrows indicate the captured cells. A higher number of captured cells is evident on (a) the anti-EpCAM functionalized half (26 cells) when compared with (b) the non-functionalized half (9 cells).*

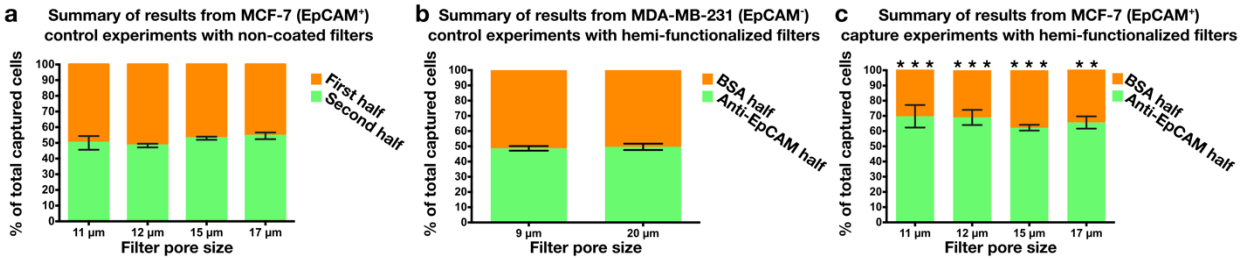

*Figure 2-4 | **Results from cell capture experiments**. (a) Control experiments with non-coated filters and EpCAM$^+$ cells, capture distribution is not biased to either half of the filter. (b) Control experiments using hemi-functionalized filters and EpCAM$^-$ cells also showed that capture distribution is not biased to either half of the filter. (c) When the hemi-functionalized filters were used for the capture of EpCAM$^+$ cells, a different capture trend is observed in comparison to the control experiment with non-coated filters. Significance of these results was evaluated using t-test analysis (*** = $p < 0.01$; ** = $p < 0.05$). Error bars represent standard deviation ($n = 3$).*

2.5 Conclusion

Differential functionalization of microfilters can be used to capture cells based on size while enriching cells expressing a given receptor, thus gaining information on receptor expression simply based on the cell distribution on the filter, without the need for specific receptor staining, simplifying the characterization process of the captured cells. Further optimization of more complex differential functionalization patterns and different flow rates will be evaluated using different cancer cell lines, so we can analyze the capture specificity of the present differential functionalization technique and its potential as a CTC characterization tool.

2.6 Acknowledgements

We acknowledge funding from NSERC-CIHR CHRP for this work. Thanks to Dr. Andy Ng for critical reading of the manuscript.

References

1. S. K. Arya, B. Lim and A. R. A. Rahman, Lab. Chip, 2013, 13, 1995–2027.

2. S. Nagrath, L. V. Sequist, S. Maheswaran, D. W. Bell, D. Irimia, L. Ulkus, M. R. Smith, E. L. Kwak, S. Digumarthy, A. Muzikansky, P. Ryan, U. J. Balis, R. G. Tompkins, D. A. Haber and M. Toner, Nature, 2007, 450, 1235–1239.

3. R. L. Fleischer, P. B. Price and E. M. Symes, Science, 1964, 143, 249–250.

4. Coumans, F. A. W.; van Dalum, G.; Beck, M.; Terstappen, L. W. M. M. *PLoS ONE* **2013**, *8*, e61774.

PREFACE TO CHAPTER 3

In the previous chapter, we introduced the use of silicon microfilters for the isolation of cancer cells spiked in buffers. After the preliminary work performed with this first generation of filters, the need for a new generation of microfilters of a different material was clear. This was the motivation to develop a fabrication method for microporous polymer membranes that could be more robust, less expensive to fabricate, and easier to handle.

In this chapter, we present a vacuum-assisted polymer microfilter fabrication method using UV-curable resins. With this technique, we successfully and reliably fabricated polymer membranes with regular pore distribution, very large pore aspect ratio (up to 14.7), large area (up to 9×9 cm^2), high porosity (up to 60%), optically transparency, and low autofluorescence. The combination of all these characteristics at once in a polymer microfilter had not been attained with other fabrication techniques, either in commercially available membranes (track-etched or mesh filters) or by microfabrication methods found in the literature. We then integrated these filters into plastic microfluidic devices and used them for the separation of a mixture of microbeads, as well as for the capture of CTC-like cells spiked in buffers.

These new polymer microfilters have then served as basis for other works performed in Prof. Juncker's and Dr. Veres' labs, namely, the development of a platform for CTC capture from blood samples (presented in more detail in Appendix I), currently being used for trials using clinical samples; and they have also been used as protective masks for selective surface treatment of plastic substrates, useful for culturing cells in regular arrays.[1]

The following manuscript was published as a *Research Article* in ***Lab on a Chip***. It was highlighted in the back cover of Issue 11 in 2017.

1. D. Polcari, J. A. Hernández-Castro, K. Li, M. Geissler and J. Mauzeroll, *Anal. Chem.*, 2017, **89**, 8988–8994.

CHAPTER 3 | FABRICATION OF LARGE-AREA POLYMER MICROFILTER MEMBRANES AND THEIR APPLICATION FOR PARTICLE AND CELL ENRICHMENT

J. Alejandro Hernández Castro,[1,2,3] K. Li,[1] A. Meunier,[2,3] D. Juncker,[2,3,4] and T. Veres[1,2]

[1]National Research Council of Canada, 75 de Mortagne Boulevard, Boucherville, Québec, Canada J4B 6Y4.

[2]Biomedical Engineering Department, McGill University, 3775 University Street, Montréal, Québec, Canada H3A 2B4.

[3]McGill University and Génome Québec Innovation Centre, McGill University, 740 Dr. Penfield Avenue, Montréal, Québec, Canada H3A 0G1.

[4]Neurology and Neurosurgery Department, McGill University, 3801 University Street, Montréal, Québec, Canada H3A 2B4.

3.1 Abstract

A vacuum assisted UV micro-molding (VAUM) process is proposed for the fabrication of freestanding porous polymer membranes based on UV-curable methacrylate polymer (MD 700). VAUM is a highly flexible and powerful method for fabricating low cost, robust, large-area membrane over 9×9 cm^2 with pore sizes from 8 to 20 µm in diameter, 20 to 100 µm in thickness, high aspect ratio (thickness of polymer over diameter of hole is up to 15:1), high porosity, and a wide variety of geometrical characteristics. The fabricated freestanding membranes are flexible while mechanically robust enough for post manipulation and handling, which allows them to be cut and integrated as a plastic cartridge onto thermoplastic 3D microfludic devices with single or double filtration strategies. Very high particle capture efficiencies (≈ 98%) have been demonstrated in the microfluidic devices integrated with polymer membranes, even when the size of the beads is very close to the size of the pores of the microfilter. About 85% of capture efficiency has been achieved in cancer cell trapping experiments, in which a breast cancer cell line

(MDA-MB-231) spiked in phosphate-buffered saline buffer when the pore size of the filter is 8 µm and the device is operated at flow rate of 0.1 mL/min.

3.2 Introduction

In the last decades, many interesting areas of research have derived from the onset of MEMS technology. The ability to fabricate devices in the micro- and nanoscale enhances our capacity to interact with particles, microorganisms, and cells in ways we had never been able to do before.

Among these, fabrication of microfilters with controllable pore size and distribution has been explored with many purposes including selection, capture, and identification of low abundance targets in clinical applications.[1,2] Among those applications of particular interest is circulating tumor cells (CTCs) isolation, for which the use of dielectrophoretic[3–6] and hydrodynamic forces,[7–11] as well as physical barriers have been explored. Fast throughputs (0.5 mL/min or more) for samples processing and very good efficiencies (CTC capture > 80 %[12–14]) have been reported using filtration techniques. Track-etched polymer membranes with a high mechanical robustness have been widely used for this purpose since the 1960s.[15–17] Although this technology allows an accurate control of the pore size dimension ranging from 0.01 to 30 µm approximately, the maximum porosity is limited due to the random nature of the track-etching process,[15] thus greatly restricting the throughput of a system using such membranes. Otherwise, metal[18,19] and silicon microfilters have been successfully used for this application as well,[14,20–22] but handling of these micro-sieves is delicate due to the brittle nature of Si, thereby making their out-of-the-lab use rather difficult.

To overcome these drawbacks, methods allowing fabrication at low-cost of high porosity polymer membranes with customizable pore sizes is of great interest. For instance, polymer casting,[23–25] hot embossing or nanoimprint lithography (NIL),[26–30] photolithography,[13,31–35] micromolding in capillaries,[36,37] phase separation microfabrication,[38–40] have been shown to work for the fabrication of through-holes of various diameters

on polymer films. More recently, Cho et al. showed that the potential of using UV curable resins for the fabrication of free-standing and residual-layer-free polymer membranes with nanoscale apertures by taking the advantage of dewetting effects.[41] However, during fabrication, most of these methods require complex processes to achieve open-through hole structures, and it remains difficult to get large-area polymeric membranes without distortion or tearing issues, especially as the membranes become thinner.

In this work, a new and low-cost method for the fabrication of free-standing polymer microfilters is presented, showing successful and relieable fabrication of very large area polymer membranes with regular distribution, high aspect ratio, and narrow size variation of pores. The characterization of the polymer membranes' thickness, pore size, and dimension, as well as the size distribution was done by both scanning electron microscopy (SEM, Hitachi S-4800) and 3D laser scanning confocal microscope (Keyence VK-X110). Moreover, proof-of-concept microfluidic devices with single or double filtration stages were fabricated to demonstrate the enrichment of micro-beads within two or three populations, results were quantified via flow cytometry analysis (BD FACSCalibur™). Very high capture efficiencies (≈ 98%) for beads with average diameters that are slightly larger than the diameter of the pores used in each case, *e.g.* 9.97 µm (± 0.23 µm) pores for 10.3 µm beads has been successfully demonstrated. The devices have been validated for the enrichment of breast cancer cells (MDA-MB-231) from buffer. The effect of pore size as well as the flow rate on the performance of CTC enrichment will be discussed.

3.3 Materials and methods

3.3.1 Chemicals

All solutions were prepared with deionized water from a Milli-Q system (resistivity of 18 MΩ cm; Millipore). Phosphate buffered saline (PBS, 1X, pH = 7.4), from Fisher Scientific, contains 11.9×10^{-3} mol/L of phosphates, 137.0×10^{-3} mol/L of sodium chloride and 2.7×10^{-3} mol/L of potassium chloride. Trypsin-EDTA, bovine serum albumin (BSA) and Tween 20 were obtained from Sigma-Aldrich. Triton X-100 and paraformaldehyde

were purchased from Fisher Scientific. Dulbecco's modified Eagle medium (DMEM), fetal bovine serum (FBS) and 4',6-diamidino-2-phenylindole (DAPI) were purchased from Life Technologies. Antibiotics (penicillin and streptomycin) were obtained from Invitrogen. Anti-pan cytokeratin-Alexa Fluor 488 was obtained from R&D systems.

AZ 9260 photoresist (AZ Electronic Materials USA Corp., Somerville, NJ) was used for all photolithographic work. Ebecryl® 3708 (Allnex Canada Inc., ON, Canada) UV-curable resin mixture was prepared in a 7:3 ratio with tripropylene glycol diacrylate (TPGDA) from Allnex Canada Inc., Darocur® 1173 (BASF Corporation, Vandalia, IL) was added as a curing agent in 1% w/w. UVA 1534 UV-curable resin was prepared by mixing Uvacure 1500 (Allnex Canada Inc.) and Capa™ 3050 (Perstrop, Sweden) in a 1:1 ratio, and Uvacure® 1600 (Allnex Canada Inc.) in 1% w/w was added as a curing agent.

Trichlorol(1H, 1H, 2H, 2H)-perfluorooctyl-silane (97%) (Sigma-Aldrich, Oakville, ON) was used for all surface silanization protocols.

Fluorolink® MD700 (Solvay Specialty Polymers USA LLC, Alpharetta, GA) UV-curable resin mixed with 2% w/w of Darocur® 1173 was used as the building material for the polymer membranes, it has a Young's modulus of approximately 10 MPa.[41]

3.3.2 Si master mold fabrication

Si master molds were prepared for different membrane designs (*e.g.* different thicknesses, footprints). AZ 9260 photoresist was spin coated at 2400 rpm for 72 s on blank Si wafers. A soft bake at 110 °C for 3 min was followed by the UV exposure of the desired pattern at 1250 mJ/cm^2. Developing was done in AZ 300MIF, and the final hard bake was done at 135° C for three hours.

The exposed pattern was etched into the Si substrate via deep reactive ion etching (DRIE) (Oxford Instruments PlasmaLab System 100). Si pillar array structures with height of approximately 20, 40, 60, and 100 µm were fabricated. After etching, the wafers were thoroughly cleaned by washing them with acetone and isopropyl alcohol (IPA) before drying them under a stream of nitrogen.

It is important to note that in the process proposed herein, the Si master molds only need to be fabricated once and are then replicated in flexible UV cured polymers (Ebecryl® 3807). The master molds could also be manufactured by lithography, or plastic micro-machining, for example.

3.3.3 Filter cartridge design and fabrication

The filter cartridge was designed with Autodesk Autocad 2015 software and machined on a Zeonor® 1060 1.7 mm-thick wafer. It encompasses 150 µm-height, 600 µm-wide channels, two 1 mm-diameter inlets, and two outlets with the same dimensions, allowing the sample to flow from both sides of the filter if desired, and avoiding the formation of any bubbles on the filter surface during the chip filling. Once the filter membranes are placed in the central recess, cover layers consisting of a hybrid structure of 300 µm of Mediprene® OF-400 and 700 µm of Zeonor® 1060 (injection molded in-house) were thermally bonded on each side of the cartridge followed by post heat treatment at 40 °C overnight. Higher temperatures can be used to speed up the thermal bonding process, however, to avoid the deterioration of attached molecules (*e.g.* antibodies for cell capture) on the filters after surface modification,[42] it is recommended to do the post thermal bonding of the devices at 40 °C. The assembled cartridge, with a 27×27 mm^2 footprint, has a total thickness of 3.7 mm, as shown in Fig4-4c, allows us to perform *in-situ* fluorescence analysis without disassembling the device.

3.3.4 Membrane embedding in thermoplastic carriers

Two different types of polymers were used as carrier materials for the microfilter membranes. Zeonor® ZF14-188 and PMMA (injection molded in-house). The shapes of the filter frames are cut from these substrates by CNC machining.

Embedding of the membranes into the frames was done by hot embossing (EVG®520). A temperature of 180 °C and 10 kN of pressing force during 7 min for ZF14-188, and 140 °C and 100 N during 3 min for PMMA.

3.3.5 Cell culture and sample preparation

All culture medium and solutions were filtered through a 0.2 µm filter before use. MDA-MB-231 (HTB-26) cells, from the American Type Culture Collection (Manassas, VA), were cultured in DMEM, supplemented with 10% FBS and 1% (v/v) antibiotics (final concentrations of 100 I.U./mL penicillin and 100 µg/mL streptomycin) and maintained in 5% CO_2 at 37 °C in 25 cm^2 flasks (Corning, NY, USA). Almost confluent monolayers (80-90%) of cells in flasks were harvested using diluted trypsin. Cell suspension (density of ≈ 10^6 cells/mL) was centrifuged 5 min at 4600 rpm then re-suspended in 50 mL of PBS. For filtration, cell suspension was diluted by a factor of 200 and 1 mL was pumped into the cartridge.

The actual number of cells within 10 µL of the suspension after dilution was manually counted under a microscope. Counting was repeated twice and averaged on 10 droplets for a more accurate measurement.

3.3.6 Cell staining

Cells were first fixed with 3.7% paraformaldehyde (PFA) diluted in PBS for 10 min. After rinsing three times (5 min each) with PBS, cells were then permeabilized with 0.2% Triton X-100 for 5 min then rinsed three times with PBS, 5 min each. BSA 1% in PBS supplemented with 0.1% Tween 20 was applied during 30 min for blocking, then cells were stained with anti-pan Cytokeratin-Alexa Fluor 488 (anti-CK, 2.0 µg/mL) diluted in PBS, for 1 hour. After rinsing with PBS for 5 min, nuclei were stained with 4',6-diamidino-2-phenylindole (DAPI, 0.1 µg/mL). Finally, the filter was rinsed with PBS and cell identification was performed by fluorescence microscopy.

3.3.7 Microbeads

Sky blue fluorescent polystyrene microbeads FP-7070-2 (nominal size: 7.0 – 8.9 µm; average size: 8.27 µm), Nile red microbeads FP-10056-2 (nominal size: 10 – 14 µm; average size: 10.3 µm), FP-15056-2 (nominal size: 15 – 19 µm; average size: 15.0 µm), and FP-20056-5 (nominal size: 20.0 – 24.9 µm; average size: 20.3 µm) were purchased from

Spherotech. These microbeads were to be used as target beads; we expected to capture them on the 8, 20, 15, and 20 µm pore size microfilters, respectively.

Green fluorescent microbeads G0500B with a nominal size of 4.8 µm (< 5% coefficient of variation (CV)) were purchased from Fisher Scientific. These were to be used as background beads, *i.e.* a population of beads we didn't wish to capture.

The beads were diluted in Milli-Q water with 0.1% v/v of Tween 20 until the following approximate concentrations were achieved: 450 beads/µL for the 4.8 µm beads, 43 beads/µL for the 8.27 µm beads, 86 beads/µL for the 10.3 µm beads, 35 beads/µL for the 15.0 µm beads, and 42 beads/µL for the 20.3 µm beads. Bead counting was done manually by inspecting five 1 µL droplets of each bead solution under the fluorescence microscope. 2 mL mixtures of each target beads and background beads were done in the following way:

- 250 µL (8.27 µm beads) + 400 µL (4.8 µm beads) + 1.35 mL (0.1% Tween 20 in Milli-Q water).
- 125 µL (10.3 µm beads) + 400 µL (4.8 µm beads) + 1.475 mL (0.1% Tween 20 in Milli-Q water).
- 200 µL (15.0 µm beads) + 400 µL (4.8 µm beads) + 1.4 mL (0.1% Tween 20 in Milli-Q water).
- 100 µL (20.3 µm beads) + 400 µL (4.8 µm beads) + 1.5 mL (0.1% Tween 20 in Milli-Q water).
- Mixture of 100 µL (20.3 µm beads) + 200 µL (15.0 µm beads) + 400 µL (4.8 µm beads) + 1.3 mL (0.1% Tween 20 in Milli-Q water).

Characterization of the bead populations were performed to corroborate the information provided by the manufacturer. Histograms of the size distribution of the beads were acquired using a Millipore Specter™ 2.0 (EMD Millipore, Darmstadt, Germany), the results are shown in the supplementary information (Figure S3-1).

3.3.8 Fluorescence microscopy

Cell counting was performed with an inverted microscope (TE-2000-E, Nikon) connected to a CCD camera (QuantEM 512SC, Photometrics) and fluorescence images were recorded with the NIS-Elements Advanced Research software (Nikon) and analyzed with the ImageJ software.[43] All the images were collected with a mercury arc lamp with fluorescence 41001 (blue, for Alexa Fluor 488), and 31000v2 (UV for DAPI) filter cubes (Chroma Technology Corp.). MDA-MB-231 was identified when it is found positive for CK and DAPI (Figure 3-6a).

3.4 Results and discussion

3.4.1 Vacuum assisted UV micro-molding fabrication process

As mentioned above, it is technically challenging to make isoporous polymer membranes, although the consistent replication of features in the micrometer range on polymers has been previously demonstrated with a wide variety of techniques, most of these are quite complex. Alternatively, we propose a robust method called vacuum assisted UV micro-molding (VAUM) to make isoporous polymer membranes.

A schematic of the proposed fabrication process for the UV-curable polymer membranes is depicted in Figure 3-1a and Figure 3-2a. First, a PDMS mold is casted from a master Si mold (Figure 3-1a, steps 1-2) after being silanized by placing it in a vacuum desiccator for two hours.

A UV-curable resin (Ebecryl®3708) was spin coated on a polyethylene terephthalate (PET) film. A silanized PDMS mold was then put on top of the UV resin and degassed to allow the resin to fully fill the cavities of the PDMS mold and be air-bubble free. After exposure to UV light (2000 EC series UV curing flood lamp, DYMAX) for 3 min and demolding, a UV-cured resin mold consisting of an array of pillars (Figure 3-1c) with the desired dimensions is created by replication from the PDMS mold (Figure 3-1a, steps 3-4). The UV cured resin mold was then covered with a PET sheet (Figure 3-1d) upon which a thin layer of the same type Ebecryl®3708 UV resin or a different UV-curable

epoxide resin (Uvacure® 1534) was previously spin-coated (Figure 3-1a, step 5). The resulting assembly is then exposed to UV radiation for curing (Figure 3-1a, step 6), leading to an enclosed pillar structure.

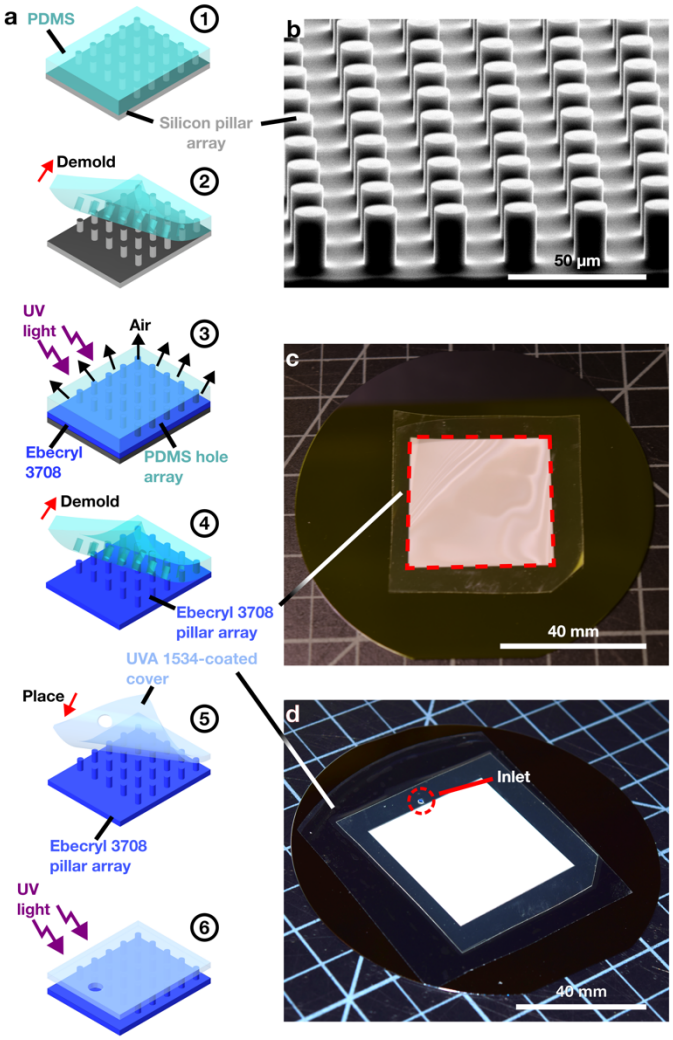

*Figure 3-1 / **VAUM process mold fabrication steps**. (a) The fabrication process begins with PDMS replication from a master Si mold (1-2), a pillar mold was replicated from the PDMS using Ebecryl®3708 (UV-curable resin) (3-4). Afterwards, an enclosed mold was assembled by placing a UVA1534 (UV-curable resin) coated film on the previously fabricated mold (5-6) to seal the cover to the posts. (b) SEM image of a silicon pillar array. (c) Picture of an Ebecryl®3708 pillar array mold after curing. The dashed line marks the area corresponding to the pillar array (4×4 cm^2). (d) Picture of an enclosed mold after assembly and curing.*

The building material for the membrane is a UV-curable methacrylate polymer (Fluorolink® MD 700). Polymerization by UV light exposure allows us to speed up the fabrication process. The filling of the UV resin is done by a vacuum assisted method,

which helps to avoid defects and cavities in the membrane structure. Following UV curing, the polymer membrane is obtained after separation from the disposable polymer mold under solvent, eliminating drawbacks like distortion or even tearing into smaller pieces that can happen with other techniques that require physical demolding steps.

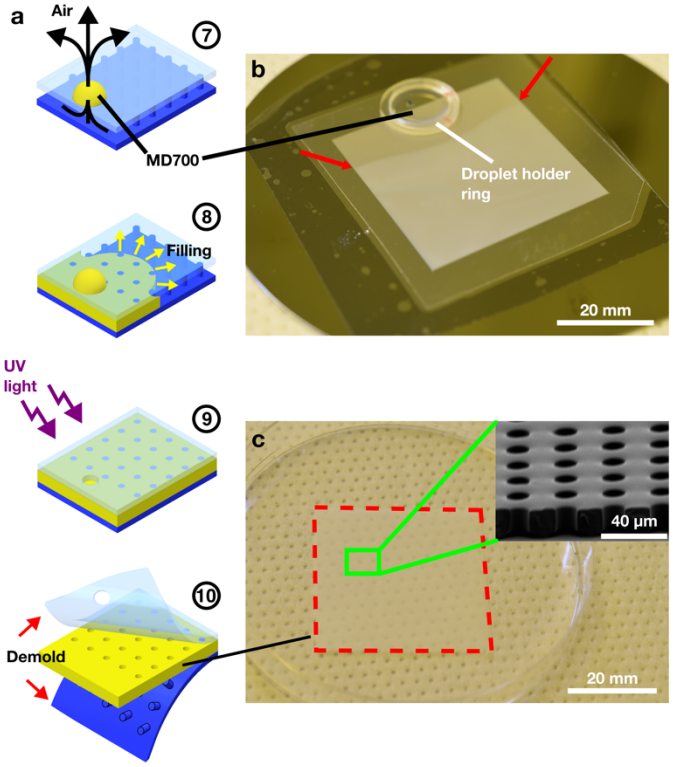

*Figure 3-2 | **Mold filling and membrane release**. (a) Fluorolink® MD 700 was applied as a droplet to the openings, and then (7) vacuum was applied to degas the air in the gap, followed by (8) re-pressurization to drive the MD700 resin into the gap. Next, (9) the MD700 was cured by UV light exposure, and (10) the membrane released from the mold. (b) Mold during the filling process, the arrows indicate the position of the resin filling front. The elastomer holder ring was placed to avoid displacement of the MD 700 droplet. (c) Fabricated polymer membrane in a Petri dish, the dashed line indicates where the membrane is placed. The insert shows and SEM image of the membrane, regular pore distribution and completely open-through holes can be observed.*

A small volume (less than 10 µL for a 4 cm^2 and 20 µm thick membranes) of MD 700 is injected inside the final mold in a vacuum assisted injection process (Figure 3-2b), and cured through UV exposure for 2 min (Figure 3-2a, steps 7-9). Finally, the PET cover layer is peeled off, and the molds are bathed in acetone for 30 mins to 1 hour, allowing the membranes to self-demold from the pillars structure (step 10).

The insert in Figure 3-2c shows a representative SEM image of the fabricated membranes, a regular pore distribution and geometry can be observed, and the presence of open-through holes is evident in a close-up of the membranes' edge. This first design consists of simple square arrays of open-through holes over the whole area of each membrane. Filters with pores with diameters of 8, 10, 12, 15, and 20 µm were successfully fabricated using this pattern.

3.4.2 Characteristics of the polymer membranes

Considering the specific application of this type of polymer membrane for CTC isolation, where the pore dimension is limited by the requirement for white blood cells (WBCs) to pass through, membranes with pore ≥ 8 µm must be used, thus we decided to focus on the single-level design of the filter membranes. The diversity and flexibility of the fabrication process were studied in terms of the distribution of pore size, thickness of membrane, aspect ratio of the pores, as well as the size of the membrane.

Si master molds with pillar structures of 30, 40, 60, and 100 µm in height were first prepared and the resulting polymer membranes with various thicknesses were characterized. Figure 3-3a, b, and c show SEM images of the 30, 60 and 100 µm thick membranes, respectively.

While the original method worked perfectly for fabrication of the polymer membranes with the thinner molds (up to 60 µm height), some issues were encountered in the demolding step of the thickest membranes. It was observed that the pillar layer of the mold folds upon itself when bathed in acetone, preventing the release of the membranes. It was thus decided to modify the last step of the fabrication process to address this issue. Prior to putting the molds in the acetone bath, they were pinned to a flat glass substrate to prevent such folding. This simple modification, not only allowed the successful release of the thicker membranes, but also greatly reduced the time needed for demolding to only ≈ 20 min for all fabricated membranes.

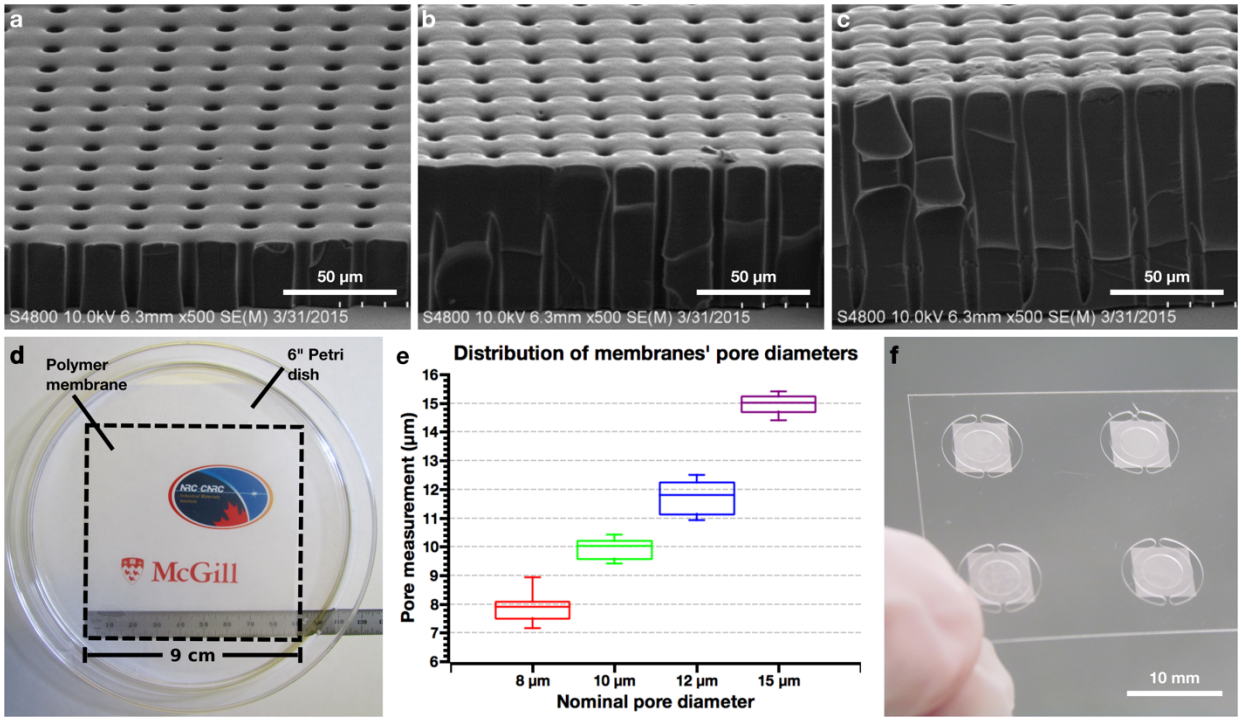

*Figure 3-3 | **Polymer membrane fabrication results**. SEM images of polymer membranes with thickness of 30 µm (a), 60 µm (b), and 100 µm (c). The pore size in (c) is ≈ 6.8 µm, which makes the aspect ratio of the pore in this membrane to be 14.7. (d) Shows a membrane of 9×9 cm in area, it also highlights the transparent properties of the material used for the fabrication of these membranes, as patterns can be seen through them. (e) The box and whisker plots show the accuracy of the fabrication process for membranes of 20 µm in thickness and target pores diameter of 8, 10, 12, and 15 µm. The boxes contain percentiles 10 to 90, whiskers correspond to the maximum and minimum values. (f) 6×6 mm² membranes embedded onto ZF14 round carrier frames. Individual filters can then be cut from the substrate for use.*

This optimized process makes possible the fabrication of polymer membranes with various thicknesses and to achieve aspect ratios as high as 14.7 for ≈ 6.8 µm diameter pores in a 100 µm thick membrane (Figure 3-3c). To our best knowledge, it is about two times higher than the value reported in porous parylene membranes.[44] For the bead and cell capture applications shown in this paper, membranes of 20 µm in thickness were used. The possibility of fabricating membranes as thin as 9.3 µm, and membranes with high porosity values (≈ 60%) has also been demonstrated, examples of these are presented in Figure S3-2.

For biological applications, these polymer membranes must be disposable; therefore, it is desirable to increase the fabrication throughput, hence to reduce the unit cost of the

membrane. The scalability of the process has been explored based on the facilities available to our group at the moment.

Since our processing equipment is limited to 6" Si wafers, after having considered the uniformity of photolithography as well as DRIE etching processes, we conservatively designed a mask for fabrication of polymer membrane with an effective surface area of 4×4 cm^2 (2 by 2 dies on a 6" wafer) and as big as 9×9 cm^2 (one die on a 6" wafer). The same fabrication process was applied for these attempts except that the degassing time was increased to make sure that the larger air volume could be extracted from the molds, to guarantee the cavities of the mold would be filled with the MD 700 resin. As shown in Figure 3-3d, polymer membranes with size as large as 9×9 cm^2 have been successfully fabricated.

The replication accuracy, in terms of feature dimension, was analysed using twenty membranes for each pore size group, and the diameter of 80 different pores (randomly selected) from each subset was measured using a 3D laser scanning confocal microscope (Keyence VK-X110).

The results were summarized as box and whisker plots shown in Figure 3-3e. The best feature replication was obtained for the group of 15 µm target pore size, where the average of the measured values was 14.97 µm with a standard deviation of 0.22. For the groups with target pore size of 8, 10 and 12 µm, the measured average diameter of pores was 7.85 ± 0.31, 9.97 ± 0.23 and 11.72 ± 0.39 µm, respectively, indicating that the fabrication process is robust and highly reproducible.

Finally, to facilitate the handling of the membranes, they are embedded onto a hard-plastic carrier frame. Smaller pieces of membranes were cut by a razor blade or scissor and placed on top of a substrate where the shapes of the carrier frames had been previously machined by CNC micro-machining (Figure 3-3f). The membranes are effectively embedded into the carriers (with penetration of Zeonor or PMMA into the holes of the membrane at the edge of the frame of the plastic carrier) by hot embosser (EVG®520)

with a protocol that is selected according to the frame material selected, as described previously.

3.4.3 Particle separation on microfilters

Figure 3-4c and d show the integrated microfilter cartridge devices with one or two filters, respectively. The cartridge device consists of three polymer layers, a hard polymer fluidic layer sandwiched between the top and bottom covers that are used to seal the microfluidic channels. The hard polymer fluidic layer (Figure 3-4a and b) hosting both the microfluidic connecting channels with the top side channels (in blue), bottom side ones (in red), and recess areas with dimension compatible with the macroscopic ZF14 inserts (part 4 in Figure 3-4a and b, 0.3 mm in thickness and 0.7 cm in diameter, also shown in Figure 3-3f) was made from cyclic-olefin polymer (COP) (Zeonor 1060R) by CNC machining. The top and bottom covers are made from thermoplastic elastomeric materials (Mediprene OF 400 M (GLS Corp., McHenry, IL, USA) which have the ability to bond to the hard thermoplastic layer holding the membrane inserts and compensate for surface unevenness while providing a very good fluidic seal.[45–47] Access inlets and outlets were connected using plastic inserts (I.D. 0.5 mm, O.D. 1.0 mm; IDEX Health & Science, Oak Harbor, WA) and silastic laboratory tubing (I.D. 0.76 mm, O.D. 1.65 mm, Dow Corning). Joints were sealed using epoxy glue to ensure leak-proof manipulation. This simple architecture allows integration of multiple membrane inserts as "LEGO-like" bricks, providing a flexible and easy way to customize the devices toward specific single or multiple target sizes of objects to be filtered.

First, separation performances were characterized using flow cytometry and solutions of fluorescent beads with diameters of 8.27, 10.3, 15.0, and 20.3 µm, chosen as target beads for their dimensions like those of the filter pores. Additionally, green-fluorescent polystyrene beads with an average diameter of 4.8 µm were used as a large population of background beads, and spiked in each sample. There are two considerations when the fluorescent beads whose diameters are like those of the filter pores are selected as the

target beads. First, it is used to mimic the real experiment condition to be carried out in the CTCs enrichment because the sizes of CTCs are usually very close to that of the filter pores. Second, it can also be used to characterize the high quality of the fabricated polymer membrane in term of its narrow pore size distribution.

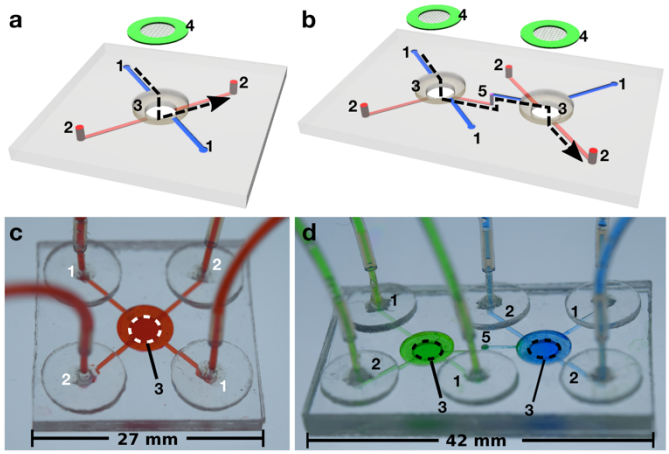

*Figure 3-4 | **Integrated microfilter cartridge devices**. (a – b) Exploded 3D schematics (top and bottom covers are not shown) of the devices with one or two filters, respectively. The top-side channels (1) are shown in blue, the bottom-side ones (2) in red, and the filter recess area (3) in yellow, and the filter cartridges (4) in green, the internal connection (5) between the two filter chambers is also shown. The flow path during filtration process is shown with a dashed arrow. (c) Photo of an assembled device with a single microfilter, it was filled with dyed water. The picture shows how the whole device is filled, no air bubbles were formed during the filling process, and no leakage is observed either. (d) Photo of an assembled device with double microfilters, it was filled with dyed water. The picture also shows that, thanks to the layout of the inlets and outlets, independent filling of each filter chamber, without trapping air bubbles, can be achieved. The labels on the pictures correspond to the same structures as in the schematics.*

The separation performance of our membrane was characterized by analysing the beads size distribution, by flow cytometry counting, within the initial solutions and after passing them through membranes having 8, 10, 15 or 20 µm pore size with help of a syringe pump at a flow rate of 0.1 mL/min (Figure 3-5).

The analysis of the filtrate after processing through 20, 15 and 10 µm pore diameter membrane showed that only background beads had passed through all pore sizes, while 20.3, 15.0 and 10.3 µm beads were successfully captured on those filters, respectively. However, a significant number of the 8.27 µm beads could still be found on the filtrate solution, suggesting that they could flow through 8 µm pores. This is caused by the

nominal size distribution of the 8.27 µm beads (range from 7.0 to 8.9 µm) with approximately 60% of the beads having a diameter of less than 8.0 µm (Figure S3-1a).

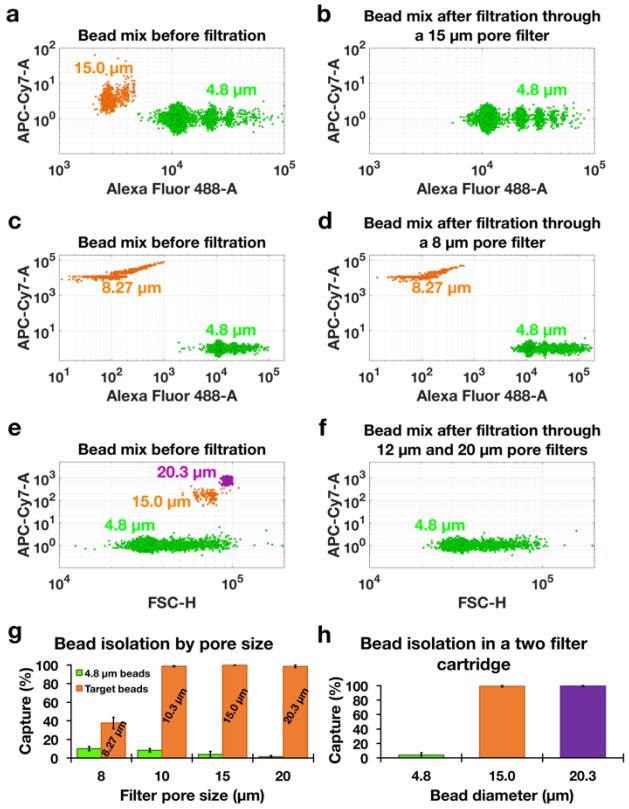

*Figure 3-5 | **Quantitative analysis of bead capture on filters**. (a, b) Dot plots of flow cytometry data of a bead mixture of 4.8 and 15.0 µm beads before and after filtration, respectively. (c, d) Dot plots of the flow cytometry data showing the composition of the 4.8 and 8 µm bead mixture before and after filtration, respectively. (e, f) Dot plots of the flow cytometry data showing the composition of the 4.8, 15.0, and 20.3 µm bead mixture before and after filtration, respectively. (g) Capture efficiency of beads after filtration by filter cartridges of different pore sizes. Green bars show the depletion rate for the background bead population (4.8 µm), while the orange ones represent the capture percentage of the target beads. Error bars correspond to SD (n=3 in all cases). (h) Capture efficiency of beads after filtration by a filter cartridge with double microfilters (12 and 20 µm pores). The 20.3 µm particles were trapped on the first filter stage (20 µm), the 15.0 µm particles passed through this first stage and were captured on the second filter (15 µm).*

Quantitative data were extracted and the depletion percentage of the target and background beads was calculated for each filter pore size and each bead population (Figure 3-5g). It is in good agreement with the narrow pore size distribution of the membrane presented in Figure 3-3e even under the dynamic flow condition. The depletion rate was found around 98% for 20.3, 15.0 and 10.3 µm beads, while it was about 40% for 8.27 µm beads because of the poor size distribution of the beads themselves, suggesting a high

potential for cell separation. Figure 3-5h shows the results carried out on a microfluidic device with double filters (12 µm and 20 µm pores). Again, the capture rate is about 100% for 15.0 µm beads on the filter with 12 µm pores and 20.3 µm beads on the filter with 20 µm pores.

3.4.4 Isolation of CTC-like cells

To validate the use of these filters for CTC enrichment, capture of MDA-MB-231, a breast cancer cell line widely used as a mimic of CTC, was performed. Once harvested from the culture flasks, MDA-MB-231 cells were spiked in PBS (approximately 100 cells were spiked per mL in each experiment) and 1 mL of the suspension was filtered through the whole available range of pore size, at a flow rate of 1 mL min^{-1}.

Cells were stained directly on the filter and the number of captured target cells (MDA-MB-231, $CK^+/DAPI^+$, Figure 3-6a) was determined and averaged on 3 experiments. Optimization of the filtration protocol was performed in parallel to determine the best parameters to use for CTC capture, further work was performed on this, as presented in a previous publication.[42]

As shown in Figure 3-6b, the number of cells captured on filters with 8, 10 and 12 µm-diameter pores remains in the same range and close to 51% (51.9 ± 2.6, 51.4 ± 2.9, 50.7 ± 2.1, respectively). When the pore diameter increases up to 15 µm, this number decreases down to about 45.5% ± 3.6 and finally reaches 36.3% ± 2.5 with 20 µm pore diameter. For the size-based capture of MDA-MB-231, this trend was expected and is in good agreement with their diameter as measured by microscopy (14.6 ± 5.1 µm).

Finally, the role of inlet pressure on cell capture efficiency was evaluated by filtering samples at different pressures. As previously mentioned, MDA-MB-231 cells were spiked in PBS, and for each flow rate condition, 1 mL of the same cell suspension was flowed through the cartridge. Filters with 8 µm-diameter pores were used to ensure the highest capture rate possible.

As the pressure decreases from 1.5×10^2, 1.0×10^2, 51, to 26 kPa (corresponding to 3.0, 2.0, 1.0, and 0.5 mL/min), 42.0 ± 4.6, 44.5 ± 5.9, 50.4 ± 2.1, and 59.7% ± 3.2 of the MDA-MB-231 were captured. When inlet pressure further decreased to 4.8 kPa (0.1 mL/min), the percentage of MDA-MB-231 cells captured on the filter increases to 84.7% ± 2.5 (Figure 3-6c). This rise approximately corresponds to a 43% gain, compared to the case with the highest inlet pressure. The initial pressure imposed to the filter clearly impacts the passage of cells through the pores and can be explained by the cell deformability, making the cell flow through easier when exposed to higher pressure.

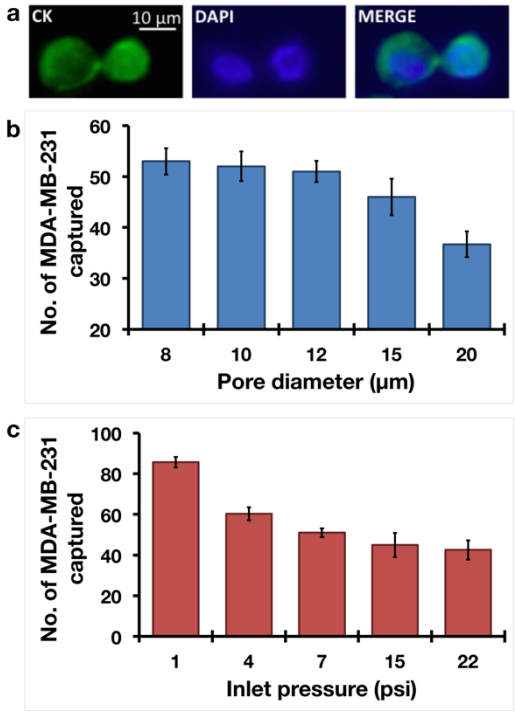

*Figure 3-6 | **Cancer cell enrichment**. (a) Fluorescently stained cancer cells trapped on filters. (b) Capture efficiency as a function of pore size; increasing the pore size reduces the capture efficiency. (c) Capture efficiency at different input pressures using a filter with 8 µm pores, the efficiency decreases with increasing inlet pressures. Error bars represent SD (n = 3).*

Cell viability was determined after filtration of MDA-MB-231 cells spiked in diluted blood. Cell viability and therefore filter cytotoxicity were characterized using a live/dead kit (Thermofisher, #L3224) after filtration, directly on the filter. Cell viability was found to be 96.5 ± 0.9 %, highlighting the non-toxicity of the filter and that the filtration conditions are soft enough to maintain cells alive.

Cell circularity, correlated with cell growth,[48] was also measured on the filter, directly after filtration and again after overnight incubation in culture medium, using ImageJ software[43] and averaged on ≈ 100 cells. A decrease in the cell circularity from 0.92 ± 0.01 to 0.61 ± 0.06 after overnight incubation reflects cell spreading, sign of increased adhesion, thus confirming cell viability and filter non-toxicity. More details are provided in the supplementary information (Figure S3-3).

Although slow flow rates must be used to enhance cell capture, higher pressure might be needed during the enrichment of CTCs from patient blood samples. Firstly, the sample viscosity will be higher due to the large amount of background blood cells, and secondly, the presence of WBCs whose size is close to that of CTCs, needs to be considered. During filtration, these WBCs will be responsible for a temporary or permanent clogging of the pores, thereby increasing the pressure. The strong robustness of these filters that can withstand fluid flow at relatively high pressures without breaking (at least 152.4 kPa corresponding to ≈ 3 mL/min) proves that the fabricated polymer membrane is mechanically stable and has been successfully applied in the enrichment of CTCs spiked into human blood.[42]

3.5 Conclusions

In summary, we have presented vacuum assisted UV micro-molding method for fabrication of polymer membranes with a wide variety of geometric characteristics. Compared to other methods previously reported in the literature, the method we propose is highly flexible and robust, allowing to fabricate polymer mebranes in large area, with various pore sizes, high aspect ratio and regular and very narrow pore size distribution (CV $<$ 4%). We have also developed the process to easily encapsulate large area (6×6 mm^2) membranes in polymer carriers which can be embeded in single or multi-stage microfluidic filtration devices composed of two thermoplastic materials. Although only single or double filtration setups were shown, the method could easily be scaled up to multiple filtration stages and easily customized for different applications.

The efficiency of the membranes for specific size filtration was characterized and quantified for the enrichment of polystyrene microbeads as well as CTCs with two populations or even three populations. The capture efficiency of polystyrene micro-beads up to 98% has been demonstarted even when the average size of the beads is approximately 0.03 to 0.40 µm larger than the size of the pores. About 85% of capture efficiency has been achieved in the enrichment of the breast cancer cells (MDA-MB-231) spiked in PBS buffer when microflter with pore size of 8 µm is used and the device is operated at a flow rate of 0.1 mL/min. The lower capture efficiency compared to that of the polystyrene beads can be explained by the more deformable nature of cells, which makes them more prone to be squeezed through the membrane pores.

Since the fabricated filters (Fluorolink® MD 700) are chemically inert, yet chemically functionalizable (using common surface modification methods[42]), easy to manipulate, mechanically stable, and resistant to high pressures (up to 1.5×10^2 kPa without breaking), it is expected that the process presented in this paper could be widely applicable for many other chemical or biological applications. In particular, microfilter membranes can be used in processes like sample concentration, sample filtration (*e.g.* separation of cell from whole blood, removal of debris, dust, or solutes), microreactors, and cell co-culture interaction experiments. There is also a growing interest in the integration of microfilter membranes into microfluidic devices,[2] which we demonstrated by successful fabrication of microfilter membranes and their integration into all-polymer microfluidic devices.

3.6 Acknowledgements

The authors acknowledge the support from the National Research Council of Canada through the Health Technologies Program (Medical Devices) and the Printable Electronics Flagship Program (Information and Communications Technologies). This research was also supported by NSERC, CONACyT, The Lloyd-Carr Harris Foundation, and the McGill University BME Department. We thank Maxence Mounier and Karel Côté for

their help with the preparation of the Si master molds used during this work. We also thank Milad Dagher for his help in the operation of the flow cytometry system and analysis of the results.

References

1. J. de Jong, R. G. H. Lammertink and M. Wessling, *Lab Chip*, 2006, **6**, 1125–1139.

2. X. Chen and J. Shen, *J. Chem. Technol. Biotechnol.*, 2016, **92(2)**, 271–282.

3. J. Yang, Y. Huang, X.-B. Wang, F. F. Becker and P. R. C. Gascoyne, *Anal. Chem.*, 1999, **71**, 911–918.

4. P. R. C. Gascoyne, J. Noshari, T. J. Anderson and F. F. Becker, *ELECTROPHORESIS*, 2009, **30**, 1388–1398.

5. A. Alazzam, I. Stiharu, R. Bhat and A.-N. Meguerditchian, *ELECTROPHORESIS*, 2011, **32**, 1327–1336.

6. F. Fabbri, S. Carloni, W. Zoli, P. Ulivi, G. Gallerani, P. Fici, E. Chiadini, A. Passardi, G. L. Frassineti, A. Ragazzini and D. Amadori, *Cancer Lett.*, 2013, **335**, 225–231.

7. A. A. S. Bhagat, H. W. Hou, L. D. Li, C. T. Lim and J. Han, *Lab. Chip*, 2011, **11**, 1870–1878.

8. K.-A. Hyun, K. Kwon, H. Han, S.-I. Kim and H.-I. Jung, *Biosens. Bioelectron.*, 2013, **40**, 206–212.

9. H. W. Hou, M. E. Warkiani, B. L. Khoo, Z. R. Li, R. A. Soo, D. S.-W. Tan, W.-T. Lim, J. Han, A. A. S. Bhagat and C. T. Lim, *Sci. Rep.*, 2013, **3**, 1259.

10. M. E. Warkiani, B. L. Khoo, D. S.-W. Tan, A. A. S. Bhagat, W.-T. Lim, Y. S. Yap, S. C. Lee, R. A. Soo, J. Han and C. T. Lim, *Analyst*, 2014, **139**, 3245–3255.

11. M. E. Warkiani, G. Guan, K. B. Luan, W. C. Lee, A. A. S. Bhagat, P. K. Chaudhuri, D. S.-W. Tan, W. T. Lim, S. C. Lee, P. C. Y. Chen, C. T. Lim and J. Han, *Lab. Chip*, 2013, **14**, 128–137.

12. I. Desitter, B. S. Guerrouahen, N. Benali-Furet, J. Wechsler, P. A. Jänne, Y. Kuang, M. Yanagita, L. Wang, J. A. Berkowitz, R. J. Distel and Y. E. Cayre, *Anticancer Res.*, 2011, **31**, 427–441.

13. T. Xu, B. Lu, Y.-C. Tai and A. Goldkorn, *Cancer Res.*, 2010, **70**, 6420–6426.

14. H. J. Lee, J. H. Oh, J. M. Oh, J.-M. Park, J.-G. Lee, M. S. Kim, Y. J. Kim, H. J. Kang, J. Jeong, S. I. Kim, S. S. Lee, J.-W. Choi and N. Huh, *Angew. Chem. Int. Ed.*, 2013, **52**, 8337–8340.

15. R. L. Fleischer, P. B. Price and E. M. Symes, *Science*, 1964, **143**, 249–250.

16. S. H. Seal, *Cancer*, 1964, **17**, 637–642.

17. G. Vona, A. Sabile, M. Louha, V. Sitruk, S. Romana, K. Schütze, F. Capron, D. Franco, M. Pazzagli, M. Vekemans, B. Lacour, C. Bréchot and P. Paterlini-Bréchot, *Am. J. Pathol.*, 2000, **156**, 57–63.

18. A. Yusa, M. Toneri, T. Masuda, S. Ito, S. Yamamoto, M. Okochi, N. Kondo, H. Iwata, Y. Yatabe, Y. Ichinosawa, S. Kinuta, E. Kondo, H. Honda, F. Arai and H. Nakanishi, *PLoS ONE*, 2014, **9**, e88821.

19. R. Negishi, M. Hosokawa, S. Nakamura, H. Kanbara, M. Kanetomo, Y. Kikuhara, T. Tanaka, T. Matsunaga and T. Yoshino, *Biosens. Bioelectron.*, 2015, **67**, 438–442.

20. L. S. Lim, M. Hu, M. C. Huang, W. C. Cheong, A. T. L. Gan, X. L. Looi, S. M. Leong, E. S.-C. Koay and M.-H. Li, *Lab. Chip*, 2012, **12**, 4388–4396.

21. J.-M. Park, J.-Y. Lee, J.-G. Lee, H. Jeong, J.-M. Oh, Y. J. Kim, D. Park, M. S. Kim, H. J. Lee, J. H. Oh, S. S. Lee, W.-Y. Lee and N. Huh, *Anal. Chem.*, 2012, **84**, 7400–7407.

22. Y. Koh, H. Kang, S. H. Lee, J.-K. Yang, J.-H. Kim, Y.-S. Lee and Y.-K. Kim, *Lab. Chip*, 2013, **14**, 237–243.

23. K. Atsuta, H. Noji and S. Takeuchi, *Lab. Chip*, 2004, **4**, 333–336.

24. T. Masters, W. Engl, Z. L. Weng, B. Arasi, N. Gauthier and V. Viasnoff, *PLoS ONE*, 2012, **7(8)**, e44261.

25. S. F. Jahn, L. Engisch, R. R. Baumann, S. Ebert and W. A. Goedel, *Langmuir*, 2009, **25**, 606–610.

26. J. Chou, N. Du, T. Ou, P. N. Floriano, N. Christodoulides and J. T. McDevitt, *Biosens. Bioelectron.*, 2013, **42**, 653–660.

27. H. Schift, S. Bellini and J. Gobrecht, *Microelectron. Eng.*, 2006, **83**, 873–875.

28. T. Shibata, S. Yukizono, T. Kawashima, M. Nagai, T. Kubota and M. Mita, *Microelectron. Eng.*, 2011, **88**, 2121–2125.

29. J. Choi, A. Roychowdhury, N. Kim, D. E. Nikitopoulos, W. Lee, H. Han and S. Park, *J. Micromechanics Microengineering*, 2010, **20**, 085011.

30. T. Yanagishita, K. Nishio and H. Masuda, *J. Vac. Sci. Technol. B Microelectron. Nanometer Struct.*, 2007, **25**, L35–L38.

31. A. M. Prenen, J. C. A. "Hans" van der Werf, C. W. M. Bastiaansen and D. J. Broer, *Adv. Mater.*, 2009, **21**, 1751–1755.

32. S. Zheng, H. Lin, J.-Q. Liu, M. Balic, R. Datar, R. J. Cote and Y.-C. Tai, *J. Chromatogr. A*, 2007, **1162**, 154–161.

33. S. Zheng, H. K. Lin, B. Lu, A. Williams, R. Datar, R. J. Cote and Y.-C. Tai, *Biomed. Microdevices*, 2011, **13**, 203–213.

34. R. A. Harouaka, M.-D. Zhou, Y.-T. Yeh, W. J. Khan, A. Das, X. Liu, C. C. Christ, D. T. Dicker, T. S. Baney, J. T. Kaifi, C. P. Belani, C. I. Truica, W. S. El-Deiry, J. P. Allerton and S.-Y. Zheng, *Clin. Chem.*, 2014, **60**, 323–333.

35. D. L. Adams, P. Zhu, O. V. Makarova, S. S. Martin, M. Charpentier, S. Chumsri, S. Li, P. Amstutz and C.-M. Tang, *RSC Adv.*, 2014, **9**, 4334–4342.

36. E. Kim, Y. Xia and G. M. Whitesides, *J. Am. Chem. Soc.*, 1996, **118**, 5722–5731.

37. Y. Tang, J. Shi, S. Li, L. Wang, Y. E. Cayre and Y. Chen, *Sci. Rep.*, 2014, **4**, 6052.

38. M. Bikel, P. Z. Çulfaz, L. A. M. Bolhuis-Versteeg, J. G. Pérez, R. G. H. Lammertink and M. Wessling, *J. Membr. Sci.*, 2010, **347**, 93–100.

39. M. Gironès, I. J. Akbarsyah, W. Nijdam, C. J. M. van Rijn, H. V. Jansen, R. G. H. Lammertink and M. Wessling, *J. Membr. Sci.*, 2006, **283**, 411–424.

40. E. J. Vriezekolk, A. J. B. Kemperman, M. Gironès, W. M. de Vos and K. Nijmeijer, *J. Membr. Sci.*, 2013, **446**, 10–18.

41. H. Cho, J. Kim, H. Park, J. Won Bang, M. Seop Hyun, Y. Bae, L. Ha, D. Yoon Kim, S. Min Kang, T. Jung Park, S. Seo, M. Choi and K.-Y. Suh, *Nat. Commun.*, 2014, **5**, 3137.

42. A. Meunier, J. A. Hernández-Castro, K. Turner, K. Li, T. Veres and D. Juncker, *Anal. Chem.*, 2016, **88**, 8510–8517.

43. C. A. Schneider, W. S. Rasband and K. W. Eliceiri, *Nat. Methods*, 2012, **9**, 671–675.

44. Y. Liu, W. Wang, W. Wu, F. Yang, W. Wang and H. Li, in 2015 Transducers - 2015 18th International Conference on Solid-State Sensors, Actuators and Microsystems (TRANSDUCERS), 2015, pp. 1767–1769.

45. M. Geissler, K. Li, X. Zhang, L. Clime, G. P. Robideau, G. J. Bilodeau and T. Veres, *Lab. Chip*, 2014, **14**, 3750–3761.

46. T. F. Didar, K. Li, M. Tabrizian and T. Veres, *Lab. Chip*, 2013, **13**, 2615–2622.

47. L. Malic, X. Zhang, D. Brassard, L. Clime, J. Daoud, C. Luebbert, V. Barrere, A. Boutin, S. Bidawid, J. Farber, N. Corneau and T. Veres, *Lab. Chip*, 2015, **15**, 3994–4007.

48. V. Chan, M. B. Collens, J. H. Jeong, K. Park, H. Kong and R. Bashir, *Virtual Phys. Prototyp.*, 2012, **7**, 219–228.

3.7 Supplementary information

3.7.1 Characterization of the bead populations

The characterization of the beads was performed using a Millipore Scepter Automated Cell Counter, which yields information regarding the size of a population of cells or beads. We were particularly interested in the characteristics of the 8.27 µm beads, since approximately only 40% of them were captured during our bead isolation experiments. The graphs in Figure S3-1 show the results obtained from these measurements.

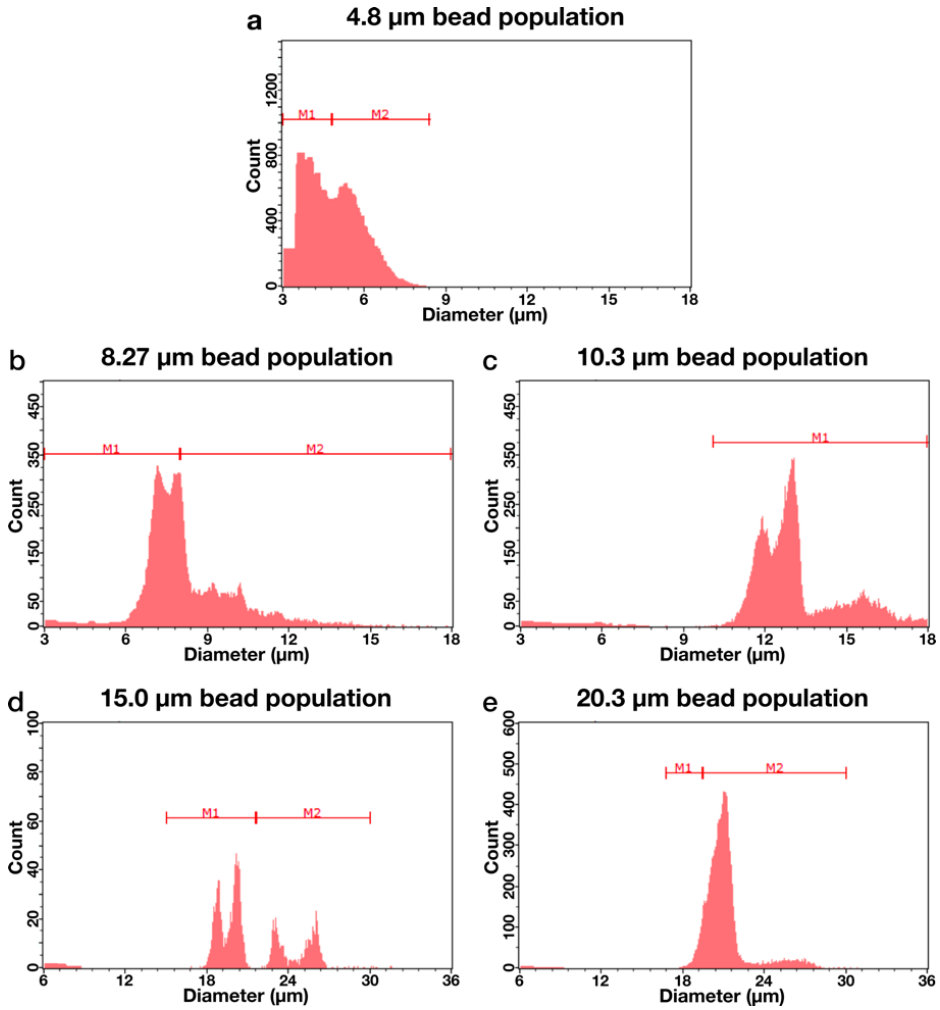

Figure S3-1 | Bead population analysis results. (a) Population of the 4.8 µm beads used as background for all the experiments, approximately 65% of the beads have a diameter < 5 µm (M1), while the rest are between 5 and 8.5 µm. (b) In the case of the 8.27 µm beads, approximately 60% of them were smaller than 8 µm (M1), while the rest were larger (M2), this helps explain the capture rates obtained in the bead isolation experiments. (c) and (d) For the 10.3 and 15.0 µm beads, respectively, close to 99% of the beads

counted had a diameter larger than 10 or 15 µm. (E) Finally, in the case of the 20.3 µm beads, approximately 96% of them were bigger than 20 µm (M2).

3.7.2 Additional examples of large-area, thin, open-through hole membranes fabricated using VAUM

Using the VAUM method, we were also able to fabricate membranes with various geometric characteristics, such as membranes as thin as 9.3 µm with pores as small as 3.2 µm, as well as membranes with higher porosity (≈ 60%).

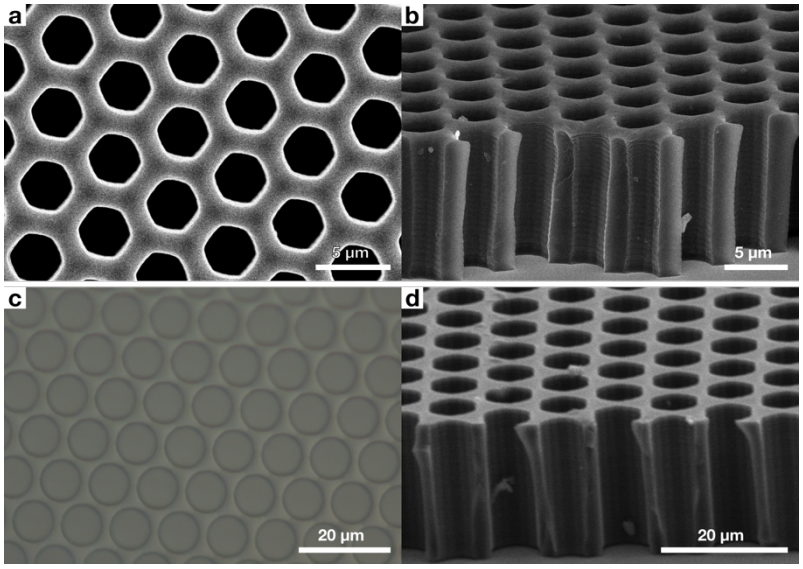

Figure S3-2 | Optical and SEM pictures of different membranes fabricated using VAUM in MD 700. (a) and (b) show SEM images of a membrane with pores of about 3.2 µm in diameter and a thickness of just 9.3 µm. The slightly hexagonal shape of the pores is a defect introduced during the photolithography process. It can be clearly seen that the pores are open-through. (c) and (d) show pictures of a high porosity membrane (≈ 60%) with pores of 8 µm in diameter fabricated in MD 700.

3.7.3 Cell viability

For control experiments, MDA-MB-231 cells were harvested from flasks and cultured in Petri dishes overnight. For positive controls, cells were kept alive in their culture medium in the incubator. For negative controls, just prior viability assay, dead cells were prepared by incubation in 70 % methanol during 45 minutes.

Cells were washed with PBS then stained by incubation in the staining solution consisting in 4.0 µmol L-1 of EthD-1 and 2.0 µmol L^{-1} of calcein AM diluted in PBS, during 45 minutes at room temperature. Viability was determined using fluorescence

microscopy on 10 images per samples and averaged on three replicated experiments (Excitation/emission wavelengths: 485/530 and 530/645 nm for calcein AM and EthD-1 respectively.) Cell viability was found to be 96.5 ± 0.9 %, highlighting the non-toxicity of the filter and that the filtration conditions are soft enough to maintain cells alive.

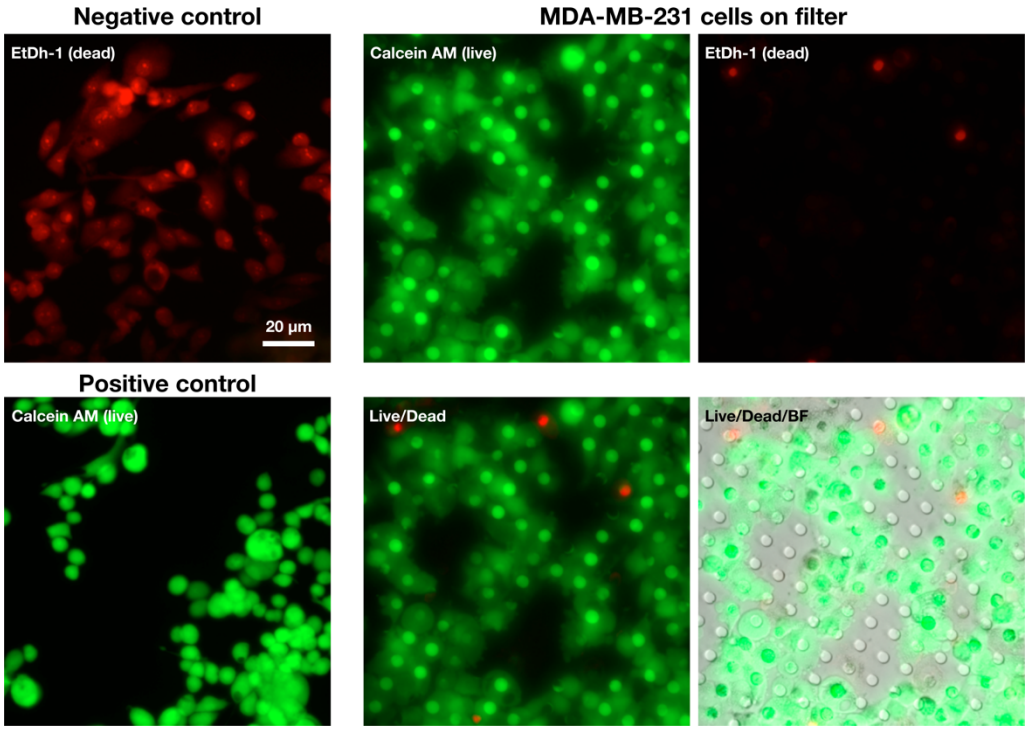

Figure S3-3 | Cell viability after filtration. Representative images of dead (negative control) and live (positive control) MDA-MB-231 cells. Cells for controls were cultured overnight in Petri dishes. Dead cells were prepared by incubation 30 minutes in 70 % methanol. Viability of captured cells was determined after filtration, directly on filter. All cells were stained with calcein AM (green, live cells) and EthD-1 (red, dead cells).

PREFACE TO CHAPTER 4

In Chapter 3, we showed a successful, reliable, and novel fabrication method for large-area, high porosity polymer membranes with a regular pore distribution. We showed that they could be efficiently used to separate mixtures of two or three different microbeads, as well as for the efficient capture of cancer cells in buffer solutions. The membranes were further used in CTC isolation experiments in healthy and patient blood samples, as presented in Appendix I.

In this chapter, we present a modification of the original vacuum-assisted polymer microfilter fabrication method to produce submicron-porous filters, we successfully made membranes with pores as small as 500 nm with the purpose of capturing populations of WBCs for a sample preparation method for downstream cell analysis. Current gold standard WBC isolation methods rely on several centrifugation and resuspension steps that have been tied to cell loss and damage, as well as wide inter-user result variability.

We achieved fabrication of theses membranes with regular submicron-pore distribution, in large area, and with enough mechanical stability to allow fast flow rates (6 mL/min) without breaking. We integrated these filters into 3D-printed microfluidic devices and used them for the high efficiency capture, multi-step staining, and release of WBCs from healthy blood samples.

These new polymer submicron filters have high potential of being used in the future as part of a minimal residual disease (MRD) diagnostic tool, and we're currently also planning their use for selective capture of lymphocytes for a rapid and inexpensive platform for CD4:CD8 ratio measurement.

The following manuscript has been published as a *Research Article* in ***Lab on a Chip***. It was highlighted in the back cover of Issue 4 in 2019.

CHAPTER 4 | TWO-LEVEL SUBMICRON HIGH POROSITY MEMBRANES (2LHPM) FOR THE CAPTURE AND RELEASE OF WHITE BLOOD CELLS

J. Alejandro Hernández Castro,[1,2,3] K. Li,[1] J. Daoud,[1] D. Juncker,[2,3,4] and T. Veres[1,2]

[1]National Research Council of Canada, 75 de Mortagne Boulevard, Boucherville, Québec, Canada J4B 6Y4.

[2]Biomedical Engineering Department, McGill University, 3775 University Street, Montréal, Québec, Canada H3A 2B4.

[3]McGill University and Génome Québec Innovation Centre, McGill University, 740 Dr. Penfield Avenue, Montréal, Québec, Canada H3A 0G1.

[4]Neurology and Neurosurgery Department, McGill University, 3801 University Street, Montréal, Québec, Canada H3A 2B4.

4.1 Abstract

A method by modifying vacuum assisted UV micro-molding (VAUM) process is proposed for the fabrication of polymer two-level submicron high porosity membranes (2LHPM). The modified process allows for the fabrication of robust, large-area membranes over 5×5 cm^2 with a hierarchical architecture made from a 200 nm-thick layer having submicron level pores (as small as 500 nm) supported by a 20 µm-thick layer forming a microporous structure with 10–15 µm diameter pores. The fabricated freestanding membranes are flexible while mechanically robust enough for post manipulation and filtration of cell samples. Very high white blood cell (WBC) capture efficiencies (≈97%) from healthy blood samples after red blood cell (RBC) lysis are demonstrated using a 3D-printed filter cartridge incorporated with these 2LHPM. A high release efficiency of ≈95% is also proved using the same setup. Finally, on-filter multistep immunostaining of captured cells is also shown.

4.2 Introduction

White blood cell (WBC) separation and isolation from peripheral blood (PB) is the precursor to many downstream analytical assays. The isolation and counting of WBCs finds many applications in disease diagnosis, including infection, myeloma, lymphoma, leukaemia, as well as for HIV/AIDS diagnostics.[1–4] To isolate WBCs, conventional methods involve density gradient centrifugation or red blood cell (RBC) depletion.[5–10] Subsequent WBC manipulation is then required to prepare samples for specific analyses, often resulting in undesired cell loss or damage. Numerous cell sample preparation methods and platforms have been introduced for a variety of applications including nucleic acid extraction, fluorescent cell labelling, and flow cytometry, amongst many others.[11–19] WBC capture rates as high as 90% have been reported in some of these methods, but downstream flow cytometry analysis still remains the gold standard in the clinic and sample preparation for it is the goal of most of these methods, however, they are limited by slow flow rates ($<$ 20 µL/min), the capacity to only process very small volumes of blood ($<$ 10 µL, while minimum recommended sample volumes for flow cytometry are typically around 300 µL in a concentration of 1000 cells/µL), or the inability to perform on-chip staining of cells for further downstream analysis.[20]

Some important prerequisite for most WBC sample preparation involves efficient (i) WBC capture/recovery and (ii) buffer exchange. This allows for effective cell washing, fluorescent labelling, as well as other processes such as lysis for nucleic acid or protein isolation. Standard methods for cell capture/recovery and buffer exchange are performed using centrifugation for cell pelleting, followed by resuspension in desired buffers. However, the use of centrifugation risks cellular damage and results can be highly variable depending on user expertise.[21] This results in cell loss during manual pipetting which adversely affects inter-assay reproducibility. In addition, WBC extracted from other media such as bone marrow (BM) or cerebral spinal fluid (CSF) require additional sample preparation steps to correct for viscosity prior to centrifugation. This presents additional

limitations when attempting to avoid any loss of rare cells-of-interest, such as leukemic cells from BM, or extremely minute WBC numbers from CSF (as low as 1 cell/µL) for cancer diagnostics. These limitations, such as the requirement for large sample volumes, high reagent consumptions, cross contamination of samples, and expensive equipment cost hinder their deployment in more novel applications.

To address these limitations, various efforts have been made to conceive more efficient WBC sample preparation technologies in miniaturized microfluidic platforms. The advantages and technical challenges of microfluidic platforms for cell isolation and downstream analysis in general have been well addressed in several recent review articles.[22–25] A popular approach involves the magnetic capture of total or subsets of WBCs using antibody-modified magnetic beads.[26] Captured WBCs may then be eluted or lysed using an appropriate buffer. However, this technique relies on label-dependent capture, with efficiency correlated with antibody activity. In addition, purified cell populations are subjected to harsh elution buffer conditions. A widely-used label-free approach involves the use of microporous membranes for size-based cell capture, recovery, and perfusion of buffers. This can be accomplished through manual filtration through polymer mesh networks.[27,28] These gentle filtration methods result in enriched and post-processed WBCs without any significant damage. However, micron-sized polymer meshes are prone to deformation and, coupled to manual filtration, often result in sub-optimal capture and recovery rates.

Herein, the use of two-level submicron high porosity membranes (2LHPM) for WBC isolation, buffer exchange, and sample preparation for downstream assays is proposed. This circumvents the need for several centrifugation/resuspension steps, as well as manual pipetting of supernatant for buffer exchange. Currently there are many different types of microfilters (MFs), several drawbacks render their utility challenging. MFs based on silicon[29–33] and polymers[34–36] can be fabricated precisely; however, the fabrication processes are proved to be cumbersome since they require the use of clean room equipment

like a mask aligner every time for fabricating each new membrane. Silicon MFs are also quite brittle and cannot withstand high pressure flow rates, they are also opaque. Parylene-C, polymer meshes, and SU-8 polymer membranes are auto-fluorescent, making it difficult for fluorescent imaging applications. Moreover, although polymer track-etched MFs are available commercially, they suffer from low porosity which in turn limits filtration flow rates,[37,38] therefore limiting the throughput.

To address the aforementioned limitations, a two-level submicron high porosity membranes (2LHPM) structure has been fabricated using a modified version of our previously published, robust, low-cost, and scalable vacuum assisted UV micro-molding (VAUM) fabrication process.[39] UV-curable polymers are utilized that allow for fabrication of transparent MFs possessing large areas, with high porosity, and with pores as small as 0.5 µm. Herein we are demonstrating the use of the two-level submicron high porosity membranes for WBC capture from small volume of blood using a perfusion-based microfiltration apparatus. Subsequent buffer exchange and cell release are also performed to demonstrate utility as a sample preparation system for downstream bioanalytical assays.

4.3 Materials and methods

4.3.1 Chemicals

All solutions were prepared with deionized water from a Milli-Q system (resistivity of 18 MΩ cm; Millipore, Burlington, MA). Phosphate buffered saline (PBS, 1×, pH 7.4), from Fisher Scientific (Hampton, NH), contains 11.9×10^{-3} mol/L of phosphates, 137.0×10^{-3} mol/L of sodium chloride and 2.7×10^{-3} mol/L of potassium chloride. Ethylenediaminetetraacetic acid (EDTA) and bovine serum albumin (BSA) were obtained from Sigma-Aldrich (St. Louis, MO). Paraformaldehyde were purchased from Fisher Scientific. SuperBlock PBS, and 4',6-diamidino-2-phenylindole (DAPI) were purchased from Life Technologies (Carlsbad, CA, USA).

AZ 5214 photoresist (AZ Electronic Materials USA Corp., Somerville, NJ) was used for all photolithographic work. UV-curable resin was prepared by mixing Ebecryl® 3708 (Allnex Canada Inc., ON, Canada) with tripropylene glycol diacrylate (TPGDA) from Allnex Canada Inc. in a ratio (weight) of 7:3, Darocur® 1173 (BASF Corporation, Vandalia, IL) was added as a photoinitiator in 1% w/w. UVA 1534 UV-curable resin was prepared by mixing Uvacure 1500 (Allnex Canada Inc.) and Capa™ 3050 (Perstorp, Sweden) in a 1:1 ratio, and Uvacure® 1600 (Allnex Canada Inc.) in 1% w/w was added as a photoinitiator.

Trichlorol(1H, 1H, 2H, 2H)-perfluorooctyl-silane (97%) (Sigma-Aldrich, Oakville, ON) was used for all surface silanization protocols.

Fluorolink® MD700 (Solvay Specialty Polymers USA LLC, Alpharetta, GA) UV-curable resin mixed with 2% w/w of Darocur® 1173 was used as the building material for the polymer membranes, it has a Young's modulus of approximately 10 MPa.[40]

4.3.2 Si master mold fabrication

Si micropillar array master molds were prepared for different membrane designs (e.g. different pore size, footprints). AZ 5214 photoresist was spin coated at 2400 rpm for 72 s on blank Si wafers. A soft bake at 110 °C for 1 min was followed by the UV exposure of the desired pattern at 1250 mJ/cm^2. Developing was done in AZ 300MIF, and the final hard bake was done at 120° C for three hours.

The exposed pattern was etched into the Si substrate via deep reactive ion etching (DRIE) (Oxford Instruments PlasmaLab System 100). Si pillar array structures with height of approximately 30 µm were fabricated. After etching, the wafers were thoroughly cleaned by washing them with acetone and isopropyl alcohol (IPA) before drying them under a stream of nitrogen.

A master mold with an array of 500 nm pillars in hexagonal lattice on a 4-inch Si wafer (with pitch size of 1.5 µm) with a pillar height of 1 µm was ordered from EULITHA, it was fabricated by PHABLE™ (photonics enabler) technology. It is important to note

that in the process proposed herein, the Si master molds only need to be fabricated once and are then replicated in flexible UV-cured polymers (Ebecryl® 3807 or UVA 1534).

4.3.3 Filter cartridge design and fabrication

The filter cartridge was designed with Autodesk Inventor 2017 software and fabricated by 3D-printing (Formlabs Form 2) using their proprietary White resin. The cartridge consists of two parts (top and bottom) that are clamped together using four screws and bolts.

The top section of the cartridge has two ports for tubing connection that lead to internal channels of 0.5 mm in diameter. It also has a 4-mm diameter opening in the middle, which defines the effective filtration area of the device, a small piece of transparent COC plastic (140 µm thick) is glued on the top of the cartridge as a cover. The bottom section contains a single port, a recess for the placement of an O-ring used for sealing the chip, and a 4-mm diameter opening sealed in the same way as the top part.

During assembly of the chip, once the filter membranes are placed in the central recess of the top piece, an O-ring is placed in the recess of the bottom one, the pieces are sandwiched together and the chip is closed using screws and bolts distributed along the corners of the chip.

4.3.4 WBC isolation from blood samples

Blood samples from healthy donors were purchased from Innovative Research (Novi, MI). WBCs for the capture rate comparisons were extracted by density gradient centrifugation, resuspended and diluted in a 2 mM EDTA in PBS solution. WBCs were obtained this way for the capture benchmark experiments to avoid confounding effects from the presence of RBCs or platelets in the cell solution.

For the rest of the experiments, fresh blood samples from finger prick draws were used. 100 µL of blood were obtained from a healthy volunteer, the blood was immediately diluted in 100 µL of 2 mM EDTA in PBS to avoid clotting of the sample. Small blood volumes were used since the fabricated device has a relatively small active filtration area,

and membrane clogging was to be avoided. The RBCs were lysed by adding a RBC lysis buffer (Pluriselect, Leipzig, Germany), used as per supplier protocols. Briefly, whole blood was incubated with 1× RBC lysis buffer (1 mL of lysis buffer per 100 µL of blood) for 15 min at 4° C. The solution was then centrifuged to pellet the WBCs and remove RBC debris. WBCs were then resuspended in PBS buffer and quantified using a hemocytometer. It is important to note that this final centrifugation step was done to remove the lysis buffer while the cell counting was being performed to avoid prolonged exposure of WBCs to the lysis solution. Direct filtration of the cell solution after RBC lysis without prior centrifugation is possible, cell debris flows through the pores and buffer exchange can be done on-chip (Figure S4-3).

4.3.5 Cell staining

Fluorescently labelled antibodies against CD3 (ab106224), CD4 (ab18282), and CD8 (ab28010) were ordered from Abcam. The anti-CD3 is tagged with Allophycocyanin (APC), with excitation and emission at 652 and 657.5 nm, respectively. Anti-CD4 is tagged with Phycoerythrin (PE), with excitation and emission at 565 and 573 nm, respectively. Anti-CD8 is tagged with fluorescein isothiocyanate (FITC), with excitation and emission at 495 and 519 nm, respectively.

4.3.6 Fluorescence microscopy

Cell imaging was done with an inverted microscope (Eclipse Ti-E, Nikon) connected to a CCD camera (iXon Ultra, Andor), fluorescence imaging was performed using an LED illumination system (X-Cite 120LED, Excelitas Technologies). Images were recorded with the NIS-Elements Advanced Research software (Nikon) and analysed with the ImageJ software.[41]

4.3.7 On-filter cell counting

Automated cell counting of the cells on the membrane surface was performed using the CellProfiler analysis software (Broad Institute, Cambridge, MA).

4.4 Results and discussion

4.4.1 Vacuum-assisted UV micro-molding fabrication process of 2LHPM

We previously presented the VAUM fabrication protocol (Figure S4-1) for the production of polymer microfilters.[39] It works well for the fabrication of microfilters with pores as small as 3.2 µm in diameter. However, fabrication of filters with pores below 3 µm according to this same protocol proved to be too challenging for a couple of reasons. First of all, the mask aligner that we have access to is not good enough to make features smaller than 3 µm; secondly, to achieve a good replication of the smallest features we could attain in our facilities, we use a photolithography process with a very thin film of photoresist, which limits the etch depth that can be achieved by DRIE in the Si etching process, and the thinner the molds are, the harder they are to be filled with the resin, due to the increased hydrodynamic resistance of the filling path; and last but not least, thinner membranes are more fragile and harder to manipulate.

It has been shown that hierarchical architectures can be used to provide mechanical stability of thin porous membranes,[40] taking this into consideration, we decided to modify our previous protocol to include a patterned cover instead of a flat cover, to create a two-level architecture combining micropores and submicron pores (Figure 4-1). The preparation of a submicron-patterned cover is critical for the fabrication of the 2LHPM, they are replicated in a similar way as the underlying micropillar array (and as presented before[39]), the differences lie in the material used for each array, and the fact that the cover is only partially cured to ensure that the micro and submicron pillars bond together after the mold assembly and curing without destroying the submicron features on the cover.

Fabrication of these two-level membranes with pores as small as ≈ 500 nm in diameter was successful using this modified process (Figure 4-1b and c). The submicron

pillar array on the cover was designed to be a continuous array covering an area of 51×51 mm^2, to avoid the need of precise alignment of the top and bottom sections of the mold.

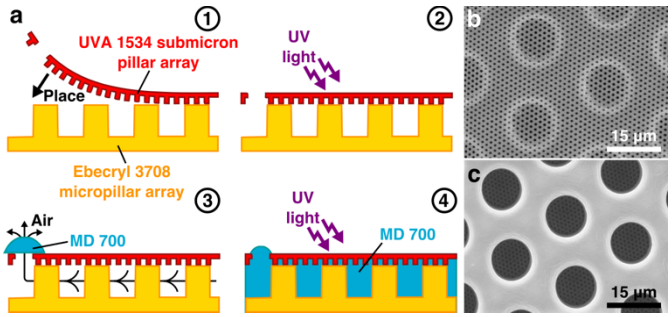

*Figure 4-1 | **Modified VAUM process for the fabrication of 2LHPM**. (a) The main difference to the previous protocol is the introduction of a cover patterned with a submicron pillar array instead of a flat cover (steps 1-2), followed by a vacuum-assisted filling process as before (steps 3-4). (b and c) Top and bottom SEM images of a 2LHPM fabricated with the proposed method. Submicron features can be seen along the entirety of the top surface, but open-through submicron pores only exist within the underlying micropores.*

4.4.2 Filter flow cells

To use the 2LHPM, both for the capture and release of cells, the fabrication of a cartridge or flow cell filter carrier was necessary, which would provide the necessary channels and inlets/outlets to flow solutions through the membranes, and to recover the captured cells afterwards.

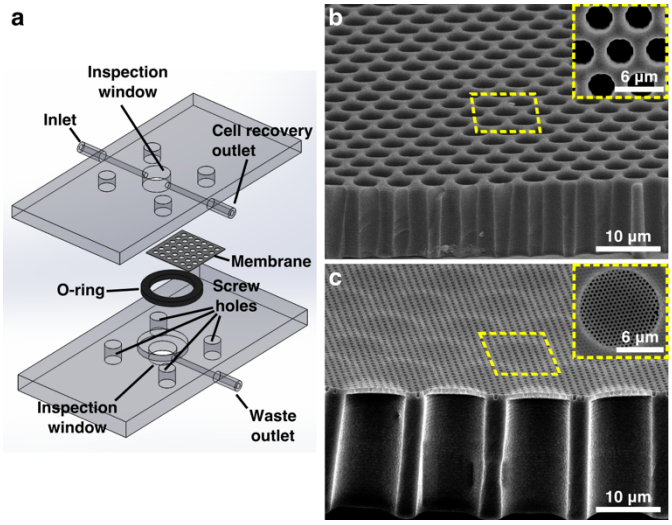

*Figure 4-2 | **The 3D-printed cartridges and membranes used**. (a) 3D exploded view of the filter cartridge, the membranes are sandwiched between the two 3D-printed parts and an O-ring, which is necessary to avoid leakages. (b and c) SEM images of the two different membrane types tested, one with 3.2 µm pores*

(b), and the new 2LHPM, with 0.5 µm pores (c), the insets show a close-up of the membrane surface for each case.

A cartridge in a simple design (Figure 4-2a) was printed using a stereo-lithography 3D printer (FormLabs Form2). The top part of the cartridge has two connections and channels, this allows the use of one of them as the inlet through which all solutions will be introduced to the chip, and the other one as an outlet that allows the creation of a lateral flow on the surface of the membranes to facilitate complete release of the captured cells during the cell recovery process.

4.4.3 White blood cell capture/release efficiencies and downstream analysis

WBC solutions were prepared by isolating them from healthy blood samples via gradient centrifugation separation, the cells were resuspended in 1 mL of a solution of 2 mM EDTA in PBS and stained by adding 5 µL of DAPI and incubating for ≈ 30 min in a rotary mixer.

The chips were assembled as shown in Figure 4-2a, and they were filled and incubated with SuperBlock™ (PBS) Blocking Buffer for 2 h. Incubation was performed at 4° C to avoid the formation of bubbles in the tubing due to evaporation.

It is known that WBCs are highly flexible and can squeeze through small constrictions, and we've also observed in previous studies using our fabricated polymer membranes with 8 µm pores[42] that, even though some WBCs are retained in these membranes, the larger portion of them goes through the filters. Our goal here was to have a platform in which we could capture as much of the cells in a sample as possible, so membranes of pores < 8 µm were needed.

We decided to test the newly fabricated 2LHPM against our other membranes with the smallest pore size made at the time (3.2 µm), we expected to have a higher capture rate using the 2LHPM membranes, since some of the cells might still be able to go through the 3.2 µm holes. We also benchmarked our in-house membranes against commercially available PluriStrainer® filters (PluriSelct, 8912 Bancroft Drive, 91977, San Diego, USA), made from a polyethylene terephthalate (PET) woven mesh with three different pore sizes

(1, 5, and 10 µm). The cell solution was then flowed through the membranes at a flow rate of 0.1 mL/min using a syringe pump. Results from these experiments showed that the 2LHPM were indeed significantly better than all other filters tested for the isolation of WBCs (Figure 4-3b). All capture rates were calculated by comparing hemocytometer cell counts of cell solutions before filtration and of the waste solutions obtained from the filtration cartridge.

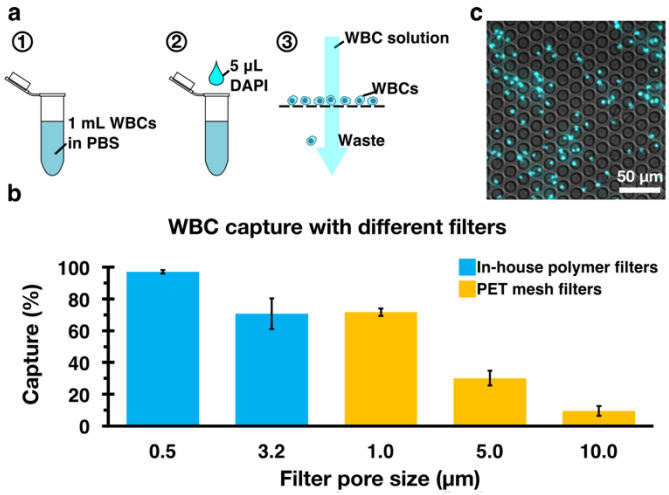

*Figure 4-3 | **WBC capture comparison of filters with different pore size**. (a) Cell filtration protocol schematic. The cells are isolated and resuspended (step 1), they are then stained with DAPI to ease their counting (step 2) before they're flowed through a filter membrane (step 3). For 2LHPM, we ensured the cells were in contact with the submicron porous region first, to avoid the cells to stack in the well-like structures created from the two-level architecture. (b) Capture rate comparison between two types of membranes tested, 2LHPM showed a capture rate of ≈ 97%, while the 3.2 µm pore microfilters had a ≈ 71% capture rate. The best performing PET mesh filter only achieved ≈ 72% isolation efficiency. Error bars are SD, n = 4. (c) Representative image of cells captured on the surface of the 2LHPM. Some DAPI-stained cells can be seen right above the spaces where the micropores are, meaning the cells sit on the submicron porous sections of the membranes.*

As expected, the use of membranes with submicron pores yields a higher capture rate compared to the one obtained with 3.2 µm pore membranes, the capture rate difference, 97.2 ± 1.1% (2LHPM) vs. 70.7 ± 9.6% (3.2 µm pores) is large enough to justify the use of the new 2LHPM for the capture of full populations of WBCs from solution. This difference is approximately the same compared to a PET mesh with 1 µm pores (71.7 ± 2.4% capture rate), the reduced capture efficiency of these filter types can be attributed to the PET mesh construction characteristics (Figure S4-2). Our membranes are

transparent and not auto-fluorescent, allowing the observation and some analysis of the cells while they sit on the filter surface. It is important to capture the WBC cells on a microfilter in an efficient way, but it is equally important and more interesting to release the captured cells for upstream analysis, which could provide more information on the population of isolated cells.

We tested the ability of our setup to perform capture and release of WBCs from fresh blood samples. Cells were extracted from finger prick draws as described above, for these experiments, they were resuspended in 1 mL of 4% PFA PBS to fix them, this was necessary to keep the cell samples for further analysis in a different day. After resuspending the cells, 5 µL of DAPI were added to the sample and incubated for ≈ 1 h in a rotary mixer. The cells were then spun down at 500 g for 10 min to remove the solution containing the PFA and DAPI, and the cells were finally resuspended in 1 mL of PBS (Figure 4-4a).

The cells from this final solution were counted with a hemocytometer, finding that approximately 230 thousand cells were in the sample. Ten 100 µL aliquots were prepared from this cell solution and diluted to 500 µL each, five of them would be processed through the 2LHPM filter setup, and the other five ones wouldn't, to be able to have a comparison point between the recovered cell solutions and the original cell sample.

Filtration is performed as described previously, at a flow rate of 0.1 mL/min with the help of a syringe pump, the filter surface was imaged under the fluorescence microscope while the cell solution was flowing through the membrane, to verify that the cells were being captured as expected. Cells were steadily deposited on the microfilters, as shown in Figure 4-4b. A 1 mL PBS wash was flowed at the same flow rate after the cell filtration.

To release the cells from the 2LHPM surface, a combination of a lateral and perpendicular flows was used (Figure 4-4a step 6). 0.5 mL of PBS were flowed in each direction at a rate of 6 mL/min to lift the cells from the filters, the recovered cell solutions were centrifuged at 500g for 10 min to remove 500 µL of the solution and to have the

same liquid volume in the non-filtered and the recovered samples. Several images of the membrane surfaces were taken before and after running the cell release process (Figure 4-4b). A clear reduction in the number of cells remaining on the filters after release can be observed under the fluorescence microscope, however, a more precise quantification is necessary to assess the cell recovery efficiency. Since the number of cells on the membranes before release is too high to count manually, we decided to use an image analysis software to do the counting instead.

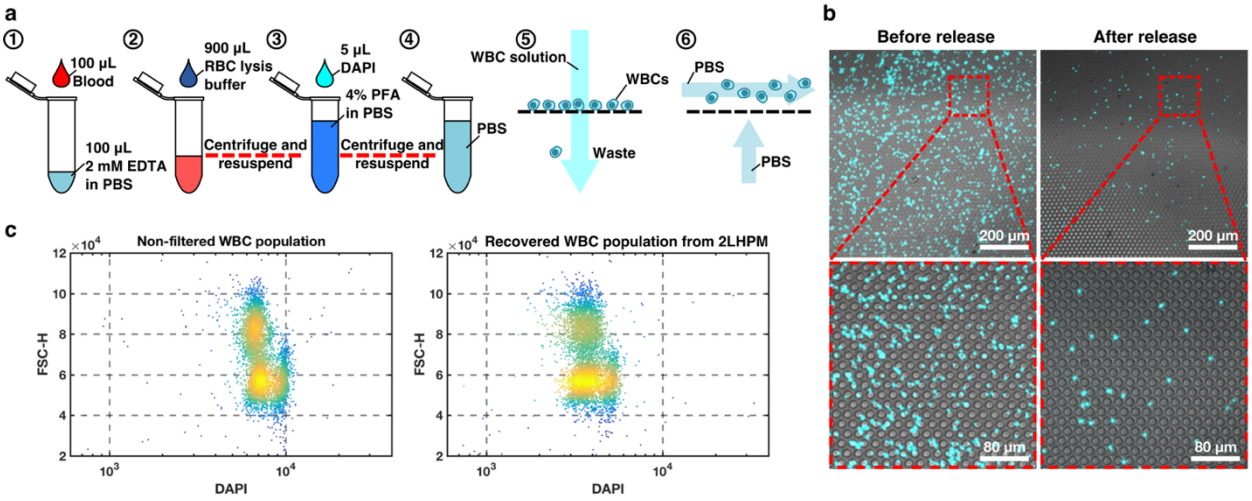

*Figure 4-4 | **WBC capture and release characterization on the 2LHPM**. (a) WBC extraction, capture, and recovery protocol schematic. A finger prick blood sample is diluted and the RBCs are lysed (steps 1 -2), after lysing, the sample is centrifuged to remove the lysis buffer and fix the cells in a 4% PFA suspension (step 3), the cell nucleus is stained with DAPI before removing the PFA containing solution and resuspending the cells in PBS (step 4). The cells are then flowed through the 2LHPM (step 5), and retrieved by using simultaneous parallel and perpendicular flows (step 6). (b) Cells were imaged on-filter in a fluorescence microscope, images of the cells sitting on the membranes' surface before and after running the cell release process were taken, a clear reduction in the number of cells can be observed after cell recovery. Image analysis measurement of the number of cells before and after release show a release efficiency of ≈ 95.5%. (c) Representative images of the flow cytometry analysis of the cell solutions from non-filtered and recovered samples. Both samples are very similar, the recovered samples have a reduced fluorescence signal (left shift), which was expected since these samples were exposed to light for a significant time while the capture experiments were running, while the non-filtered samples were not.*

Fluorescence images of the cells on the membranes' surface before and after release from five independent experiments were analysed using CellProfiler to find out the efficiency of the release protocol. All images were analysed using the same parameters.

According to the cell counts obtained by the image analysis process, an average recovery of approximately 95.5 ± 2.0% was achieved, which means that we can effectively recover 92.8% of all the cells in the original suspension using the proposed method for their capture and release. However, it could still be possible that cells could be lost by non-specific adsorption on the walls of the chip or the tubing while running the experiments.

To verify if there was a large discrepancy between the recovered cell samples and the original one, we decided to run the non-filtered cells and the retrieved ones in a flow cytometer (BD FACSCanto II), to analyze the characteristics of both populations. All flow cytometry tests ran for 1 min 50 s, so that the same volume was analyzed for every sample. From these experiments, we found an average of 5962 ± 589 cells in the non-filtered samples, and 5821 ± 361 cells for the recovered solutions, furthermore, the scatter plots (Figure 4-4c) from these measurements show that the size distribution for the samples analysed are almost identical. The only observable difference between the two populations lies on the intensity of the fluorescence signal detected, which was lower for the recovered cells, this was expected due to bleaching that might have occurred while the cells were inspected under the microscope while the capture and release experiments were being performed.

The flow cytometry experiments show that the non-filtered and recovered samples are virtually the same in terms of cell size distribution and concentration (cells/mL), which confirm the success of the proposed platform for efficient capture and release of a complete population of cells.

Finally, a multi-step on-filter staining protocol was evaluated using the proposed setup, to highlight the possibility of using the 2LHPM as an alternative sample preparation method for immunostaining of cells without the need of several centrifugation and resuspension steps.

The WBC capture protocol used was the same as presented before, cells were extracted from finger prick whole blood samples, the RBCs were lysed, and the nucleated cells were stained with DAPI before filtration (Figure 4-5a). Once the cells were captured, three steps of staining and washing were performed to stain CD3, CD4, and CD8 surface markers. After the final wash, the cells were released as per the previously discussed protocol.

The released cells were imaged on the fluorescence microscope to verify that the cells had indeed been stained (Figure 4-5b). As observed from these images, some of the cells express none, or one or more of the target surface markers. No fluorescent background was observed in any of the explored channels, confirming that the solutions containing the labeled antibodies were properly washed off after each staining step. The signals observed from the anti-CD3, -CD4, and –CD8 fluorophores are superposed to spots where DAPI-stained nuclei were observed, ensuring that the signals observed from these antibodies correspond to markers on the cells' surface and not just random agglomerations of antibodies.

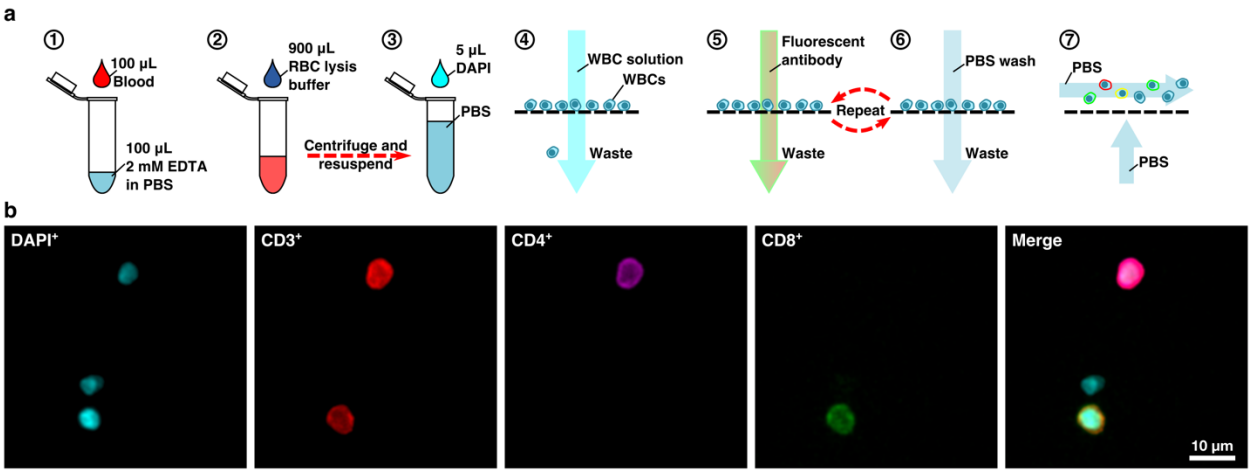

*Figure 4-5 | **Multiple on-filter staining of captured WBCs**. (a) WBC extraction, capture, and staining protocol schematic. A finger prick blood sample is diluted and the RBCs are lysed (steps 1 -2), after lysing, the sample is centrifuged to remove the lysis buffer and the cells are resuspended in 1 mL of PBS, the cell nuclei are stained with DAPI before flowing the sample through the 2LHPM (step 3). The cells are then flowed through the filter (step 4), after the cells have been captured, a solution containing fluorescently labelled antibodies is flowed through the cartridge (step 5), when the cartridge has been filled, the flow is stopped and, after a 20-min incubation time, a 2 mL PBS wash at 0.3 mL/min is performed (step 6), the staining and washing steps can be repeated several times. Finally, the cells are*

released using the same protocol explained above (step 7). (b) Fluorescence microscope images of cells released from the 2LHPM cartridge after 3 steps of on-filter staining (against CD3, CD4, and CD8 surface markers).

4.5 Conclusions

In summary, we have shown that a simple modification to our previously presented VAUM method allows for the fabrication of 2LHPM with pores as small as 0.5 µm over a 5×5 cm^2 area.

We designed and 3D-printed a simple cartridge to house the fabricated membranes. This chip includes all necessary channels to flow samples through the membranes, and allow introduction of lateral and backflows for a more efficient release of the cells captured on the surface of the 2LHPM. We've successfully used these submicron porous filters for efficient capture (≈ 97%) of full populations of WBCs. Compared to commercially available PET mesh filters (≈ 72% capture efficiency with 1 µm pores), we obtained significantly better performance.

WBCs obtained from a finger prick blood sample were isolated using our 3D-printed cartridge and 2LHPM. The recovery efficiency of these cells was analyzed by computer-assisted image analysis of pictures of the membranes' surface before and after running the release protocol, which showed a cell release efficiency of ≈ 95%. The cell populations from non-filtered and from the recovered samples were further analysed via flow cytometry, which showed that both populations had similar cell-size distributions.

On-filter multistep immunostaining of captured WBCs on the 2LHPM was also explored. We show that after arrest on the membranes, the buffers in the chip can be exchanged efficiently, allowing incubation with antibody solutions followed by a wash step, the staining efficiency was not yet optimized, which must be explored in the future in relation to specific applications. Cell staining with three different fluorescent antibodies followed by cell release is demonstrated, showing that a platform like the one suggested can be used to replace centrifuge-based protocols for cell staining if necessary. Cell

centrifugation has been linked to cell loss and damage, and the performance of these processes are known to be heavily user-dependent.

WBC isolation and separation holds great clinical importance for diagnosis of infectious disease and pathological conditions. This was the primary motivation behind the development of the perfusion-based microfiltration apparatus integrated with the 2LHPM membrane. This platform was employed for capture and release of WBCs from fresh blood samples, demonstrating exceptional recovery rates with high reproducibility. A protocol for WBCs isolation was also developed that circumvents the need for multiple centrifugation steps, which may result in stress-induced cell loss, further compromising downstream diagnosis and analysis. In addition, current protocols require a high degree of manual manipulation, which coupled with repeated centrifugation, adversely affect reproducibility, especially when processing small volumes.

The manipulation of microliter volumes in an automated fashion presents yet another application for the presented platform. This becomes even more relevant when probing rare cell populations, which typically require large sample volumes to yield significant cell populations amenable to centrifugation-based processing. Our platform remedies these shortcomings by controlling the capture area for rare cell populations, ensuring repeatable and automated high capture efficiency from small volumes. It also provides the foundational pre-requisites towards the development of a portable cell counting device. One particular application is rapid and less invasive cell-based clinical diagnoses – owing to the versatility of small sample volume processing. This may be applied to minute quantities of blood or bone marrow for identification of immature blast cells in minimal residual disease (MRD). This holds great importance for management of acute lymphoblastic leukemia (ALL), as some of the leukemic blasts are resistant to chemotherapy and can persist in very small amounts in the bone marrow and blood. Several studies have shown that the presence of detectable MRD at any stage of therapy can predict relapse in childhood and adult ALL. Therefore, it is critical to further develop

the technology for MRD detection from blood, as this process is less invasive than bone marrow biopsies. To do so, a high capture efficiency of WBCs must be coupled with a release efficiency, while minimizing cell loss, for downstream analysis. The results presented in this work lay the foundation for the development of such platform addressing, among other applications, MRD detection from blood.

Nevertheless, one drawback of having filters with such small pores is that capture of debris or background cells is highly possible, requiring a coarse sample pre-filtration step, or other form of sample preparation like RBC lysis, as we showed here.

4.6 Conflicts of interest

The authors state that there are no conflicts to declare for this work.

4.7 Ethical statement

Blood samples have been collected from healthy donors' participants that were fully informed regarding the purposes of the study and consent was obtained. All experiments performed in the study involving human samples were approved by McGill institutional ethics committee (IRB study #A05-M27-16B).

4.8 Acknowledgements

The authors acknowledge the support from National Research Council of Canada through Heath Technologies Program (Medical Devices) and Printable Electronics Flagship Program (Information and Communications Technologies). This research was also supported by NSERC, CONACyT, and McGill University BME Department.

References

1. J. J. M. van Dongen, V. H. J. van der Velden, M. Brüggemann and A. Orfao, *Blood*, 2015, blood–2015–03–580027.

2. U. Hassan, N. N. Watkins, B. Reddy Jr, G. Damhorst and R. Bashir, *Nat. Protoc.*, 2016, **11**, 714–726.

3. N. N. Watkins, U. Hassan, G. Damhorst, H. Ni, A. Vaid, W. Rodriguez and R. Bashir, *Sci. Transl. Med.*, 2013, **5**, 214ra170–214ra170.

4. U. Hassan, T. Ghonge, B. R. Jr, M. Patel, M. Rappleye, I. Taneja, A. Tanna, R. Healey, N. Manusry, Z. Price, T. Jensen, J. Berger, A. Hasnain, E. Flaugher, S. Liu, B. Davis, J. Kumar, K. White and R. Bashir, *Nat. Commun.*, 2017, **8**, 15949.

5. P. K. Dagur and J. P. McCoy, Curr. Protoc. Cytom. Editor. Board J Paul Robinson Manag. Ed. Al, 2015, **73**, 5.1.1–5.1.16.

6. C. Iliescu, G. Xu, E. Barbarini, M. Avram and A. Avram, *Microsyst. Technol.*, 2009, **15**, 1157–1162.

7. H. M. Ji, V. Samper, Y. Chen, C. K. Heng, T. M. Lim and L. Yobas, *Biomed. Microdevices*, 2008, **10**, 251–257.

8. X. Chen, D. F. Cui, C. C. Liu and H. Li, *Sens. Actuators B Chem.*, 2008, **130**, 216–221.

9. Y. Cheng, X. Ye, Z. Ma, S. Xie and W. Wang, *Biomicrofluidics*, 2017, **11**.

10. V. VanDelinder and A. Groisman, *Anal. Chem.*, 2007, **79**, 2023–2030.

11. M. J. Tomlinson, S. Tomlinson, X. B. Yang and J. Kirkham, *J. Tissue Eng.*, 2013, **4**, 2041731412472690.

12. N. J. Panaro, X. J. Lou, P. Fortina, L. J. Kricka and P. Wilding, *Biomol. Eng.*, 2005, **21**, 157–162.

13. M. Hosokawa, M. Asami, S. Nakamura, T. Yoshino, N. Tsujimura, M. Takahashi, S. Nakasono, T. Tanaka and T. Matsunaga, *Biotechnol. Bioeng.*, 2012, **109**, 2017–2024.

14. M. Hosokawa, H. Kenmotsu, Y. Koh, T. Yoshino, T. Yoshikawa, T. Naito, T. Takahashi, H. Murakami, Y. Nakamura, A. Tsuya, T. Shukuya, A. Ono, H. Akamatsu, R. Watanabe, S. Ono, K. Mori, H. Kanbara, K. Yamaguchi, T. Tanaka, T. Matsunaga and N. Yamamoto, *PLoS ONE*, 2013, **8(6)**, e67466.

15. M. Pødenphant, N. Ashley, K. Koprowska, K. U. Mir, M. Zalkovskij, B. Bilenberg, W. Bodmer, A. Kristensen and R. Marie, *Lab. Chip*, 2015, **15**, 4598–4606.

16. J. Zhang, D. Yuan, R. Sluyter, S. Yan, Q. Zhao, H. Xia, S. H. Tan, N. Nguyen and W. Li, *IEEE Trans. Biomed. Circuits Syst.*, 2017, **11**, 1422–1430.

17. H. Wei, in Studying Cell Metabolism and Cell Interactions Using Microfluidic Devices Coupled with Mass Spectrometry, ed. H. Wei, Springer Berlin Heidelberg, Berlin, Heidelberg, 2013, pp. 61–82.

18. J. K. S. Tan, S. Park, H. L. Leo and S. Kim, *IEEE Trans. Biomed. Circuits Syst.*, 2017, **11**, 1431–1437.

19. M. Borgatti, L. Altomare, M. Baruffa, E. Fabbri, G. Breveglieri, G. Feriotto, N. Manaresi, G. Medoro, A. Romani, M. Tartagni, R. Gambari and R. Guerrieri, *Int. J. Mol. Med.*, 2005, **15**, 913–920.

20. G.-H. Lee, S.-H. Kim, K. Ahn, S.-H. Lee and J. Y. Park, *J. Micromechanics Microengineering*, 2016, **26**, 013003.

21. M. Delahaye, K. Lawrence, S. J. Ward and M. Hoare, *Biotechnol. Bioeng.*, **112**, 997–1011.

22. C. M. Yousuff, E. T. W. Ho, I. Hussain K. and N. H. B. Hamid, *Micromachines*, 2017, **8**, 15.

23. C. W. S. Iv, C. D. Reyes and G. P. López, *Lab. Chip*, 2015, **15**, 1230–1249.

24. J. Wu, Q. Chen and J.-M. Lin, *Analyst*, 2017, **142**, 421–441.

25. A. Dalili, E. Samiei and M. Hoorfar, *Analyst*, 2018, **144**, 87–113.

26. S. Miltenyi, W. Müller, W. Weichel and A. Radbruch, *Cytometry*, 1990, **11**, 231–238.

27. D. Okuzaki, S. Kimura, N. Yabuta, T. Ohmine and H. Nojima, *BMC Clin. Pathol.*, 2011, **11**, 9.

28. L. Yu, P. Warner, B. Warner, D. Recktenwald, D. Yamanishi, A. Guia and A. Ghetti, *Cytom. Part J. Int. Soc. Anal. Cytol.*, 2011, **79**, 1009–1015.

29. L. S. Lim, M. Hu, M. C. Huang, W. C. Cheong, A. T. L. Gan, X. L. Looi, S. M. Leong, E. S.-C. Koay and M.-H. Li, *Lab. Chip*, 2012, **12**, 4388–4396.

30. H. J. Lee, J. H. Oh, J. M. Oh, J.-M. Park, J.-G. Lee, M. S. Kim, Y. J. Kim, H. J. Kang, J. Jeong, S. I. Kim, S. S. Lee, J.-W. Choi and N. Huh, *Angew. Chem. Int. Ed.*, 2013, **52**, 8337–8340.

31. J.-M. Park, J.-Y. Lee, J.-G. Lee, H. Jeong, J.-M. Oh, Y. J. Kim, D. Park, M. S. Kim, H. J. Lee, J. H. Oh, S. S. Lee, W.-Y. Lee and N. Huh, *Anal. Chem.*, 2012, **84**, 7400–7407.

32. Y. Koh, H. Kang, S. H. Lee, J.-K. Yang, J.-H. Kim, Y.-S. Lee and Y.-K. Kim, *Lab. Chip*, 2013, **14**, 237–243.

33. C. J. M. Rijn, W. Nijdam and M. Elwenspoek, *J. Dyn. Syst. Meas. Control-Trans. Asme - J DYN SYST MEAS CONTR*, 1995, 995–1000.

34. Y. Liu, W. Wang, W. Wu, F. Yang, W. Wang and H. Li, in 2015 Transducers - 2015 18th International Conference on Solid-State Sensors, Actuators and Microsystems (TRANSDUCERS), 2015, pp. 1767–1769.

35. T. Xu, B. Lu, Y.-C. Tai and A. Goldkorn, *Cancer Res.*, 2010, **70**, 6420–6426.

36. M. E. Warkiani, A. A. S. Bhagat, B. L. Khoo, J. Han, C. T. Lim, H. Q. Gong and A. G. Fane, *ACS Nano*, 2013, **7**, 1882–1904.

37. R. L. Fleischer, P. B. Price and E. M. Symes, *Science*, 1964, **143**, 249–250.

38. G. Vona, A. Sabile, M. Louha, V. Sitruk, S. Romana, K. Schütze, F. Capron, D. Franco, M. Pazzagli, M. Vekemans, B. Lacour, C. Bréchot and P. Paterlini-Bréchot, *Am. J. Pathol.*, 2000, **156**, 57–63.

39. J. A. Hernández-Castro, K. Li, A. Meunier, D. Juncker and T. Veres, *Lab. Chip*, 2017, **17**, 1960–1969.

40. H. Cho, J. Kim, H. Park, J. Won Bang, M. Seop Hyun, Y. Bae, L. Ha, D. Yoon Kim, S. Min Kang, T. Jung Park, S. Seo, M. Choi and K.-Y. Suh, *Nat. Commun.*, 2014, **5**, 3137.

41. C. A. Schneider, W. S. Rasband and K. W. Eliceiri, *Nat. Methods*, 2012, **9**, 671–675.

42. A. Meunier, J. A. Hernández-Castro, K. Turner, K. Li, T. Veres and D. Juncker, *Anal. Chem.*, 2016, **88**, 8510–8517.

4.9 Supplementary information

4.9.1 Vacuum-assisted UV micro-molding (VAUM) fabrication process

The process is described in detail elsewhere.[1] Briefly, a micropillar array was replicated from molds obtained by standard photolithography and DRIE. The structure was then closed using a polyester film coated with a UV-curable resin to form an enclosed 3D microcavity. By using a vacuum chamber, the enclosed mold can be fully filled by the UV-curable Fluorolink® MD 700 resin (80 µL are usually enough to fill most molds), afterwards, it's cured by a 2 min UV exposure (2000-EC Series UV curing flood lamp, DYMAX). Finally, the cover is peeled off, and the molds are placed in an acetone bath during 15-20 minutes, allowing the membranes to self-de-mold from the pillar array. Membrane pores as small as 3.2 µm in diameter have been successfully produced with this fabrication process.

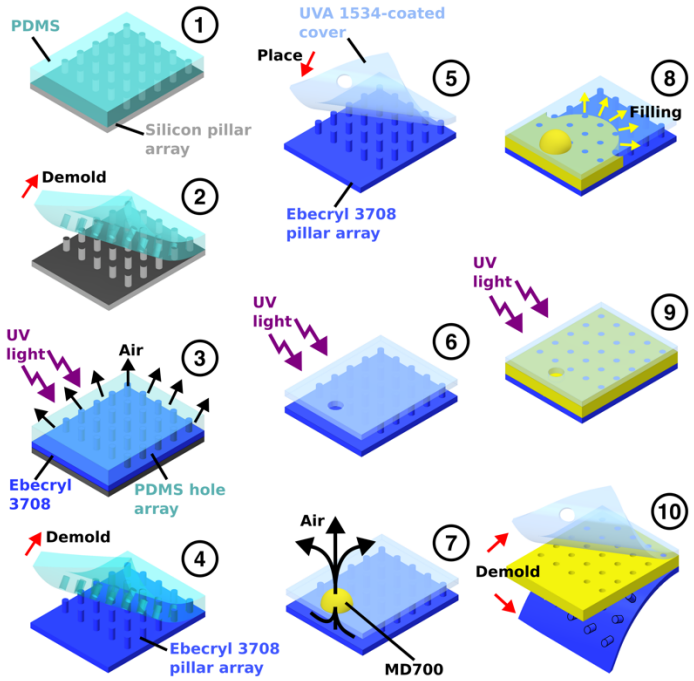

*Figure S4-1 | **Schematic of the VAUM fabrication process**. An enclosed mold is fabricated using a sacrificial pillar array replicated on a UV-curable resin (Ebecryl 3708), and a polystyrene cover coated with a partially cured second resin (UVA 1534). The membrane building material is introduced with the help of a vacuum process, by degassing the mold, a pressure difference is established, which drives the*

MD700 material inside the mold and allows for a complete filling. After curing, freestanding, microporous polymer membranes are obtained.

4.9.2 SEM images of PET mesh filter

The mesh materials used in PluriStrainer® 1 µm filter is polyethylene terephthalate. It is formed by interlaced by PET wires in diameter of about 40 µm and packed with three layers vertically, resulting in a mesh filter with thickness of about 100 µm. The pores are formed at the crossing point among the wires as shown by the elliptical circles in the SEM images depicted in Figure S2. The pores are not perfectly uniform in terms of the height (1-3 µm) and width (20-30 µm in lateral direction).

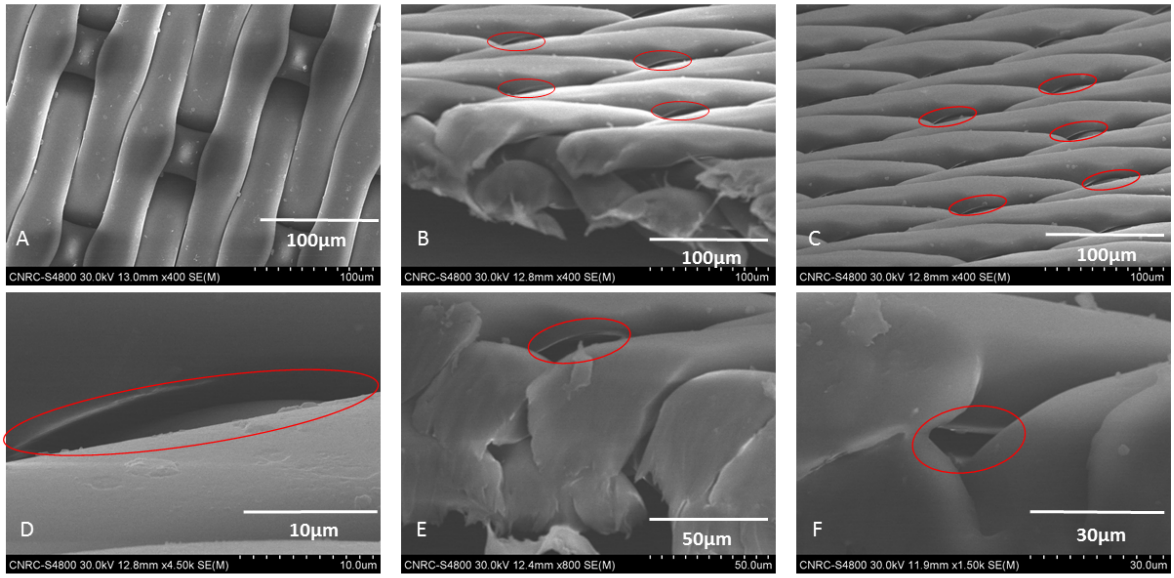

*Figure S4-2 | **SEM images of the PluriStrainer® mesh filters.***

4.9.3 WBC capture and staining without centrifugation steps

For the experiments presented in the main text of this manuscript, some centrifugation steps were done prior to flowing the cell solutions through the filter membranes. This was done to remove harsh buffers while the cells were being counted and the cartridges primed for the filtration protocol. However, it's possible to do without these centrifugation steps while still maintaining the same capture efficiency stated in the text.

Some WBC capture experiments were performed by running the samples through the filter cartridge right after the RBC lysis step, no filter clogging issues were encountered. Successful capture of the WBCs, buffer exchange, and multi-step staining were also validated, as shown in Figure S3. A capture efficiency of ≈ 96% was measured for this experiment, which is in accordance to the results obtained in the tests presented in the main text.

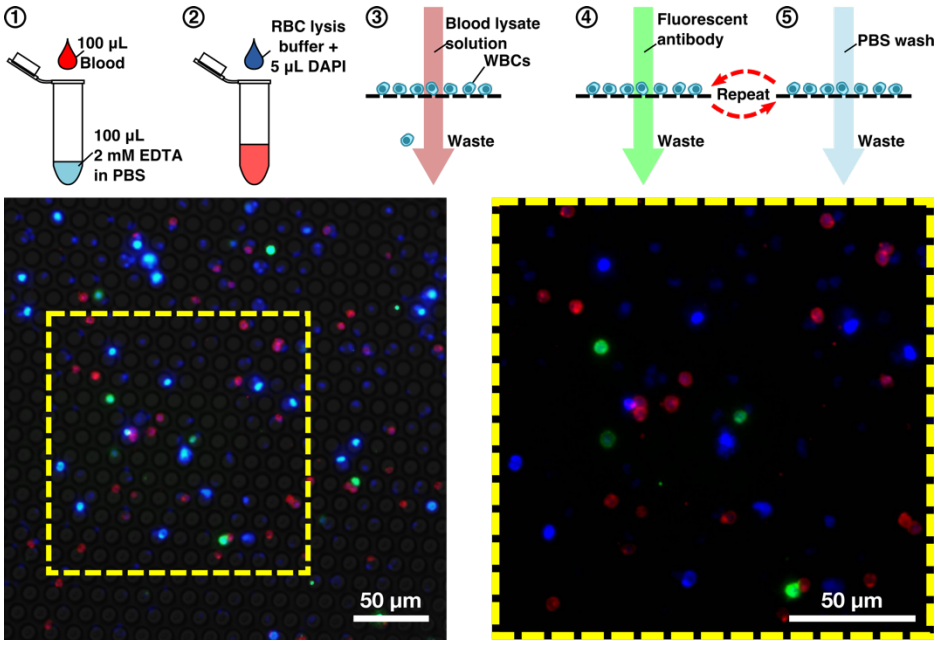

*Figure S4-3 | **WBC capture and staining from solution right after RBC lysis**. The only difference between this experiment and the ones for WBC capture and release presented in the manuscript is the removal of the centrifugation and resuspension step to remove the RBC lysis buffer before filtration. Cells were stained for DAPI (blue), CD4 (red), and CD20 (green).*

References

1. J. A. Hernández-Castro, K. Li, A. Meunier, D. Juncker and T. Veres, Lab. Chip, 2017, 17, 1960–1969.

CHAPTER 5 | CONCLUSIONS AND OUTLOOK

5.1 Summary

In this dissertation we set out, first, to develop a fabrication method for the production of optically transparent, freestanding, high porosity polymer microfilters, and then, to use these newly developed porous membranes for different cell isolation applications.

We successfully devised the VAUM protocol presented in Chapter 3, which allowed us to fabricate polymer microfilters with regular and controllable pore size and distribution, over very large areas (9×9 cm^2), high porosity (up to 60%), non-autofluorescent, optically transparent, and robust enough to manipulate and integrate to fluidic cartridges for cell filtration experiments. We showed successful use of the microfilters for the separation of a mixture of microbeads of different sizes into distinct populations, as well as isolation of cancer cells spiked in buffer solutions.

In Chapter 2 we had shown that the addition of capture antibodies on the surface of a silicon filter enhances the capture of the specific cells expressing the target antigen, a combined approach that had not been explored before. In Appendix I we demonstrate the use of our polymer microfilters for the efficient enrichment of circulating tumor cells from blood samples. Furthermore, we took the ideas from Chapter 2 and applied them using the new polymer filters, a surface functionalization protocol was developed to attach antibodies onto the polymer membranes, we finally demonstrated that the capture of CTCs from blood can be significantly enhanced using antibody-functionalized polymer microfilters. By using a hybrid or two-pronged approach for the isolation of CTCs, we are able to harness the advantages of both methods and avoid some of the limitations that either method alone might have. Furthermore, the high base-line capture of CTCs with our filtration platform ensures that most of these rare cells will be captured, regardless of their surface marker expression properties. In more recent experiments (not yet published), we were able to use these microfilters for the analysis of ovarian cancer patient

samples and we detected the presence of CTC clusters in all samples tested. It is believed these clusters might hold a higher metastatic potential than single CTCs, having a platform that can efficiently target both is thus of high relevance.

Finally, in Chapter 4 we show that, by using a submicron pillar patterned cover, the original VAUM process can be used to achieve fabrication of two-level porous membranes with pores as small as 500 nm in diameter. We demonstrated that these submicron filters can be used for efficient capture, staining, and release of white blood cells from RBC-lysed blood samples. Standard WBC isolation methods rely on centrifugation methods that have been shown to be tied to cell loss and damage, as well as to result variability (dependent on the technical expertise of the person performing the assay). Having a platform that avoids the use of sample centrifugation for WBC isolation, can potentially be automated, and allows multi-step cell staining is a valuable technology for sample preparation, especially useful in applications where cell loss must be minimized as much as possible, and where result variability is undesired, like in leukemia screening tests.

5.2 Conclusions

We present a novel polymer filter fabrication process that relies on the replication of an original silicon master mold onto disposable sacrificial molds made from UV-curable polymers. It is important to note that the use of photolithography equipment is only necessary for the preparation of the silicon master molds, which, if handled carefully, can last for years. Furthermore, the way our method was designed enables us to obtain large area (up to 9×9 cm^2), optically transparent, non-autofluorescent, non-cytotoxic, high porosity (up to 60%), and regular pore distribution polymer microfilters, it is important to note that the combination of all these characteristics at once has not been achieved by other fabrication methods to date. Out of the discussed methods in the literature, only the mold-based dewetting method allows for the fabrication of membranes with smaller regularly distributed pores (50 nm vs 500 nm).[1]

The material used for the fabrication of our microfilters was chosen due to several characteristics that made it highly desirable for biological applications: It is optically transparent and non-autofluorescent, which allows optical and fluorescence microscopy imaging through the membranes. It is a fluorinated methacrylate, which makes it chemically inert, we tested the membranes to be resistant to organic solvents, acidic, and basic solutions. Also, the cytotoxicity of the material was investigated, we found cells don't die after prolonged exposure to it, however, they don't readily attach to it either, making on-filter culture not straightforward. Furthermore, in its prepolymer form, the liquid material is fluid enough to flow into the enclosed molds with submicron and microstructures and fill them completely. Finally, the cured polymer is not thermoplastic, which allows the thermal bonding integration or encapsulation of the manufactured membranes onto hard plastic carrier frames or microfluidic chips, which is important for easier manipulation and use in filtration cartridges.

The combination of the material properties and fabrication method characteristics allowed us to successfully use these polymer microfilters for cell isolation from buffer or blood samples. Spiked cancer cell isolation, as well as highly efficient WBC capture, staining, and release from healthy donors' blood were demonstrated. We also showed that a combined physical and immunocapture approach can significantly increase the capture efficiency of specific cell types without decreasing the purity of the captured cells sample. The developed platform can also be used for the efficient isolation of clustered CTCs, an important advantage compared to other cell isolation methods that are only tailored for the capture of single cells. The study of CTC clusters is garnering attention, if our platform had only been useful for single CTC capture, it is possible it would have been rendered obsolete in a few years.

The results obtained here make the use of these polymer membranes very promising, we have so far focused on their use for biological applications, but given their physical

and chemical properties, they could also be implemented for different purposes, like chemical sample purification, surface patterning, and fuel cells, among others.

5.3 Limitations

The proposed polymer microfilter fabrication process overcomes some limitations present in other methods found in the literature, namely: the necessity of performing a photolithography process for fabrication of each new membrane, even though fabrication of the master mold requires the use of photolithography equipment, once this is made, the next steps in the process can be carried out outside of the clean room; the autofluorescence of materials used to produce the microfilters, which is important for on-filter identification of the captured cells by immunocytochemistry; or the presence of residual layers that need to be etched before through-hole structures are created in the polymer membranes. However, our process is not without its own limitations and could still be improved.

The fabrication method could be perfected by replacing the use of the intermediate PDMS mold for one made of another material that could be reused indefinitely. As it stands, these molds can be effectively used 5 or 6 times before accurate replication of the features becomes impossible. Thus, to adapt the fabrication protocol for the mass production of polymer microfilters, an alternative material must be found. Being able to streamline the fabrication of the polymer membranes would not only be helpful for commercialization of the technology, but also to be able to perform clinical tests more rapidly.

It would also be interesting to analyze the stability or shelf life of the antibodies attached to the surface of the microfilters. The typical shelf life for antibodies kept in aqueous solution at 4° C has been reported to be of approximately 1 month under optimized conditions,[2] which might be a limiting factor in the storage of functionalized antibodies for future use. It would also be important to perform thermostabilization of the capture antibodies[3] to allow the functionalization of the membranes prior to their integration into monolithic chips, usually done by thermal bonding at high temperatures,

which can result in fast degradation or denaturation of proteins. Finally, replacing antibodies with more stable capture molecules, like aptamers, could also be investigated, it would be necessary to see if the same capture rates can be achieved using these alternative molecules.

Very high capture efficiencies of CTCs from blood samples has been achieved, as presented in Appendix I. The polymer membranes can be successfully integrated into hard plastic or 3D-printed cartridges, with optimized filtration parameters, consistent capture rates can be achieved. Cells can be stained on-filter and inspected afterwards. One aspect of the process that can be improved is the detection and enumeration of the captured cells, the integration of an artificial-intelligence-assisted method for an automated detection and counting of the isolated cells would be helpful to have a faster and more standardized protocol for the discrimination of the captured cells. Furthermore, this would help remove human bias and errors, making the adoption of the CTC capture platform much easier.

As presented in Chapter 4, the use of a submicron-patterned cover during the membrane mold fabrication process makes the fabrication of two-level polymer filters with submicron pores. The fabrication of this patterned covers is somewhat challenging, as precise control on the UV exposure times is necessary. A possible alternative would be to make a two-level master mold, moving the submicron features onto the micropillars on the silicon mold, and reverting to the use of flat covers. By doing this, the complexity in the fabrication method is moved to the master mold preparation, for which there are already well established and documented protocols. The disadvantage is that not all clean room facilities have access to the necessary equipment to perform the photolithography processes needed for replicating submicron structures onto silicon substrates.

5.4 Outlook

I believe future work based on the results presented in this dissertation could go in two directions: new applications, and translation of the technology into a user-friendly

platform for clinical use. As mentioned previously, there are still some challenges related to the fabrication process itself, like the limitation of relying on a PDMS intermediate mold that must be replaced after a few uses, or the complexity of fabricating the submicrometer patterned cover for the 2LHPM. While tackling these issues might be important to achieve commercialization of the technology, these issues can be mostly considered engineering or technical problems.

On the other side, we have achieved very promising results on the use of this technology for the isolation of rare and abundant cells. Translation of the use of these polymer filters in clinical tests is already under way, with projects related to the capture of clustered CTCs from patient blood samples, and also on the detection of minimal residual disease (MRD) in leukaemia patients. Filter cartridge optimizations can lead to having an easy-to-use, automated platform for cell capture and detection, with future work being focused on the downstream manipulation and analysis of the captured cells, useful discoveries on their biology might be achieved through the use of our proposed technology.

Having been able to fabricate polymer filters with pores as small as 500 nm, it would be interesting to explore the limits of the fabrication process to see if pores of < 100 nm can be obtained. There is currently a growing interest in the development of exosome capture and analysis platforms,[4] exosomes are extracellular vesicles with sizes ranging from 30 to 100 nm. Their most common isolation process is through ultra-centrifugation, but the use of track-etched polymer membranes with pores between 30 to 100 nm has begun to be explored for exosome capture.[5-7] As mentioned previously, track-etched membranes have intrinsic limitations on the maximum porosity values they can have (limiting throughput), and the autofluorescence of the materials they're made from (making detection more complicated). The dewetting fabrication method mentioned in the introduction[1] showed that pores as small as 50 nm could be obtained using the material used for our own polymer microfilters, thus, it's highly probable we can achieve fabrication

of nanofilters with pore sizes ranging from 50 to 100 nm, which could then be used for efficient and high-throughput exosome filtration.

Overall, the continued development of the technology and the techniques presented in this thesis will further increase their potential uses, perfecting their use for some of the applications presented here can lead to the development of clinical tools for CTC detection and analysis, MRD assessment, or the study of other blood or immune system pathologies. The refinement of the fabrication protocol can lead to a mass-production-ready method that could permit commercialization of this technology and the development of other novel applications.

References

1. H. Cho, J. Kim, H. Park, J. Won Bang, M. Seop Hyun, Y. Bae, L. Ha, D. Yoon Kim, S. Min Kang, T. Jung Park, S. Seo, M. Choi and K.-Y. Suh, *Nat. Commun.*, 2014, **5**, 3137.

2. M. Johnson. *Materials and Methods*, 2012, **2**, 120.

3. A. McConnell, X. Zhang, J. Macomber, B. Chau, J. Sheffer. *mAbs*. 2014, **6**, 1274-1282.

4. B. Yang, Y. Chen and J. Shi, *Adv. Mater.*, 2019, **31**, 1802896.

5. P. Li, M. Kaslan, S. H. Lee, J. Yao and Z. Gao, *Theranostics*, 2017, **7**, 789–804.

6. F. Liu, O. Vermesh, V. Mani, T. J. Ge, S. J. Madsen, A. Sabour, E.-C. Hsu, G. Gowrishankar, M. Kanada, J. V. Jokerst, R. G. Sierra, E. Chang, K. Lau, K. Sridhar, A. Bermudez, S. J. Pitteri, T. Stoyanova, R. Sinclair, V. S. Nair, S. S. Gambhir and U. Demirci, *ACS Nano*, 2017, **11**, 10712–10723.

7. L.-G. Liang, M.-Q. Kong, S. Zhou, Y.-F. Sheng, P. Wang, T. Yu, F. Inci, W. P. Kuo, L.-J. Li, U. Demirci and S. Wang, *Scientific Reports*, 2017, **7**, 46224.

PREFACE TO APPENDIX I

In the previous chapters, we showed the results pertaining the fabrication of our microporous polymer membranes and demonstrated successful applications for the isolation of microbeads and cancer cells from buffer solutions.

The work I performed for this thesis also formed part of a larger effort towards building a platform for CTC capture from patient blood samples. This part of the project was led by Dr. Anne Meunier, a postdoctoral researcher at Prof. Juncker's lab.

In the next chapter, we show the first applications of the polymer microfilters for the isolation of CTCs spiked in healthy blood samples, the filtration conditions (filter pore size, flow rate) were optimized to achieve the best possible capture rate of the cancer cells while avoiding non-specific arrest of WBCs as much as possible.

Furthermore, building on the work presented in Chapter 2, I helped develop a functionalization protocol to attach antibodies to the polymer filters' surface, it was then demonstrated that, by using functionalized filters, the capture efficiency for cells expressing the complimentary antigen was significantly increased, which was expected as per the previously presented results. This hybrid CTC capture method using polymer microfilters had not been explored before by other authors.

A method to encapsulate the membranes onto hard plastic carriers was also devised to aide in the handling of the filters and their integration into the 3D-printed cartridge designed for the filtration experiments.

A high capture efficiency and purity of CTCs from blood was achieved with the use of our polymer microfilters. These results were promising to attempt the use of the platform for CTC capture from patient blood samples.

The following manuscript was published as a *Research Article* in ***Analytical Chemistry***.

APPENDIX I | COMBINATION OF MECHANICAL AND MOLECULAR FILTRATION FOR ENHANCED ENRICHMENT OF CIRCULATING TUMOR CELLS

A. Meunier,[1,2] **J. Alejandro Hernández Castro**,[1,2,3] K. Turner,[1,2] K. Li,[3] T. Veres,[3] and D. Juncker,[1,2,4]

[1]Biomedical Engineering Department, McGill University, 3775 University Street, Montréal, Québec, Canada H3A 2B4.

[2]McGill University and Génome Québec Innovation Centre, McGill University, 740 Dr. Penfield Avenue, Montréal, Québec, Canada H3A 0G1.

[3]National Research Council of Canada, 75 de Mortagne Boulevard, Boucherville, Québec, Canada J4B 6Y4.

[4]Neurology and Neurosurgery Department, McGill University, 3801 University Street, Montréal, Québec, Canada H3A 2B4.

AI.1 Abstract

Circulating Tumor Cells (CTCs) have been linked to cancer progression, but are difficult to isolate, as they are very rare and heterogeneous, covering a range of sizes and expressing different molecular receptors. Filtration has emerged as a simple and powerful method to enrich CTCs, but only captures cells above a certain size regardless of molecular characteristics. Here, we introduce antibody-functionalized microfilters to isolate CTCs based on both size and surface receptor expression. We present a 3D printed filtration cartridge with microfabricated polymer filters with 8, 10, 12, 15 or 20 µm-diameter pores. Pristine filters were used to optimize sample dilution, rinsing protocol, flow rate and pore size, leading to $>$ 80 % for the recovery of spiked cancer cells with very low white blood cell contamination ($<$ 1000). Then, filters were functionalized with antibodies against either epithelial cell adhesion molecule (EpCAM) or epidermal growth factor receptor (EGFR) and the cartridges were used to enrich breast (MDA-MB-231, MCF-7) and renal (786-O, A-498) cancer cells expressing various levels of EpCAM and EGFR. Cancer cells

were spiked into human blood, and when using filters with antibodies specific to a molecular receptor expressed on a cell, efficiency was increased to > 96 %. These results suggest that filtration can be optimized to target specific CTC characteristics such as size and receptor expression, and that a diverse range of CTCs may be captured using particular combinations of pore size, filtration parameters, and antibody functionalization.

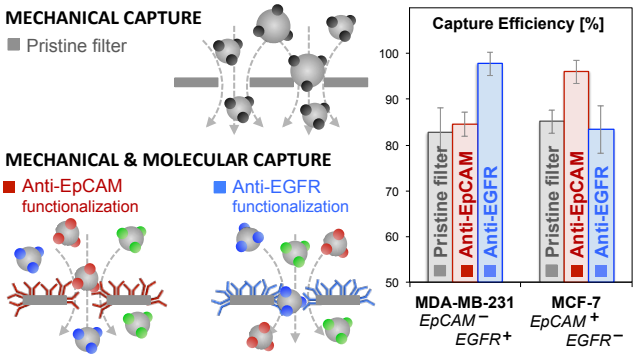

AI.2 Introduction

Circulating Tumor cells (CTCs) are cancer cells that have detached from a primary tumor, entered the bloodstream, and thought to invade distant tissues where they adapt and proliferate, leading to the formation of metastases (secondary tumors).[1,2] Metastasis is a highly frequent complication responsible for as much as 90 % of cancer-associated mortality. CTCs, found in blood, have emerged as a prognostic indicator for disease progression.[3,4] CTCs are extremely rare (1-10 CTCs per milliliter of blood, compared to $< 10^6$ leucocytes and $< 10^9$ erythrocytes),[3,5,6] and the detection of one CTC in five milliliters of blood is clinically relevant. However, one of the main obstacles to characterize these cells is the difficulty of obtaining sufficient numbers for analysis. This has prompted the development of many technologies, where selective enrichment is typically achieved using molecular (surface receptor expression) or mechanical (size, density, electric charges, deformability) properties, known to be different from blood cells.

Filtration was first used to concentrate cancer cells from saline in 1956 using cellulose ester filters with 0.5-3.0 µm pore diameter.[7] Track-etching technique, developed in the

1960s and used to this day,[6,8] allows an accurate control of pore dimensions. However, the random arrangement of pores and the need to prevent pore overlapping inherently limit membrane porosity using this approach.

Microfabrication, allowing precise control of sub-micrometric dimensions, was used to design filtration systems with micropillars or microholes.[9-11] However, the high flow resistance of microfluidic devices limits the throughput, while fabrication processes can be complex and costs high. Filters can provide multiple parallel paths and microfabrication has been used to make filter membranes with higher porosities,[12] as well as rectangular or conical shapes,[13-15] and 3 dimensional configurations,[16] permitting higher flow throughput. However, the heterogeneity of CTCs is becoming increasingly appreciated, and the diameter of small CTCs falls within the range of white blood cells (WBCs), making their capture difficult as the pore size is constrained by the requirement for WBCs to pass through without clogging the pores.

Another successful strategy is targeting molecular receptor expression using antibodies. CTCs of epithelial origin and unlike any blood cells, express the epithelial cell adhesion molecule (EpCAM). Currently, CellSearch® (Veridex LLC, Raritan, NJ, USA), using magnetic beads coated with anti-EpCAM antibodies is the only system approved by the US Food and Drug Administration for the enumeration of CTCs of epithelial origin in whole blood.[17] Affinity-based strategies using antibody-functionalization of nanostructured substrates[18-22] or magnetic beads,[23,24] have been widely used in microfluidic devices for magnetic separation.[25-28] For instance, using anti-EpCAM functionalization, Soper et al. captured EpCAM positive cancer cells spiked in blood, and showed their possible detachment by enzymatic digestion of the extracellular domain of EpCAM or anti-EpCAM with high yield.[29] Released cells were then enriched based on their electrical charges for further molecular profiling.

However, CTCs heterogeneity extends to the expression of molecular receptors as well. CTCs can undergo epithelial-mesenchymal transition (EMT), that may lead to

EpCAM downregulation.[30] A number of techniques are emerging to address the intrinsic heterogeneity of CTCs. Cancer cells with stem cell features were shown to preferentially adhere to extracellular matrix proteins for example.[31] Negative selection allows for targeting WBCs with magnetic beads conjugated with anti-CD45 instead of enriching CTCs.[32] Toner *et al.* developed a complex microfluidic chip with a size-based RBC separation followed by magnetic isolation of either CTCs by capture on anti-EpCAM magnetic beads, or to preserve CTC diversity, in a negative selection mode by removing WBCs using anti-CD45 magnetic beads.[33] Negative selection however is costly as large amounts of antibody-conjugated magnetic beads are needed, and some CTCs may be removed along with the other cells.

A promising strategy to isolate a wider range of heterogeneous CTCs is to isolate cells based on both molecular and mechanical features. First steps have been taken in this direction by Chung *et al.* who, using a multi-step procedure, first enrich cancer cells on magnetic beads conjugated with anti-EpCAM, rinse, and then capture the cells with beads on a filter, and finally detach them by inverting the flow.[34] Zhang *et al.* used a reverse protocol where anti-EpCAM beads are also added to the sample and labeled cancer cells are first enriched on a filter, and then detached from the filter using magnetic force.[35] It is EpCAM expression that dictates isolation, and the cells, enlarged by the magnetic beads, are thus captured by the filter. In both approaches yields were excellent, but they were dependent on EpCAM expression and only used for $EpCAM^+$ cells, the protocols required multiple steps while the magnetic beads interfered with fluorescence imaging, and most importantly, it is not known whether the intrinsic mechanical properties of the cells influence this filtration method.

Here, we introduce antibody-functionalized microfilters to isolate CTCs based on both their intrinsic mechanical properties including size and rigidity, and their expression of surface receptors. Microfabricated polymer filters with 8, 10, 12, 15 or 20 µm-diameter pores were used, and various parameters such as sample dilution, rinsing protocol, flow

rate and filter pore size were optimized for the enrichment of MDA-MB-231 breast cancer cells spiked into blood while considering both cell recovery and WBCs contamination. We designed and made a 3D printed filtration cartridge that can be rapidly assembled, and that was used for all experiments. Upon processing, cells were fluorescently stained directly in the cartridge. Then, transparent filters were removed from the cartridge and imaged by microscopy. Using the optimal conditions, breast (MDA-MB-231, MCF-7) and renal (786-O and A-498) cancer cells, chosen for expressing various levels of EpCAM and epidermal growth factor receptor (EGFR), were then enriched with pristine filters, and filters functionalized with anti-EpCAM and anti-EGFR antibodies.

AI.3 Experimental section

AI.3.1 Filter fabrication

The process, described in detail elsewhere[36] and briefly in supporting information (AI.7.1), allows for the fabrication of 20-40 micrometer-thick filters with precise pore dimensions (Figure AI-1A). Pore diameters, measured by microscopy and averaged on 20 pores from three different filters and for each pore size, were found to be 7.9 ± 0.3, 10.0 ± 0.2, 11.7 ± 0.4, 15.0 ± 0.2 and 20.1 ± 0.3 µm.

AI.3.2 Cartridge design

The filtration cartridge (70 mm long and 40 mm large) was designed using AutoCAD software (Autodesk Inc.) and 3D printed (Perfactory Micro EDU, Envision Tech) (Supporting information AI.7.1). It consists of a bottom (15 mm high) and a top part (10 mm high) in between which a microfilter can be inserted (Figure AI-1B).

AI.3.3 Filter functionalization

Covalent immobilization of antibodies was performed through EDC/NHS coupling after surface activation with oxygen plasma (PE-50, Plasma Etch) for 2 minutes at 150 W and O_2 pressure of 200 mTorr. Filters were incubated for 20 minutes in EDC (0.5 mol L^{-1})/NHS (0.5 mol L^{-1}) solution, prepared immediately before use and diluted 10 times in MES buffered saline (0.1 mol L^{-1} MES, and 0.5 mol L^{-1} NaCl) supplemented with 2.0 %

BSA. After rinsing with MES buffer, filters were incubated in the antibody solution containing 10.0 µg mL^{-1} of anti-EGFR or anti-EpCAM for 3 hours. The filters were then rinsed with PBS and directly used for filtration.

AI.3.4 Cell culture

MDA-MB-231, MCF-7 and A-498 cells were cultured in DMEM, supplemented with 10 % FBS and 1 % (v/v) antibiotics. 786-O renal cells were cultured in RPMI 1640 medium supplemented with 10 % FBS. For spiking experiments, cells were harvested from flasks, centrifuged then re-suspended in PBS. Additional details are provided in supporting information (AI.7.1).

AI.3.5 Blood collection

Blood was drawn from healthy volunteers (IRB study reference number: BMB-08-012) into 10 mL CTAD tubes (Citrate-based anticoagulant containing the platelet inhibitors theophylline, adenosine, and bipyridamole, BD Vacutainer). Samples were maintained at 4 °C and processed within 72 hours of blood collection.

AI.3.6 Cell staining

After filtration, cells were treated directly on the filter, within the cartridge. Cells were fixed with 3.7 % paraformaldehyde (PFA) in PBS then rinsed with PBS. Cells were then permeabilized with 0.2 % Triton X-100 and rinsed with PBS. Afterwards, blocking was performed with 1.0 % BSA in PBS supplemented with 0.1 % Tween 20, then cells were stained with Anti-Pan-cytokeratin Alexa Fluor 488 (2.0 µg mL^{-1}) and Anti-Human CD45 Phycoerythrin (PE, 1.0 µg mL^{-1}). Cells were rinsed with PBS then their nucleus was stained by 4',6-diamidino-2-phenylindole (DAPI, 0.1 µg mL^{-1}). Finally, the filter was rinsed with PBS and cell identification was performed by fluorescence microscopy. Additional practical details are provided in supporting information (AI.7.1).

AI.3.7 Cell identification by fluorescence microscopy

Filters were placed upside down on the platform of an inverted microscope (TE-2000-E, Nikon) connected to a CCD camera (QuantEM 512SC, Photometrics) and

fluorescence images were recorded with NIS-Elements Advanced Research software (Nikon) and analyzed with ImageJ.[37] Images were collected with a mercury arc lamp and 41001 (blue, for Alexa fluor 488), 41004 (green, for PE) and 31000v2 (UV for DAPI) filter cubes (Chroma Technology Corp.) were used. Cells are defined as CTC-like cells when they have a nucleus (DAPI staining) and when they express cytokeratin, a cytoplasmic protein from epithelial origin (anti-pan-CK staining). WBCs also possess a nucleus (DAPI) but express the cluster of differentiation 45 (anti-CD45 staining) (Figure AI-1D).

AI.4 Results and discussion

Transparent polymer membranes with pore diameter of 8-20 µm, an open ratio of 8-20 %, and 33-80 thousand pores[36] were inserted into a 3D printed cartridge (Figure AI-1A); unless specified 8-µm-pore-filters were used in all experiments. The porous membrane is heat bonded to a PMMA ring that defines an 8 mm-diameter filter. Filters were used in pristine condition for initial optimization and for pure mechanical filtration, and functionalized with antibodies for combined mechanical and molecular filtration in subsequent experiments. The filters are positioned between the cartridge and a pair of toric joints, and clamped with screws and bolts for sealing. A precise number of cancer cells (Supporting information AI.7.1) was spiked into 1.0 mL of blood diluted with PBS. The sample was inserted from the inlet (top) and flowed through the cartridge at a defined flow rate using a programmable syringe pump (Figure AI-1C). Red blood cells (RBCs) and white blood cells (WBCs) with diameters of 7-8 and 8-14 µm respectively, are known to be deformable and could pass through all filters used here.[38] The larger and less deformable cancer cells were captured, stained and imaged on the filter for identification (Figure AI-1D).

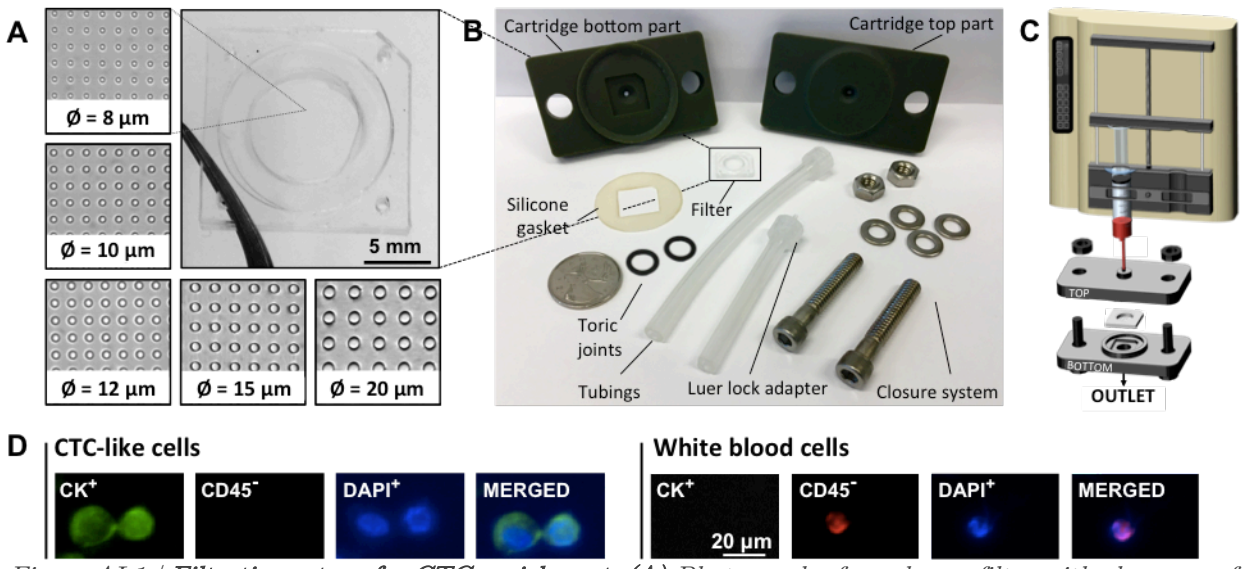

*Figure AI-1 | **Filtration set-up for CTC enrichment.** **(A)** Photograph of a polymer filter with close-ups of membranes with 8, 10, 12, 15 and 20 µm-diameter pores. **(B)** Photograph of the disassembled filtration set-up. **(C)** Schematic representation of the filtration set-up comprising programmable syringe pump and exploded view of the cartridge. **(D)** Examples of fluorescence images of cancer (MDA-MB-231) cells and white blood cells on 8-µm-pore filters.*

AI.4.1 Mechanical capture of CTCs

The influence of experimental conditions such as sample dilution, rinsing protocol, flow rate and filter pore size on the enrichment performance was studied. Enrichment performance can be quantified by measuring efficiency and purity.[32] Efficiency corresponds to the recovery ratio between cells that are captured versus spiked into the sample:

$$efficiency = \frac{NTC\ captured}{NTC\ initially\ spiked\ in\ blood} \times 100$$

Purity is measured as the number of white blood cells (WBCs) concurrently captured with cancer cells. A higher purity corresponds to a lower number of WBCs, which is desirable as WBCs can confound further biological analysis.

An important parameter that could not be directly controlled but was considered is the pressure drop across the microfilter, which is determined by the flow rate divided by the flow resistance of the microfilter. Dilution of blood in buffer would contribute to reduce the pressure by reducing the viscosity. However, although the flow rate was fixed, the pressure could not easily be derived because of the non-Newtonian characteristic of blood, and more importantly, because clogging of the pores by captured cells reduces the number

of open pores, leading to increased resistance and higher pressures for a given flow rate. It is expected that increases in pressure will affect the enrichment of CTCs, as well as the WBCs contamination. For increasing pressure, less CTCs and less WBCs would be captured, while it may also help reduce clogging of the microfiltration membrane as cells are displaced.

Sample dilution

The effect of sample dilution was evaluated with a known number of MDA-MB-231 cells (161.82 ± 8.1 cells) spiked into 1.0 mL of blood diluted with different volumes of PBS (1.0, 2.0, 5.0, 6.0, 10.0 and 15.0 mL) and filtered at 1.0 mL min^{-1}.

For increasing dilutions of 1.0 mL of blood with up to 6.0 mL of PBS, efficiency increased from about 20 to about 50 % (Figure AI-2A). This trend is in good agreement with the work of Coumans *et al.* who have previously demonstrated that for a fixed flow rate, diluting samples reduces the pressure drop and helps increase efficiency.[6] Since enrichment is based on cell size and deformability, it is not surprising that a lower pressure undergone by cells would make them pass through the filter less easily, therefore increasing efficiency. As the sample is further diluted up to 1:15 of blood:PBS, no significant improvement is observed, consistent with only minor changes in viscosity. The reproducibility in efficiency and in the initial number of spiked cells was found to be very good with very low standard deviation. In order to limit the processing time, for all further experiments, 1 mL blood samples were diluted with 6 mL of PBS. For all dilutions we observed a high accumulation of WBCs on the filter, indicating that dilution is not an effective means of improving purity.

Rinsing

We tested the effect of rinsing on purity by flowing various volumes of PBS. 101.3 ± 2.4 MDA-MB-231 cells, spiked in 1:6 mL of blood:PBS, were filtered, then rinsed at 1.0 mL min^{-1}.

Using 5.0 mL of PBS, the number of WBC captured on the filter was greatly reduced, from the experiments without rinsing, to a low density that permitted their enumeration, and in this case corresponding to ≈ 1000 WBCs (Figure AI-2B). WBCs concentration is $> 10^6$ per mL of blood,[32] thus < 0.1 % were captured on the filter. Without and with rinsing, respectively 50 ± 2 % and 50 ± 3 % of cancer cells were captured, indicating that this rinsing did not reduce efficiency. Increasing the rinsing volume to 10.0 or 20.0 mL did not improve purity significantly. However, rinsing in several steps (2 or 3 rinses with 5.0 mL of PBS) further reduced the number of WBCs, but for three rinses efficiency was only 41 ± 3 %. Contrary to a single rinse with 10.0 mL of PBS, when rinsing twice with 5.0 mL of PBS, the syringe was unplugged to be re-filled. This procedure creates a small negative pressure (back pulse) that may displace cancer cells and WBCs captured into a pore, thus they may be washed during the second rinsing step. Therefore, while increasing the number of rinsing steps, cells are exposed to more successive negative and positive pressure cycles, which may eventually facilitate the passage of any cells and explain the decrease in both efficiency and purity. Based on these results, we identified rinsing twice with 5.0 mL of PBS as the optimal compromise between high efficiency and high purity, and adopted it for all subsequent experiments.

The number of WBCs captured on the filter varies to a larger extent than the efficiency, which is consistent with person-to-person variability of blood cell counts and cell properties.[6] Jones *et al.* showed that both WBCs and RBCs (to a lesser extent) are responsible for pore occlusion, leading to changes in the pressure drop across the filter.[39] Only ≈ 1000 WBCs were left following rinsing, filling 1-3 % of the total number of pores, and thus inducing a negligible change in pressure. During filtration, many more cells are expected to be on the filter surface and transiting through the pores, yet efficiency was reproducible for many different blood samples, suggesting that WBCs and RBCs do not affect CTC capture when the samples are sufficiently diluted. In conclusion, whereas the

number of WBCs on the filter is subject to greater variation, < 0.1 % were retained on the filters in all scenarios tested here.

Flow rate

The influence of flow rate on efficiency and purity was investigated by spiking 101.3 ± 3.3 MDA-MB-231 cells in 1.0:6.0 mL of blood:PBS. Samples were filtered at different flow rates (0.1, 0.5, 1.0, 2.0 or 3.0 mL min^{-1}). No rinsing was done.

As the flow rate decreased from 3.0 to 0.1 mL min^{-1}, efficiency increased from 42 ± 5 to 85 ± 3 % (Figure AI-2C). The number of WBCs on the filter was evaluated by imaging them after filtration. Since for low flow rates there were too many WBCs captured to be counted, the surface coverage of WBCs was compared, which was smaller for higher flow rates (supporting information AI.7.2). Both the number of cancer cells and WBCs on the filter diminish with increasing flow rates, consistent with a higher pressure and results in the literature,[6,22] manifesting a trade-off between efficiency and purity. Reducing the flow rate will reduce the pressure on cells, including WBCs, through pores. This would explain the increase not only in the number of captured target cells, thus increasing efficiency, but also in the number of WBCs, reducing purity.

Finally, we determined purity after filtration and rinsing twice with 5 mL of PBS at 0.1 mL min^{-1}. The number of WBCs was found to be 694 ± 161, consistent with our previous results, obtained at 1.0 mL min^{-1}. A flow rate of 0.1 mL min^{-1} was therefore selected as optimal for our system. It is worth mentioning that the overall process could be further sped up by increasing membrane porosity or filter size, both resulting in increased flow rate for a given pressure.

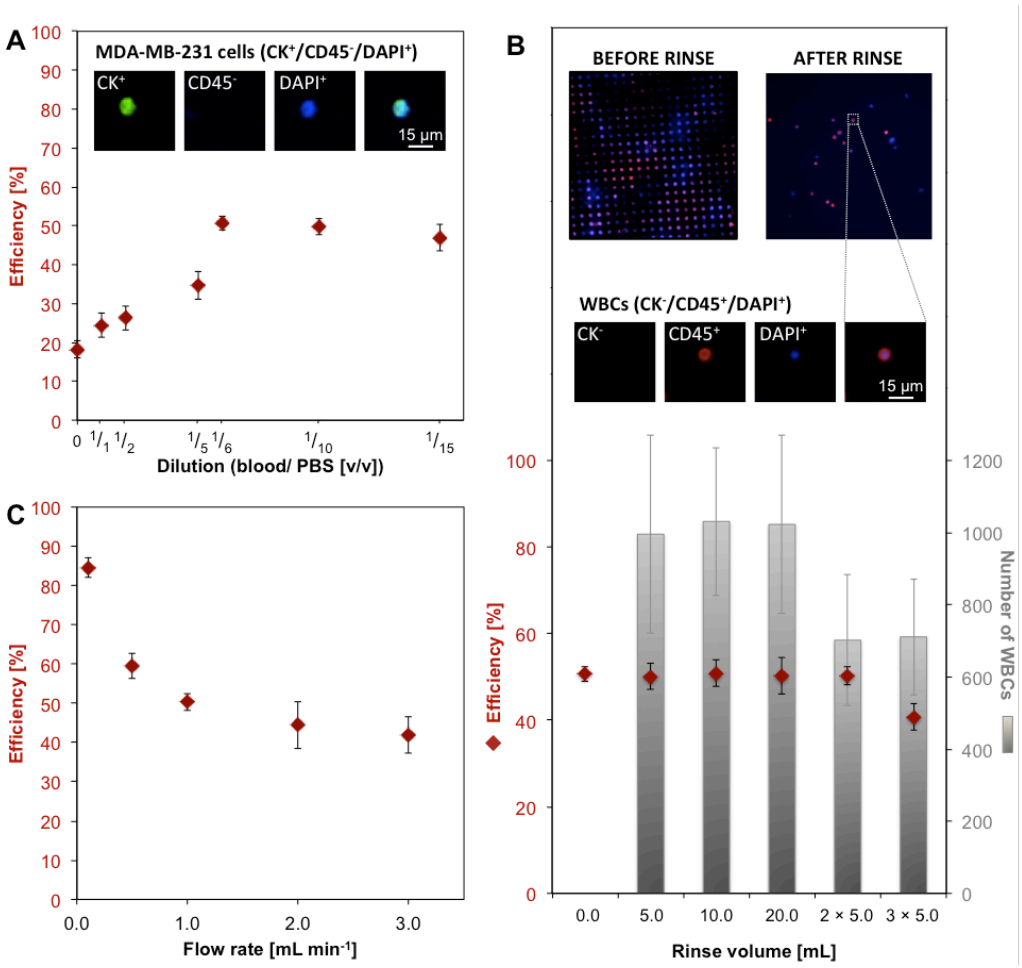

*Figure AI-2 | Capture efficiency and WBC contamination for different dilutions factors, rinsing protocols, and flow rates. **(A)** Effect of sample dilution on capture efficiency. 161.8 ± 8.1 MDA-MB-231 cells were spiked in 1.0 mL of blood diluted with 1.0, 2.0, 5.0, 6.0, 10.0 or 15.0 mL of PBS, and filtered at 1.0 mL min^{-1}. Insets show a MDA-MB-231 cell stained on filter. **(B)** Qualitative (top, WBCs stained on filter) and quantitative (bottom) effect of rinsing on efficiency (red symbols) and the number of WBCs (grey bars). 101.1 ± 5.1 MDA-MB-231 cells were spiked in 1.0:6.0 mL of blood:PBS, filtered, then rinsed with 5.0, 10.0, 20.0, 2 × 5.0 or 3 × 5.0 mL of PBS at 1.0 mL min^{-1}. Without rinsing, the number of WBC is too high to be counted. **(C)** Effect of flow rate on efficiency. 101.3 ± 3.3 MDA-MB-231 cells were spiked in 1.0:6.0 mL of blood:PBS, and filtered at 0.1, 0.5, 1.0, 2.0 or 3.0 mL min^{-1} (no rinse). The results identify 1:6 dilution, 0.1 mL min^{-1} and 5.0 mL rinsing volume (twice) as the optimal conditions. Error bars correspond to the standard deviation of three independent experiments.*

Filter pore size

The pore size is expected to play a dominant role in the efficiency and purity of captured CTCs. 8 µm-diameter pores were selected as lower limit based on the results in the literature that showed it to be the smallest dimension before clogging by WBCs becomes significant. Indeed, the smaller the pores, the more efficient enrichment, but as they become too small they retain a small fraction of WBCs, which rapidly leads to a

clogging of the pores. As the fraction of open pores in the filter is reduced, the pressure drop across the filter rapidly increases under constant flow rate conditions, and the flow rate in the remaining open pores also increases rapidly, which can then lead to lower capture efficiency. We thus tested filters with nominal pore size of 8, 10, 12, 15 and 20 µm. Based on the results obtained earlier, optimal conditions were chosen as follows. MDA-MB-231 cells were spiked in 1 mL of blood diluted 1:6 in PBS, and filtered at 0.1 mL min^{-1}, then rinse twice with 5.0 mL of PBS at the same rate.

In good agreement with the previous data, efficiency was found to be > 80 % for small pore sizes (Figure AI-3, red symbols). Efficiency decreased for 15 and 20 µm pores, falling to 76 ± 5 and 63 ± 3 respectively. The number of WBCs was 694 ± 161 on 8 µm-filters, in the same range as in previous experiments (702 ± 181 using 1.0 mL min^{-1}) and found to decrease for increasing pore sizes (Figure AI-3, grey bars). The mean diameter of MDA-MB-231 cells, measured on 180 cells by microscopy, was 14.6 ± 5.1 µm and these cells are expected to easily flow through the bigger pores (decreasing efficiency). Likewise, the number of WBCs was also reduced (increasing purity).

Number of spiked cells

To test whether the number of cells spiked into the blood sample affect the enrichment for the different pore sizes, 6.1 ± 1.5, 26.6 ± 1.4 or 101.1 ± 5.1 MDA-MB-231 cells were added to the sample, (Supporting information AI.7.3). As expected, efficiency was not dependent on the spiking numbers, thus also validating our methodology for as little as 6 cells spiked into blood.

As a conclusion, using optimized conditions, the mechanical capture configuration provides a good efficiency (87 ± 2 % of MDA-MB-231 cells were captured with 8 µm-diameter pores at 0.1 mL min^{-1}) and a good purity (less than 1000 WBCs on the filter after rinsing twice with 5 mL of PBS).

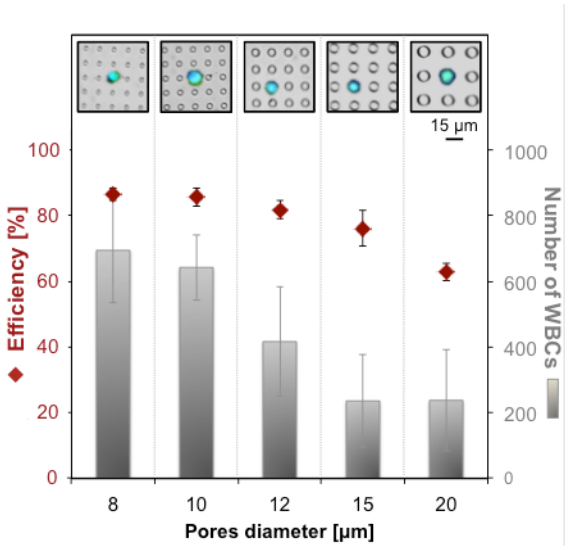

Figure AI-3 | Performance of the mechanical capture for various pore sizes. Efficiency (red symbols) and number of WBCs (grey bars) were determined for 26.2 ± 1.9 MDA-MB-231 cells spiked in 1.0:6.0 mL of blood:PBS. Samples were filtered through with 8, 10, 12, 15 or 20 µm-diameter pores at 0.1 mL min^{-1} and rinsed twice with 5.0 mL of PBS at 0.1 mL min^{-1}. Insets show cells, stained for nucleus (blue) and CK (green), captured on filters with the corresponding pore size. Error bars correspond to the standard deviation of three independent experiments.

AI.4.2 Mechanical and molecular capture of CTCs

To help target specific cell types, we sought to functionalize filters with antibodies directed against receptors expressed in particular CTCs.

Filter functionalization

Different functionalization protocols were tested using pristine filters or using a chemical activation by oxygen plasma or ozone treatment followed by covalent linkage using EDC/NHS or CNBr-based chemistry of antibodies (Supporting information AI.7.4). Filters were functionalized with anti-rabbit IgG antibody fluorescently labeled with FITC (Fluorescein isothiocyanate), and the Δfluo between pristine and functionalized filter was used to evaluate the efficacy of each protocol (Figure AI-4A).

Interestingly, a high fluorescence was observed on pristine filters incubated with IgG indicating that antibodies were adsorbed on the filter. O_3 treatment followed by EDC/NHS or CNBr-based chemistry leads to moderate fluorescence increases. For oxygen plasma treated filters, CNBr-based functionalization gave the lowest fluorescence variation of all tested conditions, while EDC/NHS chemistry gave the highest, which was thus

selected for subsequent experiments. The influence of IgG concentration on functionalization was tested by varying the concentration from 2.0 to 50.0 µg mL^{-1} (Figure AI-4B and C). For 2.0 and 5.0 µg mL^{-1}, the surface coverage was not uniform, leaving areas where fluorescence intensity was close to that of pristine filters. For 10.0 and 25.0 µg mL^{-1}, fluorescence was found approximately constant on the entire filter surface. As the antibody concentration increased to 50.0 µg mL^{-1}, Δfluo also increased but the overall uniformity of the coating was not significantly improved compared to 10.0 and 25.0 µg mL^{-1}. Therefore, in further experiments, filters were functionalized by incubation in a 10.0 µg mL^{-1} antibody solution.

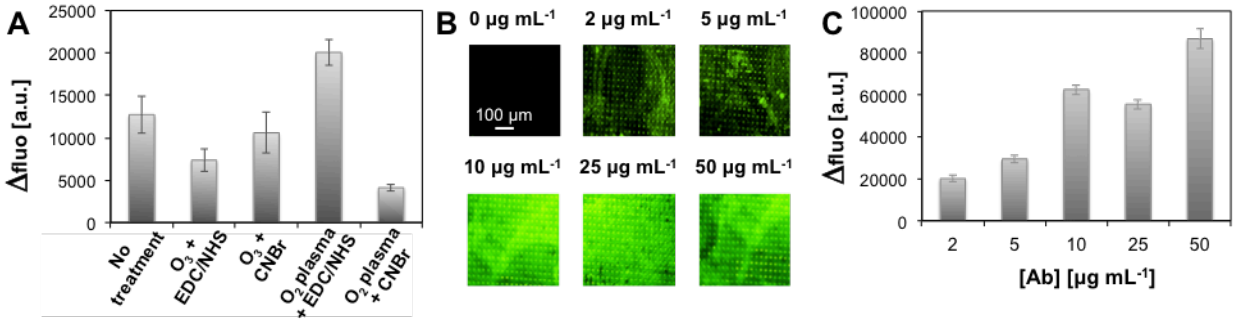

*Figure AI-4 | Filter functionalization. (A) Fluorescence increase of filters coated with 2.0 µg mL^{-1} of fluorescent IgG. Antibodies were applied to filters in a pristine state, or after activation by oxygen plasma or ozone treatment followed by EDC/NHS or CNBr-based chemistry. Δfluo was determined by comparison with the filter before incubation. **(B)** Qualitative and **(C)** quantitative evaluation of O_2 plasma + EDC/NHS filter functionalization with 2.0, 5.0, 10.0, 25.0 or 50.0 µg mL^{-1} of antibody solutions. Δfluo was averaged on 10 images per filter. Error bars correspond to the standard deviation of three independent experiments.*

AI.4.3 CTC enrichment on functionalized filters

To evaluate the feasibility of improving efficiency by combining mechanical and molecular enrichment, filters were used as is or functionalized with antibodies against EpCAM (epithelial cell adhesion molecule) or EGFR (epidermal growth factor receptor) (Figure AI-5A). These two receptors are expressed on a variety of cancer cells, and cells that only express one or the other receptor were used here to test the enrichment and selectivity of single receptor targeting. MDA-MB-231 cells are a triple negative breast cancer cell with low EpCAM[40] and high EGFR expression.[41] MCF-7 breast cancer highly express EpCAM[42] but no or a low level of EGFR.[41] In addition, we filtered two renal

cancer cells: 786-O and A-498 that are both EpCAM negative[43] but EGFR positive.[44,45] The filtration parameters were selected based on the optimal conditions for mechanical capture as per our previous experiments. 27-32 cells of each type were spiked separately into 1.0:6.0 mL of blood:PBS, and filtered at 0.1 mL min^{-1}. Filters were rinsed twice with 5 mL of PBS at the same rate.

The efficiency for MDA-MB-231 cells was increased to 98 ± 3 % with anti-EGFR coating compared to non-functionalized filters (83 ± 5 %) and anti-EpCAM (85 ± 3 %) (Figure AI-5B). Likewise, for 786-O and A-498 cells that also overexpress EGFR, efficiency was increased with anti-EGFR filters (93 ± 3 and 96 ± 1 %, respectively) but similar when filters were not functionalized (78 ± 2 and 86 ± 2 %, respectively) or functionalized with anti-EpCAM (81 ± 2 and 87 ± 4 %, respectively). Conversely, anti-EpCAM functionalization helped increase the capture of EpCAM expressing MCF-7 cells to 96 ± 3 % (compared to 85 ± 3 % with non-functionalized filter), while anti-EGFR functionalization does not significantly affect efficiency (83 ± 5 %).

These results show that antibody-functionalized filters used in the 3D printed cartridge achieved very high efficiency for all tested cell lines, and indicate that antibody functionalization helped improve the efficiency specifically for cells that overexpress the targeted receptors from ≈ 80 % (pristine filters) to > 95 %, underscoring the advantage of combining mechanical and molecular capture. In both configurations, WBCs contamination was very low, with < 0.1 % WBCs captured on the filter. In consideration of the high efficiency values and the broad size distribution of all cell lines used here (Supporting information AI.7.1, Table SAI-1), it is expected that patient CTCs, that are on average smaller, will also be captured with high efficiency.

Only few groups made use of antibody targeting and filtration. However, in all cases, isolation was performed in two steps, and none of them enrich cells both based on their size and molecular expression. Chung *et al.* used magnetic beads conjugated with anti-EpCAM to target cancer cells. A magnet was used first to attract labeled cells when

pushing blood cells out, then cancer cells were finally isolated from residual WBCs by filtration, leading to 70-90 % efficiency.[34] More recently, Zhang *et al.* labeled cancer cells with anti-EpCAM functionalized magnetic beads to increase their size. RBCs and free beads were first removed by filtration, then labeled cells were magnetically isolated from WBCs. Using this strategy, Zhang *et al.* reported 80-94 % for the recovery of MCF-7 spiked in blood, and > 98 % purity (number of WBCs near each MCF-7 cells).[35] In both cases, cell selection was based on the expression of a single marker only, and filtration was performed to improve purity.

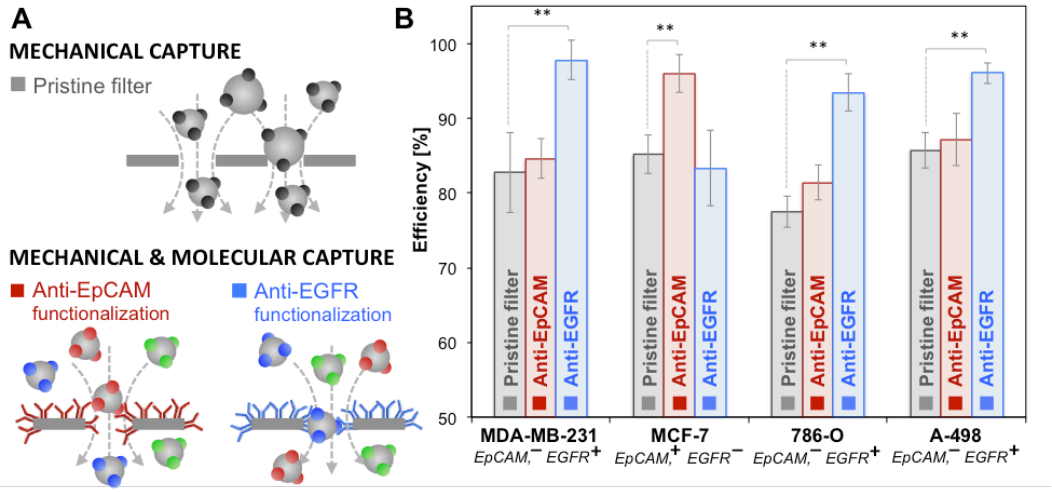

*Figure AI-5 | Filter functionalization enhances efficiency. (A) Schematic representation of the filtration process using pristine filter and filters functionalized with anti-EpCAM or anti-EGFR. **(B)** Efficiency for MDA-MB-231, MCF-7, 786-O and A-498 cells using pristine filters (grey) and filters functionalized with anti-EpCAM (red) or anti-EGFR (blue). 26.9 ± 2.3 MDA-MB-231, 27.6 ± 3.7 MFC-7, 34.2 ± 2.3 786-O or 32.0 ± 2.3 A-498 cells were spiked in 1.0:6.0 mL of blood:PBS, filtered and rinsed twice with 5.0 mL of PBS at 0.1 mL min^{-1}. For all cells tested, filters functionalized with antibodies against cells overexpressed receptors significantly increased efficiency. Error bars correspond to the standard deviation of three independent experiments. ($p \leq 0.01$: **).*

The method we presented here is the only method that selects cells based on mechanical and molecular features. Very high performances are reached, with efficiency and purity in the same range or higher than device described in the literature. The whole isolation process occurs in one single step, and is simpler to implement. Moreover, the use of transparent filters allows imaging and cell identification directly on the filter.

AI.5 Conclusion

In this study we introduced combined mechanical and molecular filtration using antibody-functionalized polymer filters and a new 3D printed cartridge permitting rapid assembly and disassembly for retrieval of the filters for analysis. Filters are transparent with low autofluorescence and are thus compatible with image-based identification of CTCs. Multiple processing parameters were systematically optimized (sample dilution, rinsing procedure, filtration flow rate and filter pore size) allowing to obtain high enrichment of breast and kidney tumor cells spiked into fresh blood with very low WBCs contamination (< 0.1 %), in less than 3h. The enrichment efficiency with pristine filters was 80 %, and was reliable for between as little as 6-100 cells spiked into 1 mL of blood. After filter functionalization with antibodies against cell surface receptors, efficiency increased to > 96 % with good reproducibility for all studied breast and renal cancer cell types. Further improvements are possible, for example processing time may be reduced by increasing membrane porosity or doubling the filter diameter (allowing for quadrupling of flow rates while maintaining the same shear stress), as well as by improving and shortening the rinsing protocol.

To address the challenge of enriching a population of heterogeneous CTCs, it may be possible to stack multiple filters with different pore sizes and functionalized with different antibodies each. Alternatively, a single filter might be coated with multiple different antibodies, thus targeting a broad spectrum of CTCs.

For use in cancer disease management, CTC enrichment technologies should be fast, sensitive and selective. The proposed cartridge with antibody-functionalized microfabricated filters is simple to use and efficiently captures a cancer cells from whole blood, and thus represented a promising technology for clinical enrichment of CTCs from different cancers with a diversity of mechanical and molecular features.

AI.6 Acknowledgements

A.M. acknowledges funding from National Science and Engineering Research Council of Canada (NSERC). D.J. acknowledges support from Canada Research Chair (CRC). J.A. H.-C. thanks the Lloyd-Carr Harris Foundation and CONACyT for funding. We acknowledge Dr. Kebin Li and Dr. Matthias Geissler for their help in the filter fabrication and functionalization. Finally, we thank Dr. Bernard Nisol and Gina Zhou for their critical reading of the manuscript.

References

1. Chaffer, C. L.; Weinberg, R. A. *Science* **2011**, *331*, 1559-1564.

2. Nguyen, D. X.; Bos, P. D.; Massague, J. *Nat. Rev. Cancer* **2009**, *9*, 274-284.

3. Arya, S. K.; Lim, B.; Rahman, A. R. A. *Lab Chip* **2013**, *13*, 1995-2027.

4. Alix-Panabières, C.; Pantel, K. *Clin. Chem.* **2013**, *59*, 110-118.

5. Allard, W. J.; Matera, J.; Miller, M. C.; Repollet, M.; Connelly, M. C.; Rao, C.; Tibbe, A. G. J.; Uhr, J. W.; Terstappen, L. W. M. M. *Clin. Cancer Res.* **2004**, *10*, 6897-6904.

6. Coumans, F. A. W.; van Dalum, G.; Beck, M.; Terstappen, L. W. M. M. *PLoS ONE* **2013**, *8*, e61774.

7. Seal, S. *Cancer* **1956**, *9*, 866-868.

8. Balic, M.; Cote, R. J. In *Genomic Applications in Pathology*; Springer, 2015, pp 71-84.

9. Lv, P.; Tang, Z.; Liang, X.; Guo, M.; Han, R. P. *Biomicrofluidics* **2013**, *7*, 034109.

10. Sun, W.; Jia, C.; Huang, T.; Sheng, W.; Li, G.; Zhang, H.; Jing, F.; Jin, Q.; Zhao, J.; Li, G. *PLoS ONE* **2013**, *8*, e75865.

11. Tan, S. J.; Yobas, L.; Lee, G. Y. H.; Ong, C. N.; Lim, C. T. *Biomed. microdevices* **2009**, *11*, 883-892.

12. Mohamed, H.; Murray, M.; Turner, J. N.; Caggana, M. *J. Chromatogr. A* **2009**, *1216*, 8289-8295.

13. Harouaka, R. A.; Zhou, M.-D.; Yeh, Y.-T.; Khan, W. J.; Das, A.; Liu, X.; Christ, C. C.; Dicker, D. T.; Baney, T. S.; Kaifi, J. T. *Clin. Chem.* **2014**, *60*, 323-333.

14. Hosokawa, M.; Yoshikawa, T.; Negishi, R.; Yoshino, T.; Koh, Y.; Kenmotsu, H.; Naito, T.; Takahashi, T.; Yamamoto, N.; Kikuhara, Y. *Anal. Chem.* **2013**, *85*, 5692-5698.

15. Tang, Y.; Shi, J.; Li, S.; Wang, L.; Cayre, Y. E.; Chen, Y. *Sci. Rep.* **2014**, *4*.

16. Zheng, S.; Lin, H. K.; Lu, B.; Williams, A.; Datar, R.; Cote, R. J.; Tai, Y.-C. *Biomed. microdevices* **2011**, *13*, 203-213.

17. Tibbe, A. G. J.; Miller, M. C.; Terstappen, L. W. M. M. *Cytometry A* **2007**, *71A*, 154-162.

18. Gleghorn, J. P.; Pratt, E. D.; Denning, D.; Liu, H.; Bander, N. H.; Tagawa, S. T.; Nanus, D. M.; Giannakakou, P. A.; Kirby, B. J. *Lab Chip* **2010**, *10*, 27-29.

19. Hou, H. W.; Warkiani, M. E.; Khoo, B. L.; Li, Z. R.; Soo, R. A.; Tan, D. S.-W.; Lim, W.-T.; Han, J.; Bhagat, A. A. S.; Lim, C. T. *Sci. Rep.* **2013**, *3*.

20. Shen, Q.; Xu, L.; Zhao, L.; Wu, D.; Fan, Y.; Zhou, Y.; OuYang, W. H.; Xu, X.; Zhang, Z.; Song, M. *Adv. Mater.* **2013**, *25*, 2368-2373.

21. Zhao, L.; Lu, Y. T.; Li, F.; Wu, K.; Hou, S.; Yu, J.; Shen, Q.; Wu, D.; Song, M.; OuYang, W. H. *Adv. Mater.* **2013**, *25*, 2897-2902.

22. Nagrath, S.; Sequist, L.; Maheswaran, S.; Bell, D.; Irimia, D.; Ulkus, L.; Smith, M.; Kwak, E.; Digumarthy, S.; Muzikansky, A.; Ryan, P.; Balis, U.; Tompkins, R.; Haber, D.; Toner, M. *Nature* **2007**, *450*, 1235 - 1239.

23. Earhart, C. M.; Wilson, R. J.; White, R. L.; Pourmand, N.; Wang, S. X. *J. Magn. Magn. Mater.* **2009**, *321*, 1436-1439.

24. Saliba, A.-E.; Saias, L.; Psychari, E.; Minc, N.; Simon, D.; Bidard, F.-C.; Mathiot, C.; Pierga, J.-Y.; Fraisier, V.; Salamero, J. *Proc. Natl. Acad. Sci. U.S.A.* **2010**, *107*, 14524-14529.

25. Mohamadi, R. M.; Besant, J. D.; Mepham, A.; Green, B.; Mahmoudian, L.; Gibbs, T.; Ivanov, I.; Malvea, A.; Stojcic, J.; Allan, A. L.; Lowes, L. E.; Sargent, E. H.; Nam, R. K.; Kelley, S. O. *Angewandte Chemie International Edition* **2015**, *54*, 139-143.

26. Murlidhar, V.; Zeinali, M.; Grabauskiene, S.; Ghannad - Rezaie, M.; Wicha, M. S.; Simeone, D. M.; Ramnath, N.; Reddy, R. M.; Nagrath, S. *Small* **2014**, *10*, 4895-4904.

27. Sequist, L. V.; Nagrath, S.; Toner, M.; Haber, D. A.; Lynch, T. J. *J. Thorac. Oncol.* **2009**, *4*, 281-283.

28. Stott, S. L.; Hsu, C.-H.; Tsukrov, D. I.; Yu, M.; Miyamoto, D. T.; Waltman, B. A.; Rothenberg, S. M.; Shah, A. M.; Smas, M. E.; Korir, G. K. *Proc. Natl. Acad. Sci. U.S.A.* **2010**, *107*, 18392-18397.

29. Dharmasiri, U.; Njoroge, S. K.; Witek, M. A.; Adebiyi, M. G.; Kamande, J. W.; Hupert, M. L.; Barany, F.; Soper, S. A. *Anal. Chem.* **2011**, *83*, 2301-2309.

30. Pantel, K.; Saad, F. *Future Oncol.* **2012**, *8*, 321-331.

31. Zhang, Y.; Wu, M.; Han, X.; Wang, P.; Qin, L. *Angewandte Chemie International Edition* **2015**, *54*, 10838-10842.

32. Sajay, B. N. G.; Chang, C.-P.; Ahmad, H.; Khuntontong, P.; Wong, C. C.; Wang, Z.; Puiu, P. D.; Soo, R.; Rahman, A. R. A. *Biomed. microdevices* **2014**, *16*, 537-548.

33. Ozkumur, E.; Shah, A. M.; Ciciliano, J. C.; Emmink, B. L.; Miyamoto, D. T.; Brachtel, E.; Yu, M.; Chen, P.-i.; Morgan, B.; Trautwein, J. *Sci. Transl. Med.* **2013**, *5*, 179ra147-179ra147.

34. Chung, Y.-K.; Reboud, J.; Lee, K. C.; Lim, H. M.; Lim, P. Y.; Wang, K. Y.; Tang, K. C.; Ji, H.; Chen, Y. *Biosens. Bioelectron.* **2011**, *26*, 2520-2526.

35. Zhang, H.; Wang, Y.; Li, Q.; Zhang, F.; Tang, B. *Chem. Commun.* **2014**, *50*, 7024-7027.

36. J. A. Hernández-Castro, K. Li, A. Meunier, D. Juncker and T. Veres, *Lab. Chip*, 2017, **17**, 1960–1969.

37. Rasband, W. *Astrophysics Source Code Library* **2012**, *1*, 06013.

38. Seal, S. H. *Cancer* **1964**, *17*, 637-642.

39. Jones, J. G.; Holland, B. M.; Humphrys, J.; Quew, R.; Wardrop, C. A. *Br. J. Haematol.* **1984**, *57*, 457-466.

40. Gorges, T.; Tinhofer, I.; Drosch, M.; Rose, L.; Zollner, T.; Krahn, T.; von Ahsen, O. *BMC Cancer* **2012**, *12*, 178.

41. Charafe-Jauffret, E.; Ginestier, C.; Monville, F.; Finetti, P.; Adelaide, J.; Cervera, N.; Fekairi, S.; Xerri, L.; Jacquemier, J.; Birnbaum, D. *Oncogene* **2006**, *25*, 2273-2284.

42. Rao, C.; Chianese, D.; Doyle, G.; Miller, M.; Russell, T.; Sanders, R.; Terstappen, L. *Int. J. Oncol.* **2005**, *27*, 49 - 57.

43. Patriarca, C.; Macchi, R. M.; Marschner, A. K.; Mellstedt, H. *Cancer Treat. Rev.* **2012**, *38*, 68-75.

44. Franovic, A.; Gunaratnam, L.; Smith, K.; Robert, I.; Patten, D.; Lee, S. *Proc. Natl. Acad. Sci. U.S.A.* **2007**, *104*, 13092-13097.

45. Gemmill, R.; Zhou, M.; Costa, L.; Korch, C.; Bukowski, R.; Drabkin, H. *Brit. J. Cancer* **2005**, *92*, 2266-2277.

AI.7 Supporting information

Additional data regarding material and methods (AI.7.1), the effect of the flow rate on purity (AI.7.2), the effect of the number of spiked cells (AI.7.3) and filter functionalization (AI.7.4) are provided in supporting information.

AI.7.1 Materials and methods

Materials and reagents

All solutions were prepared with water from a Milli-Q system (resistivity: 18 MΩ cm; Millipore). Phosphate buffered saline (PBS, 1X, pH=7.4, Fisher Scientific), contains 11.9 10^{-3}, 137.0 10^{-3} and 2.7 10^{-3} mol L^{-1} of phosphates, NaCl and KCl, respectively. Trypsin-EDTA, sulfuric acid, 1-ethyl-3-(3-dimethyl aminopropyl) carbodiimide (EDC), N-hydroxysuccinimide (NHS), 2-(N-morpholino)ethanesulfonic acid (MES), NaCl, bovine serum albumin (BSA) and Tween 20 were obtained from Sigma-Aldrich. Triton X-100 and paraformaldehyde were purchased from Fisher Scientific. Dulbecco's modified Eagle medium (DMEM), RPMI 1640 medium, fetal bovine serum (FBS) and 4',6-diamidino-2-phenylindole (DAPI) were purchased from Life Technologies. Antibiotics (penicillin/streptomycin) were obtained from Invitrogen. Anti-EGFR (epidermal growth factor receptor), anti-EpCAM (epithelial cell adhesion molecule), anti-pan cytokeratin-Alexa Fluor 488 and anti-human CD45-phycoerythrin were obtained from R&D systems.

Filter fabrication

The process described in detail elsewhere.[1] Briefly, a pillar structure was created by replication of molds obtained by standard photolithography and DRIE. The structure was then closed using a UV curable polymer cover coated on polyethylene terephthalate (PET) carrier to form an enclosed 3D microcavity, which was fully filled by the UV-curable Fluorolink® MD 700 resin (about 10 µL, depending on the surface area of the device and the height of the pillar) thereafter, and cured through UV exposure (2000-EC Series UV curing flood lamp, DYMAX). Finally, the blank cover was peeled off, and the molds were bath in acetone during 15-20 minutes, allowing the membranes to self-de-mold from the

pillars. Filter pore diameters, determined by microscopy and averaged on 20 pores from three different filters and for each pore size, were 7.9 ± 0.3, 10.0 ± 0.2, 11.7 ± 0.4, 15.0 ± 0.2 and 20.1 ± 0.3 µm.

Cartridge design

The filtration cartridge used in this work was designed with AutoCAD software (Autodesk Inc.) and 3D printed (Perfactory Micro EDU, Envision Tech). The cartridge is made of two parts in between which the microfilter can be inserted. A small notch (1 mm deep) with the filter shape and size is located at the center of bottom part, on the inside, to allow perfect alignment of the filter with the inlet and outlet. These notches are connected to the inlet and outlet through conical junctions allowing a homogeneous flow to reach the filter surface. Two toric joints, a silicone gasket and a pair of screws and bolts are used to ensure proper sealing.

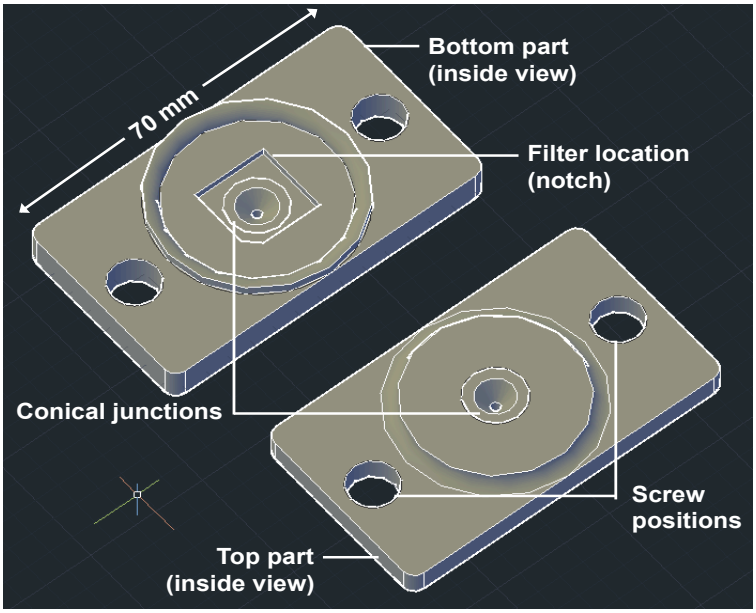

Figure SAI-1 | Design of the filtration cartridge. Screen capture of the AutoCAD design showing the insides of the top and bottom part of the cartridge. The filter is inserted in the notch located on the inside of the bottom part, and the cartridge is closed with the top part and clamp with screws.

Cell culture

All culture medium and solutions were initially sterile and filtered through a 0.2 µm filter. MDA-MB-231 (HTB-26) and MCF-7 (HTB-22) cell lines were obtained from the

American Type Culture Collection (Manassas, VA). 786-O and A-498 renal cells were kindly provided by Dr. Y. Riaz Alhosseini (McGill University, Montreal, Canada). MDA-MB-231, MCF-7 and A-498 cells were cultured in DMEM, supplemented with 10 % FBS and 1 % (v/v) antibiotics (final concentrations of 100 I.U. mL^{-1} penicillin and 100 µg mL^{-1} streptomycin). 786-O renal cells were cultured in RPMI 1640 medium supplemented with 10 % FBS. All cell cultures were maintained in 5 % CO_2 at 37 °C in 25 cm^2 flasks (Corning, NY, USA). Almost confluent monolayers (80-90 %) of cells in flasks were harvested through scratching in 2 mL of PBS (for MDA-MB-231 cells) or using diluted trypsin (for MCF-7, 786-O and A-498 cells). 1 mL of the cell suspension was re-suspended in 5 mL of culture media in a new flask while, for spiking experiments, the second milliliter was centrifuged at 4600 rpm for 5 minutes and re-suspended in 1 mL of PBS (density of ≈ 10^6 cells mL^{-1}). Information regarding the size distribution and the level of expression of EpCAM and EGFR antibodies for all cell lines is provided in Table SAI-1.

*Table SAI-1 | Summary of cell types used in this study. * Diameters, measured by microscopy, are reported as mean ± standard deviation.*

Cell Type	Cancer	Diameter* (µm)	EpCAM expression	EGFR expression
MDA-MB-231	Breast	14.6 ± 5.1	Low/negative[2]	High[3]
MCF-7	Breast	15.2 ± 4.1	High[4]	Low/negative[3]
786-O	Kidney	15.6 ± 5.8	Negative[5]	High[6,7]
A-498	Kidney	15.8 ± 3.8	Negative[5]	High[6,7]

Cell counting

For cell spiking experiments, the cell suspension was first diluted by a factor of 50 to obtain approximately 10-20 cells per microliter. In order to precisely determine the amount of cells within each suspension, 10 µL droplets were placed between a microscope glass slide and a coverslip. The actual number of cells within the 10-µL suspension was manually counted under a microscope. Counting was repeated twice on each slide and averaged on 10 droplets.

Cell enrichment

The sample preparation was directly performed in a syringe. 1.0 mL of blood was diluted with the desired volume of PBS (from 0.0 to 15.0 mL). Once the exact number of (MDA-MB-231, MCF-7, 786-O or A-498) cells in suspension was determined (Supporting information AI.7.1), the volume corresponding to the desired number of cells was then spiked into the mixture.

After mixing, the syringe was plugged in the cartridge with a polyetheretherketone (Peek) tube (i.d. 0.75 mm, length 10 cm, Sigma Aldrich) at the inlet (top). The desired flow rate (0.1, 0.5, 1.0, 2.0 or 3.0 mL min-1) was applied, making the sample pass through the filter with pore diameters ranging from 8 to 20 µm. Where specified, samples were rinsed with PBS (5.0, 10.0, 20.0, 2 × 5.0 or 3 × 5.0 mL) at the same flow rate as for filtration; in that case, the syringe was re-filled with the chosen volume of PBS.

Cell staining

Cell staining was performed on the filter, directly in the cartridge after filtration. Before each step described below (from a. to i.), the tubes were unplugged and the outlet was closed with a suitable stopper. Then, 100 µL of appropriate solution was introduced into the cartridge through the inlet with a pipette. After the required incubation time, the cartridge was plugged again to the tubes and a 0.1 mL min^{-1} air flow was applied to push the solution out.

(a.) Cells fixation with 3.7 % paraformaldehyde (PFA) in PBS for 10 minutes.

(b.) Rinsing twice, 5 min each, in PBS.

(c.) Cells permeabilization with 0.2 % Triton X-100 for 5 min.

(d.) Rinsing twice, 5 min each, in PBS.

(e.) Blocking with 1.0 % BSA in PBS supplemented with 0.1 % Tween 20.

(f.) Cells staining with Anti-Pan-cytokeratin Alexa Fluor 488 (2.0 µg mL^{-1}) and Anti-Human CD45 Phycoerythrin (PE, 1.0 µg mL^{-1}), diluted in PBS, for 1 hour.

(g.) Rinsing with PBS.

(h.) Nucleus staining with 4',6-diamidino-2-phenylindole (DAPI, 0.1 µg mL^{-1}).

(i.) Rinsing with PBS.

AI.7.2 Effect of the flow rate on purity

The effect of flow rate on the number of white blood cells (WBCs) remaining on the filter was estimated directly after filtration (no rinse). For these experiments, 101.3 ± 3.3 MDA-MB-231 cells were spiked in 1.0 mL of blood, and samples, diluted with 6.0 mL of PBS, were filtered through 8 µm diameter pores at different flow rates (0.1, 0.5, 1.0, 2.0 or 3.0 mL min^{-1}). Fluorescence images were acquired after cell staining.

As expected, the number of WBCs seems to decrease when the flow rate increases (Figure SAI-2A). However, for some flow rate conditions, that number can reach high values (< 1000), preventing the direct count of WBCs. In order to overcome this issue, the surface of the filter covered by fluorescently labeled WBCs was estimated using ImageJ software (Wayne Rasband). All images were acquired with the same exposure time (3 seconds) allowing the direct comparison of their fluorescence intensity. For each filter, 10 images were collected and converted to 8 bit greyscale images. The level of fluorescence intensity of WBCs was used as threshold value (fixed for all images and all conditions) to separate background (areas of the filter with intensity lower than the threshold) and areas covered by WBCs (intensity higher than the threshold).

The percentage of the filter surface covered by WBCs, averaged on the 10 images per filter and on three samples is plotted in Figure SAI-2B. In good agreement with the qualitative observation (Figure SAI-2A), the surface covered by WBCs decreases from 29 ± 4 % at 0.1 mL min^{-1} to 8 ± 3 % at 3.0 mL min^{-1}, indicating that higher flow rate improves purity.

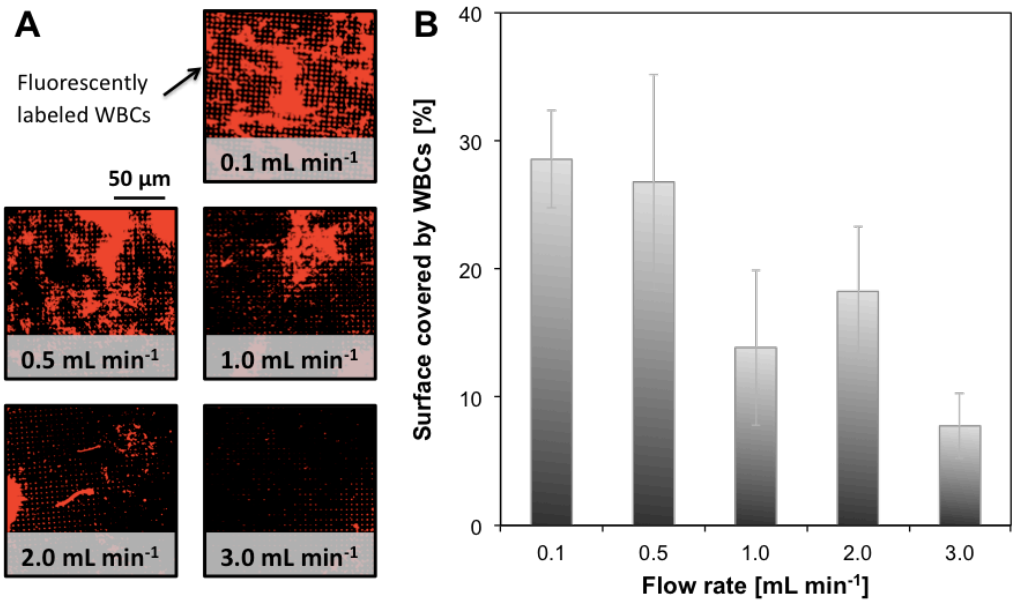

Figure SAI-2 | WBCs captured on filter as function of flow rate. ***(A)*** *Representative images of the filter surface covered by fluorescently labeled WBCs (anti-CD45-Phycoerythrin) for various flow rates.* ***(B)*** *Percentage of the filter surface covered by WBCs, averaged on 10 images per filter and on three samples. 101.3 ± 3.3 MDA-MB-231 cells were spiked in 1.0 mL of blood and diluted with 6.0 mL of PBS. Samples were filtered through filters with 8 µm diameter pores at 0.1, 0.5, 1.0, 2.0 or 3.0 mL min-1. The error bars correspond to the standard deviation of three independent experiments.*

AI.7.3 Effect of the number of cells spiked in blood

Circulating tumor cells (CTCs) are typically in the range of 1 to 10 per milliliter of blood.[8-12] However, depending on the type and stage of cancer, this count can strongly vary. For instance, up to 115 and 224 CTCs per milliliter have been detected in metastatic breast and gastric cancer patients respectively.[13] The influence of that number on capture efficiency was therefore investigated on a large range, by spiking 6.1 ± 1.5, 26.6 ± 1.4 or 101.1 ± 5.1 MDA-MB-231 cells in 1.0 mL of blood diluted with 6.0 mL of PBS. Samples were filtered through 8, 10, 12, 15 or 20 µm diameter pores at 1.0 mL min^{-1}. Fluorescence images were recorded after immunostaining.

As previously observed, for each number of MDA-MB-231 cells spiked in blood, efficiency clearly decreases when pore size increases. For instance, 61 ± 10 % of MDA-MB-231 were captured with 8 µm diameter pores and 6.1 cells spiked in blood, and this value decreases down to 38 ± 10 when filters with 20 µm diameter pores are used (Figure SAI-3).

For each single pore size, efficiency values obtained for various number of MDA-MB-231 spiked in blood (6.1 ± 1.5, 26.6 ± 1.4 or 101.1 ± 5.1 MDA-MB-231 cells) were compared using Fisher test. In all cases, p values are higher than 0.05, indicating that the number of MDA-MB-231 initially spiked in blood has no effect on efficiency.

Moreover, one can notice that the errors bars (standard deviations of three independent experiments) are in the same range for a single number of MDA-MB-231 cells spiked in blood but clearly decreases when the number of MDA-MB-231 cells spiked in blood increases. This is due to the fact that missing a cell will impact more on the efficiency for small number of cells. Indeed, one missed cell when spiking about six MDA-MB-231 cells, corresponds to about 16 % of error, while when spiking about a hundred cells, it approximately corresponds to 1 %.

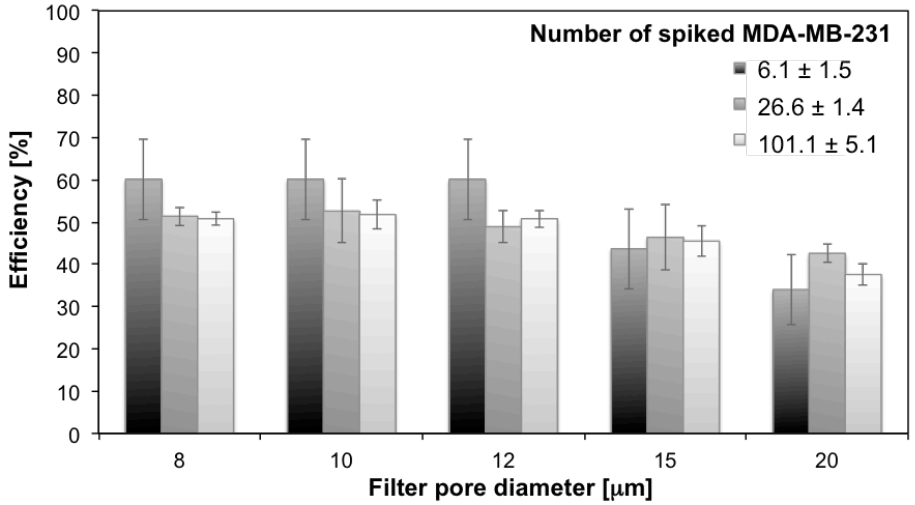

Figure SAI-3 | Effect of the number of MDA-MB-231 spiked in blood on efficiency. ■ 6.1 ± 1.5, ■ 26.6 ± 1.4 or □ 101.1 ± 5.1 MDA-MB-231 cells were spiked in 1.0 mL of blood and diluted with 6.0 mL of PBS. Samples were filtered at 1.0 mL min^{-1} through filters with 8, 10, 12, 15 or 20 µm diameter pores. The error bars correspond to the standard deviation of three independent experiments.

AI.7.4 Filter functionalization

The performance of various treatments of the filter surface for antibody functionalization was evaluated using fluorescently labeled antibody (FITC-labeled anti-rabbit antibodies). Following each surface treatment describe in Table SAI-2, 100 µL of the antibody solution (2 µg mL^{-1}) was added on the filter surface for three hours at 4 °C

to avoid evaporation. The filter was then rinsed with PBS, deionized water, and dried under a nitrogen stream.

Table SAI-2 | Surface treatments studied to optimize filter surface functionalization. EDC: 1-ethyl-3-(3-dimethyl aminopropyl) carbodiimide, NHS: N-hydroxysuccinimide, CNBr: Cyanogen bromide.

Labels in Figure AI-4A (main paper)	Surface treatment before antibody incubation
No treatment	Pristine filter
O_3 + EDC/NHS	Ozone treatment (20 minutes in an ozone generator, OzoMax, Inc., Shefford, Quebec, Canada) + 20 minutes incubation in EDC/NHS (0.05 mol L^{-1})
O_2 plasma + EDC/NHS	Oxygen plasma (2 minutes, 150 W, O_2 pressure of 200 mTorr, Plasmalab 80 Plus, Oxford Instruments, Bristol, United Kingdom) + 20 minutes incubation in EDC/NHS (0.05 mol L^{-1})
O_3 + CNBr	Ozone treatment (20 minutes in an ozone generator) + 20 minutes incubation in CNBr (0.5 mol L^{-1} in nitric acid).
O_2 plasma + CNBr	Oxygen plasma treatment (2 minutes, 150 W, O_2 pressure of 200 mTorr) + 20 minutes incubation in CNBr (0.5 mol L^{-1} in nitric acid).

The presence of antibodies on the surface was directly evidenced using fluorescence microscopy. For each condition, fluorescence images were collected before and after functionalization with 3 second exposure. The mean fluorescence intensity was determined from four randomly chosen areas of the filter. Finally, the variation between the fluorescence intensity of the pristine filter and that obtained after functionalization (Δfluo), averaged on three independent experiments, is plotted in Figure AI-4A of the main paper.

Briefly, the highest variation of fluorescence intensity was obtained after oxygen plasma followed by EDC/NSH based-chemistry. Therefore, in order to obtain the highest

antibody density, filters were functionalized after O_2 plasma treatment and EDC/NHS chemistry. For cells experiments, same protocol was used and antibody concentrations were optimized (Figure AI-4B and C of the main paper).

References

1. J. A. Hernández-Castro, K. Li, A. Meunier, D. Juncker and T. Veres, *Lab. Chip*, 2017, **17**, 1960–1969.

2. Gorges, T.; Tinhofer, I.; Drosch, M.; Rose, L.; Zollner, T.; Krahn, T.; von Ahsen, O. *BMC Cancer* **2012**, *12*, 178.

3. Charafe-Jauffret, E.; Ginestier, C.; Monville, F.; Finetti, P.; Adelaide, J.; Cervera, N.; Fekairi, S.; Xerri, L.; Jacquemier, J.; Birnbaum, D. *Oncogene* **2006**, *25*, 2273-2284.

4. Rao, C.; Chianese, D.; Doyle, G.; Miller, M.; Russell, T.; Sanders, R.; Terstappen, L. *Int. J. Oncol.* **2005**, *27*, 49 - 57.

5. Patriarca, C.; Macchi, R. M.; Marschner, A. K.; Mellstedt, H. *Cancer Treat. Rev.* **2012**, *38*, 68-75.

6. Franovic, A.; Gunaratnam, L.; Smith, K.; Robert, I.; Patten, D.; Lee, S. *Proc. Natl. Acad. Sci. U.S.A.* **2007**, *104*, 13092-13097.

7. Gemmill, R.; Zhou, M.; Costa, L.; Korch, C.; Bukowski, R.; Drabkin, H. *Brit. J. Cancer* **2005**, *92*, 2266-2277.

8. Allard, W. J.; Matera, J.; Miller, M. C.; Repollet, M.; Connelly, M. C.; Rao, C.; Tibbe, A. G. J.; Uhr, J. W.; Terstappen, L. W. M. M. *Clin. Cancer Res.* **2004**, *10*, 6897-6904.

9. Arya, S. K.; Lim, B.; Rahman, A. R. A. *Lab Chip* **2013**, *13*, 1995-2027.

10. Coumans, F. A. W.; van Dalum, G.; Beck, M.; Terstappen, L. W. M. M. *PLoS ONE* **2013**, *8*, e61774.

11. Hajba, L.; Guttman, A. *Trends Anal. Chem.* **2014**, *59*, 9-16.

12. Ma, Y.-C.; Wang, L.; Yu, F.-L. *Technol Cancer Res Treat* **2013**, *12*, 295-309.

13. Galletti, G.; Sung, M. S.; Vahdat, L. T.; Shah, M. A.; Santana, S. M.; Altavilla, G.; Kirby, B. J.; Giannakakou, P. *Lab Chip* **2014**, *14*, 147-156.